Universidade do Minho
Escola de Medicina

Beatriz Rocha Ferreira

Establishing the relevance of Tau isoform imbalance in the onset and progression of Machado-Joseph disease

fevereiro de 2022

Establishing the relevance of Tau isoform imbalance in the onset and progression of Machado-Joseph disease

Beatriz Ferreira

UMinho | 2022

Universidade do Minho
Escola de Medicina

Beatriz Rocha Ferreira

Establishing the relevance of Tau isoform imbalance in the onset and progression of Machado-Joseph disease

Dissertação de Mestrado
Mestrado em Ciências da Saúde

Trabalho efetuado sob a orientação de
Doutora Andreia Alexandra Neves de Carvalho
e
Doutora Sara Carina Duarte da Silva

AGRADECIMENTOS

Em primeiro lugar, gostaria de deixar um especial agradecimento ao Doutor Nuno Sousa, Presidente da Escola de Medicina da Universidade do Minho, ao professor Jorge Correia-Pinto, Presidente do Instituto de Investigação das Ciências da Vida e Saúde da Universidade do Minho (ICVS/3B's), ao Doutor João Bessa, Coordenador do Domínio das Neurociências, e à professora Doutora Patrícia Maciel, diretora do Mestrado em Ciências da Saúde pela oportunidade de desenvolver este trabalho e pelas excelentes condições que me proporcionaram. Um enorme agradecimento à professora Patrícia Maciel pela oportunidade de integrar a sua equipa. Foi um privilégio enorme e agradeço todo o conhecimento profundo e simpatia que me transmitiu. A toda a equipa, agradeço o vosso apoio e ensinamento, assim como as críticas construtivas e ferramentas que me forneceram, incentivando a minha curiosidade, empenho e dedicação nas características fundamentais para desenvolver investigação científica. Aos que dedicaram parte do seu tempo para me transmitirem conhecimentos mais práticos, relacionados com o biotério e o laboratório, agradeço a disponibilidade, pois foram fundamentais no meu percurso. Sem tudo isto, este trabalho não seria possível. Por isso, um sincero obrigado a todos! Em particular, à minha orientadora Andreia Carvalho e co-orientadora, Sara Silva, agradeço o acompanhamento próximo, por me ajudarem a encontrar o caminho e as soluções para as dúvidas com que me fui confrontando ao longo deste percurso. Foram particularmente importantes o rigor e a dedicação transmitidos em todas as tarefas que mobilizam o trabalho científico e que me auxiliaram grandemente na concretização deste objetivo e no meu crescimento pessoal. Estou profundamente grata pela vossa preciosa ajuda! A todos os NeRDs, agradeço a vossa disponibilidade para me ajudar, pelas discussões interessantes, pela simpatia e pelo bom ambiente de trabalho. A todos os meus amigos, que têm acompanhado o meu percurso académico, agradeço a paciência e os momentos de descontração que foram essenciais para superar os momentos de maior tensão. Obrigado pelas conversas e desabafos e por estarem presentes na minha vida. Para vocês um abraço especial, Adoro-vos! Por fim, às pessoas mais importantes da minha vida, os meus pais. Obrigada por todas as oportunidades que me proporcionaram e por acreditarem sempre em mim, vocês são os grandes impulsionadores do meu sucesso. À minha irmã, por me transmitires confiança e força em todos os momentos. Um enorme obrigada pelo vosso apoio incondicional.

FUNDING

The work presented in this thesis was performed in the Life and Health Sciences Research Institute (ICVS), Minho University. Financial support was provided by grants from the ICVS Scientific Microscopy Platform, member of the national infrastructure PPBI - Portuguese Platform of Bioimaging (PPBI-POCI-01-0145-FEDER-022122; by National funds, through the Foundation for Science and Technology (FCT) - project UIDB/50026/2020 and UIDP/50026/2020;

STATEMENT OF INTEGRITY

I hereby declare having conducted this academic work with integrity. I confirm that I have not used plagiarism or any form of undue use of information or falsification of results along the process leading to its elaboration.

I further declare that I have fully acknowledged the Code of Ethical Conduct of the University of Minho.

RESUMO

Estabelecer a relevância do desequilíbrio das isoformas da Tau no início e na progressão da doença de Machado-Joseph

A doença de Machado-Joseph (DMJ), também conhecida como Ataxia Espinocerebelosa Tipo-3 (SCA3), é uma ataxia hereditária dominante causada por uma expansão instável do trinucleotído citosina-adenina-guanina (CAG) dentro da sequência codificante do gene *ATXN3*, que é traduzido num trato de poliglutamina anormalmente longo na proteína ataxina-3 (ATXN3). Este distúrbio neurodegenerativo de início tardio é caracterizado por uma apresentação clínica altamente complexa. A nível neuropatológico, a neurodegeneração também afeta várias áreas do sistema nervoso central (SNC). Nos últimos anos, a nossa compreensão acerca do mecanismo patológico da DMJ/SCA3 progrediu notavelmente, e a comunidade científica fez alguns avanços no desenvolvimento de possíveis estratégias terapêuticas para este transtorno incapacitante. Atualmente, os tratamentos ou terapias existentes para a DMJ/SCA3 são escassos e dirigidos principalmente para o alívio dos sintomas. Além disso, essas abordagens não têm sido muito eficientes em desacelerar ou reverter o processo de neurodegeneração. No entanto, o(s) mecanismo(s) preciso(s) subjacente(s) a esta doença permanecem indefinidos e poucos biomarcadores foram identificados. Trabalho anterior da equipa sugeriu que a expressão da ATXN3 mutante perturba o fator de splicing SRSF7(9G8), levando a uma desregulação do splicing do exão 10 do gene da MAPT (Tau). Este estudo mostrou uma diminuição nos níveis da isoforma 4R-Tau no cérebro do modelo de ratinho CMVMJD135 (ratinho SCA3) a uma idade sintomática tardia e também, em amostras de cérebro de pacientes com DMJ/SCA3. Com base nessas observações, o objetivo principal deste trabalho foi restaurar os níveis de expressão da proteína 4R-Tau no cérebro de ratinhos SCA3 e avaliar se esta abordagem modulatória poderia melhorar a progressão da DMJ/SCA3. Nesse sentido, recorremos a injeções estereotáxicas, no quarto ventrículo, de vetores virais adeno-associados (VAA), expressando a proteína 4R-Tau humana, no cérebro de um modelo de ratinho SCA3 que recapitula de perto a doença humana tanto a um nível fenotípico como neuropatológico. O efeito da modulação dos níveis de expressão da proteína 4R-Tau foi avaliado ao longo da progressão da doença através da realização de um conjunto de testes comportamentais para avaliar a (dis)função motora. No geral, os nossos resultados mostraram que nas condições aqui testadas, e embora a expressão viral tenha sido detetada no final do ensaio (na semana 20) em algumas áreas do SNC, a administração de AAV-CAG-4R-Tau falhou em reverter ou melhorar a disfunção motora dos ratinhos SCA3. No entanto, e porque o equilíbrio entre as isoformas da Tau precisa de ser estritamente regulado nos neurónios, outras condições experimentais devem ser testadas em estudos futuros.

Palavras-chave DMJ/SCA3 ● modelo de ratinho CMVMJD135 ● VAA ● 4R-Tau ● SNC

ABSTRACT

Establishing the relevance of Tau isoform imbalance in the onset and progression of Machado-Joseph disease

Machado-Joseph disease (MJD), also known as Spinocerebellar Ataxia Type-3 (SCA3), is a dominantly inherited ataxia caused by an unstable cytosine-adenine-guanine (CAG) trinucleotide expansion within the coding sequence of the *ataxin-3* gene, which is ultimately translated to an abnormally long polyglutamine tract in the disease protein, named ataxin-3 (ATXN3). This late-onset neurodegenerative disorder is characterized by a highly complex clinical presentation. At the neuropathological level, neurodegeneration also affects multiple areas within the central nervous system (CNS). In the past years, our understanding of MJD/SCA3 pathological mechanism remarkably progressed, and the scientific community made some advances towards development of possible therapeutic strategies for this disabling disorder. Currently, the existing treatments or therapies for MJD/SCA3 are scarce and mainly focused on the relief of symptoms. Furthermore, these approaches have not being very efficient in slowing down or reversing the process of neurodegeneration. However, the precise mechanism(s) underlying this disease remains elusive and few readouts/biomarkers have been identified. Previous work from our team suggested that expression of mutant ATXN3 perturbs the splicing factor SRSF7 (or 9G8), leading to a deregulation of MAPT(Tau) exon 10 splicing. This study showed a decrease in the levels of 4R-Tau isoform in the brain of the CMVMJD135 mouse model (SCA3 mice) at a late symptomatic age as well as in brain samples of MJD/SCA3 patients. Based on these observations, the main aim of this work was to restore the 4R-Tau protein expression levels in the brain of our SCA3 mice and evaluate whether this modulatory approach could delay SCA3 progression. To accomplish this, we took advantage of stereotaxic injections of Adeno-Associated Viral Vectors (AAV) expressing the human 4R-Tau protein into the fourth ventricle of the brain of our SCA3 mouse model, that closely recapitulates the human disease both at the phenotypical and neuropathological levels. The effect of the modulation of 4R-Tau protein expression levels was evaluated along disease progression by performing a set of behavioural tests to assess motor (dys)function. Altogether, our results showed that, in the conditions herein tested, and although viral expression was detected at the end of the trial (at week 20) in some areas of the CNS, the administration of AAV-CAG-4R-Tau failed to reverse or ameliorate the motor dysfunction of the SCA3 mice. Nevertheless, and because the balance between Tau isoforms needs to be strictly regulated in neurons, other experimental conditions should be tested in future studies.

Key words MJD/SCA3 ● CMVMJD135 mouse model ● AAV ● 4R-Tau ● CNS

INDEX

ABBREVIATION LIST

17-DMAG - 17-dimethylaminoethylamino-17-Demethoxygeldanamycin

3R-Tau - 3 repeat Tau isoform

4R-Tau - 4 repeat Tau isoform

AAV - Adeno-associated viral vector

APP - Amyloid precursor protein

ATG - autophagy-related gene proteins

ATXN3 - Ataxin-3

Ca2+ - Calcium ion

CAG - Chicken beta actin promoter

CAG - Cytosine-Adenine-Guanine

CBD - Corticobasal degeneration

CBP - cAMP response element-binding protein-binding protein

ChAT - Choline Acetyltransferase

CHIP - C-terminus of Hsc70 interacting protein

CK2 - casein kinase 2

CMV - Cytomegalovirus

CNS - Central nervous system

CSF - Cerebrospinal fluid

CYP46A1 - Cholesterol 24-hydroxylase

DAPI - 4',6-diamidino-2-phenylindole

DNA - Deoxyribonucleic Acid

DUB - Deubiquitinating enzyme

E1 - Ubiquitin-activating enzyme

E2 - Ubiquitin-conjugating enzyme

E3 - Ubiquitin-protein ligase

EYA - Nuclear protein eyes absent protein

Fit-1S - Interleukin 1 receptor-related Fos-inducible transcript

FOXO – forkhead box O

FTDP-17 - Frontotemporal dementia with parkinsonism linked to chromosome 17

GFP – Green Fluorescent Protein

GSK 3β - glycogen synthase kinase 3β

HDAC - Histone deacetylase inhibitor

HDAC3 - Histone deacetylase 3

ICV - intracerebroventricular

IGF-1 - Insulin-like growth factor-1

IL-1ra - Interleukin-1 receptor antagonist

IL-6 - interleukin-6

IP3R1 - inositol 1,4,5-trisphosphate receptor type 1

MAPT - Microtubule-associated protein Tau

MJD – Machado Joseph Disease

MMP-2 - Matrix metalloproteinase-2

MRI – Magnetic resonance imaging

mRNA - Messenger RNA

NcoR - Nuclear receptor co-repressor

NNI - Neuronal nuclear inclusion

NPY - Neuropeptide Y

PBS - Phosphate-buffered saline

PCAF - p300/CREB-binding protein-associated factor

PNKP - polynucleotide kinase 3'-phosphatase

PolyQ - Polyglutamine

PSP - Progressive supranuclear palsy

PTM - Post-Translational Modifications

qRT-PCR - Quantitative Real-Time Polymerase Chain Reaction

REM - Rapid eye movement sleep

ROCK - Rho-kinase

S12 – serine 12

SCA - Spinocerebellar ataxias

SCA3 – Spinocerebellar ataxia type 3

SDF1α - cytokine stromal cell-derived factor 1α

SOD2 - superoxide dismutase 2

SRSF7 - Serine/arginine-rich splicing factor 7

TBP - TATA-binding protein

UPP - Ubiquitin Proteasome pathway

VCP/p97 - Valosin-containing protein

WT- Wild-type

LIST OF FIGURES

LIST OF TABLES

CHAPTER 1 -

INTRODUCTION

CHAPTER 1 – INTRODUCTION

1.1. Machado-Joseph Disease / Spinocerebellar Ataxia Type-3

Machado-Joseph disease (MJD), also designated as Spinocerebellar Ataxia Type-3 (SCA3), is a neurodegenerative disorder of the nervous system that belongs to a large group of diseases called polyglutamine diseases (PolyQ)[1]. Additionally, MJD/SCA3 is part of a large group of autosomal dominantly inherited ataxias. Considering its prevalence and, although considered a rare disease (global prevalence of 1 per 100 000 inhabitants reviewed in [2]), it is among the commonest spinocerebellar ataxias worldwide[3,4,5].

The first reports of MJD/SCA3 described families of Azorean origin and emerged with distinct designations, which demonstrates the heterogeneity of the disease. In 1972, Nakano and colleagues examined family members descending from an individual named William Machado that were reported as having autosomal dominant ataxia, thus assigning the name "Machado disease"[6]. In the same year, Woods and Schaumburg identified a family with "nigro-spino-dentatal degeneration with nuclear ophthalmoplegia" that, although presenting common clinical features to the "Machado disease", had a different pathological pattern[7]. In 1976, Rosenberg and colleagues described the "autosomal dominant striatonigral degeneration" in the Joseph family and proposed a new genetic entity due to the identification of different pathological findings when comparing to previously reported descriptions of the disease[8]. In 1977, Romanul and colleagues studied members of a family suffering from a neurological disease and identified in the literature similarities with other previously reported families with inherited autosomal dominant ataxia, which led them to propose the "Azorean disease of the nervous system" as the same disease but with distinct patterns of expression[9]. In the following year, Coutinho and Andrade reported different families of Azorean descent as having "autosomal dominant system degeneration" with a remarkable broad range of clinical and pathological manifestations[10]. This study helped to clarify the assignment of distinct entities for the same disease. In 1980, Lima and Coutinho proposed the name "Machado-Joseph disease" in an attempt to unify this disorder and proposed some clinical criteria for a more accurate diagnosis[11]. In the following years, the scientific community uncovered the broad geographic distribution of MJD/SCA3 and found that this disease is particularly common in Portugal (57.8%)[12], Thailand (46.5%)[13], Germany (42%)[14], Singapore (41%)[15], Taiwan (32%)[16], France (32%)[17], Netherlands (28%)[18], Japan (28%)[19], Venezuela (25%)[20], USA (21%)[21] and Spain (15%)[22].

1.1.1. Clinical Presentation

MJD/SCA3 is an incurable disorder characterized by a range of symptoms which manifest to a variable degree (Figure 1), mainly including progressive gait and limb ataxia, progressive external ophthalmoplegia, pyramidal and extrapyramidal signs, fasciculations of facial and lingual muscles, difficulties in the movement of the eyes, bradykinesia, dystonia, rigidity and spasticity[10,23,24]. The mean age of disease onset is estimated as 37 years and the average survival time after onset is 21 years[25].

The marked clinical heterogeneity of disease onset and presentation led to its classification into four subtypes: **Type I**, with the earliest onset, which includes pyramidal and extrapyramidal abnormalities, dystonia, rigidity and spasticity and progresses faster[24, reviewed in 3]; **Type II**, the most frequent with middle age of onset (20 to 45 years), which includes ataxia, pyramidal and extrapyramidal deficits and progressive external ophthalmoplegia[24, reviewed in 3,]; **Type III**, with later onset (40 to 60 years) and slow disease progression, being the most common type[24, reviewed in 3]; some authors described a **Type IV**, the rarest, that includes parkinsonism signs associated with the overall clinical features of the disease[24,26, reviewed in 3]. Whichever the subtype, MJD/SCA3 is usually a late-onset disorder, with symptoms emerging during adulthood.

Besides the wide range of symptoms affecting the motor function, MJD/SCA3 patients also present non-motor symptoms that can include sleep disorders, depression symptoms, fatigue, pain, cramps, olfactory and autonomic dysfunction, and cognitive deficits[reviewed in 27].

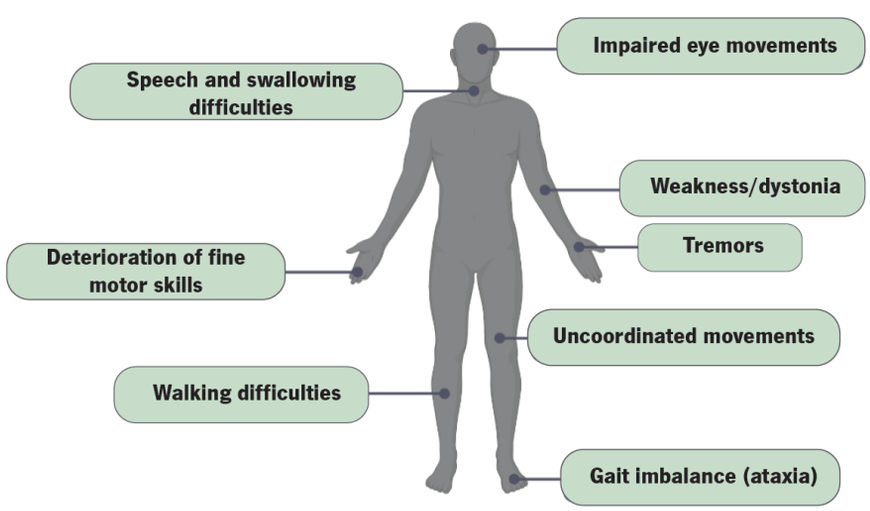

Figure 1. Schematic representation of the core clinical symptoms of MJD/SCA3. Adapted from [28].

1.1.2. Pathological findings of MJD/SCA3

Neuropathological examinations of *post-mortem* brains of MJD/SCA3 patients reveal a severe and widespread degeneration that affects specific areas of the central nervous system (CNS) (Figure 2): *(i)* The cerebellum, which plays a critical role in the control of balance and locomotion, presents pronounced atrophy with a marked degeneration of the dentate nucleus due to a severe neuronal loss with grumose degeneration in surviving neurons, and degeneration of the efferent cerebellar tracts - namely the superior cerebellar peduncle[29,30]. Although the cerebellar cortex is normally preserved, some studies have reported a loss of Purkinje cells[29,31,32]; *(ii)* The brainstem generally reveals atrophy[29,31]. A prominent neuronal loss with astrogliosis is observed in the pontine nuclei and in the red nucleus[reviewed in 33]; *(iii)* In the medulla oblongata a neuronal loss in the motor nuclei has been reported[31]; *(iv)* The basal ganglia, which encompass a group of several nuclei, have been reported to show degeneration in the internal segment of the globus pallidus, subthalamic nucleus and substantia nigra, with severe neuronal loss together with astrogliosis[29,30]; *(v)* The cranial nerves, particularly the oculomotor (III), abducens (VI), facial (VII), vestibular (VIII), and hypoglossal nucleus (XII), have shown prominent neuronal loss[31, reviewed in 33]; *(vi)* At the level of the spinal cord, a marked neuronal loss has been detected in the Clarke's columns and the anterior horns as well as severe degeneration of the spinocerebellar tracts[7,32,reviewed in 33]. Besides neurodegeneration, there was a progressive replacement by glial cells – with gliosis - that has been detected in the medulla oblongata (hypoglossal nucleus, ambiguus nucleus, dorsal vagal nucleus, medial and lateral vestibular nuclei), cerebellum (dentate nuclei), pars compacta of the substantia nigra, and spinal cord (dorsal and ventral spinocerebellar tracts)[7]. Additionally, myelin loss has been documented in the pyramidal and spinocerebellar tracts, namely in the fasciculus gracilis and anterior horn of the spinal cord[9,10].

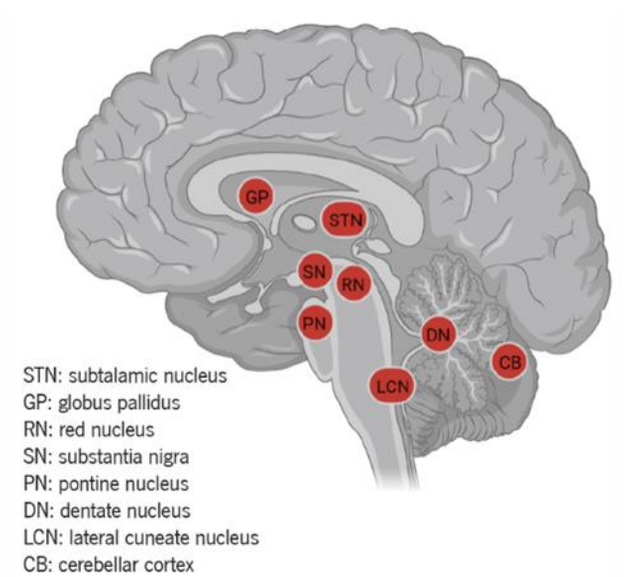

Figure 2. Main sites of neurodegeneration (depicted in red) of MJD/SCA3 human brain. Adapted from [34].

Neuroimaging studies of MJD/SCA3 patients enabled a wider understanding of the degeneration pattern of this disorder. Several studies have revealed considerable atrophy of the cerebellum (cerebellar hemispheres and cerebellar vermis), brainstem (midbrain, pontine basis, pontine tegmentum, pons, and medulla oblongata), and superior and middle cerebellar peduncles. The frontal and temporal lobes and basal ganglia (caudate, putamen and globus pallidus) were also seen to be atrophic[35–41]. Additionally, a considerable enlargement of the fourth ventricle was observed among MJD/SCA3 patients[14]. Also, the brain weight of MJD/SCA3 patients at an advanced disease stage has shown a size reduction when compared with normal individuals[42]. Important to note, however, the participants involved in the mentioned studies were of different ages and were at different stages of the disease, which might explain the different extent of atrophy in the different brain areas identified. Additionally, a positive correlation was documented between the degree of cerebellar and brainstem atrophy and the size of the CAG repeat expansion, as well as the age of the patients, that contributes to disease progression and, consequently, to the process of neurodegeneration[38,43].

MJD/SCA3 neuropathology does not affect exclusively the brainstem and cerebellum and some studies documented that several functional and neurotransmitter systems are impaired in this disease, which results in widespread neuropathology throughout the brain[reviewed in 44]. The complex pattern of degeneration became more evident with the identification of several affected CNS circuits and its associated disease-related motor symptoms: the cerebellothalamocortical loop (that may lead to ataxia, dysdiadochokinesia, dysarthria, intentional tremor, amyotrophy, fasciculations, muscles weakness, hypoflexia or areflexia, spasticity, hyperreflexia and positive Babinski sign), the basal ganglia–thalamocortical motor loop (that may cause ataxia, bradykinesia, dystonia and myoclonia), the visual system (visual attentional deficits and abnormal visual evoked potentials), the auditory system (brainstem auditory abnormalities), the somatosensory system (ataxia, falls, decreased proprioception, decreased sense of vibration, decreased temperature discrimination, abnormal somatosensory evoked potentials), the vestibular system (instable posture, falls, horizontal gaze-evoked nystagmus, impaired vestibolo-ocular reaction and optokinetic nystagmus), the oculomotor systems (diplopia, saccadic smooth pursuits, dysmetrical and slowed saccades, vertical and horizontal gaze palsy), the ingestion-related brainstem system (dysphagia, malfunctions of the preparatory phase of ingestion, dysfunctions detrimental to the lingual, pharyngeal and oesophageal phases of swallowing), the pre-cerebellar brainstem system (ataxia, dysarthria, horizontal gaze-evoked nystagmus), the midbrain dopaminergic (parkinsonian signs such as akinesia and rigidity), the cholinergic systems (REM sleep disorder), and the pontine noradrenergic system (REM sleep disorder)[reviewed in 44]. The recognition of impairments on these neuronal circuits helps us to understand the variability of the clinical symptoms that characterize MJD/SCA3.

The most remarkable pathological feature of this neurodegenerative disorder is the propensity of the expanded

disease protein to misfold and aggregate within the nucleus of neurons, leading to the formation of neuronal intranuclear inclusions, making the nucleus the primary site of pathogenesis[45–47].

1.1.3. MJD/SCA3 disease protein: Ataxin-3 (ATXN3)

The genetic basis of MJD/SCA3 disease is an unstable cytosine-adenine-guanine (CAG) trinucleotide expansion within the coding sequence of the *Ataxin-3* (*ATXN3*) gene, located at chromosome 14, which is translated to an abnormally long polyglutamine (PolyQ) tract in the disease protein, named Ataxin-3 (ATXN3)[48,49].

The CAG repeat length is highly variable, presenting a distinct repeat size between the normal population and affected patients; in healthy individuals, it ranges from 12 to 44 units whereas in MJD/SCA3 patients lies between 61 and 87 repeats[50–52]. The severity of the clinical symptoms correlates with the length of this CAG tract and negatively correlates with the age at onset of disease, with the longer repeats leading to earlier disease onset. Taking advantage of this difference in the CAG repeat size that divides healthy from non-healthy individuals, a diagnostic test for MJD/SCA3 was developed and proved to be a valuable tool for the detection of the disease at a pre-symptomatic age[51,52]. Some other particularities of MJD/SCA3 are also important to highlight; *(i)* an intergenerational instability is observed, that is, an unstable transmission of the CAG repeat expansion from the parent that carries the mutation to the offspring occurs, and is more evident in paternal transmission than in maternal transmission[53,50,54,55]; *(ii)* the existence of a genetic anticipation effect observed in some patients, that is, an earlier age of disease onset in successive generations, thought to be correlated with the instability of the CAG repeat tract in the disease gene[30,53,56]; and *(iii)* somatic mosaicism, defined by the presence of distinct CAG repeat sizes among different brain regions. In particular, the presence of a smaller CAG repeat size in the cerebellar cortex in comparison to other brain areas of the central nervous system such as the frontal cortex has been described[57–60].

In physiological conditions, ATXN3 is predominantly localized in the cytoplasm. Both normal and expanded ATXN3 are widely distributed in the brain and throughout the body, but the expression of the expanded ATXN3 in certain brain areas may influence the pattern of neurodegeneration[45,61].

Despite the efforts to understand the physiological role(s) of ATXN3, they are not fully elucidated yet, with the best known cellular role of this protein being its involvement in the ubiquitin-proteasome pathway (UPP) as a deubiquitinating enzyme (DUB)[62–65]. The UPP is a fundamental molecular mechanism for the degradation of incorrectly folded, non-necessary and/or short-lived proteins[66]. Thus, it is not surprising that dysregulation of

this pathway can compromise cellular protein homeostasis. Protein degradation by the Ubiquitin Proteasome System (UPS) is mediated by a process called ubiquitination, in which ubiquitin moieties are attached to a target substrate and further degraded by the proteasome. This sequential action requires the interaction of three classes of enzymes: (*i)* activation of the ubiquitin by an ubiquitin-activating enzyme (E1); (*ii)* action of ubiquitin-conjugating enzyme (E2) that accepts the ubiquitin from E1 enzyme; (*iii)* action of ubiquitin-protein ligase (E3) that accepts the ubiquitin molecules from E2 enzyme and catalyse their binding to lysine residues of the target substrates. Besides protein degradation, ubiquitination also regulates other important cellular events such as regulation of translation, activation of transcription factors and kinases, and DNA repair[reviewed in 67,68]. Besides, ubiquitination is a dynamic and reversible post-translational modification and is counterbalanced by deubiquitination through the action of DUBs (such as ATXN3) which are responsible for the disassembly of ubiquitin molecules from the target substrates and that are critical to maintaining cellular homeostasis[reviewed in 69,70].

1.1.3.1. ATXN3-interacting partners

The efforts made so far enabled the scientific community to unravel some protein interactors of ATXN3 and define molecular mechanisms in which this protein may be involved, and thus provide new clues about its physiological functions. A growing number of proteins have been shown to interact with ATXN3 which might support its involvement in many cellular pathways. The known molecular interactors of ATXN3 are highlighted in Table 1.

Table 1. Molecular interactors of ATXN3 and their function.

Protein	Function	Ref
HHR23A and HHR23B	Protein degradation and DNA repair	71,72
VCP/p97	AAA ATPase	73,74, reviewed in 75,76
CHIP	E3 ubiquitin ligase	77
Parkin		78
P53	Regulates apoptosis	79
BCL-xL	Mitochondrial protein related to oxidative stress	80
Chk1	DNA damage response	81
PNKP	DNA strand break repair enzyme	82
LC3C/GABARAP	Autophagy receptors	83

The human homologs of the yeast Rad23 protein (HHR23A and HHR23A), which are involved in protein degradation and DNA repair, have been identified to interact with both normal and pathological forms of ATXN3[71,72]. ATXN3 also binds to valosin-containing protein (VCP/p97) - a member of a highly conserved AAA ATPase family which participates in several cellular events that include cell cycle regulation, membrane fusion, transcriptional control and degradation of polyubiquitinated substrates in the proteasome[reviewed in 73,74]. These interactions with Rad23 and VCP/p97 point towards a role of ATXN3 in proteasomal protein degradation, with VCP/p97 being suggested to be required for the delivery of ubiquitinated substrates by Rad23 to ATXN3[63]. Moreover, the interaction between ATXN3 and VCP/p97 regulates the extraction of misfolded proteins from the endoplasmic reticulum to the cytosol for elimination through the proteasome[75,76,84].

ATXN3 also binds to the C-terminus of Hsc70 interacting protein (CHIP), which is also implicated in protein quality control[77]. ATXN3 is thought to modulate CHIP substrates' ubiquitination cycle through its DUB activity[77]. ATXN3 also exerts its DUB activity towards parkin, an E3 ligase, another evidence of its involvement in the ubiquitin signalling pathway[78]. Interaction with p53, a regulator of apoptosis, has also been shown and suggested to contribute to the stability of p53 protein and regulation of its ubiquitination levels[79]. BCL-xL, a protein that represses apoptosis, also interacts with ATXN3 suggesting that this protein plays a protective role against cellular oxidative stress[80]. ATXN3 was also shown to interact with Chk1, a protein kinase involved in DNA damage response, regulating its ubiquitination and degradation and, thus, promoting Chk1 stability and DNA repair[81].

In collaboration with others, our laboratory also found that ATXN3 interacts with polynucleotide kinase 3'-phosphatase (PNKP), a DNA repair enzyme[82]. It has also been shown that the presence of the expanded version of ATXN3 perturbs this interaction leading to inactivation of enzymatic activity of PNKP, resulting in inefficient DNA repair[82]. ATXN3 was also found to interact, *in vitro*, with the autophagy receptors LC3 and GABARAP, thus having a regulatory function in autophagy[83].

1.2. Molecular mechanism(s) underlying MJD/SCA3: lessons from ATXN3 function

Several studies have been dedicated to uncovering the cellular role(s) of ATXN3 and its involvement in disease-related mechanism(s). It has been highlighted that the interaction of pathological ATXN3 with several proteins contributes to disturbances in cellular pathways which, in turn, may be relevant for MJD/SCA3 pathogenesis (Figure 3)[85].

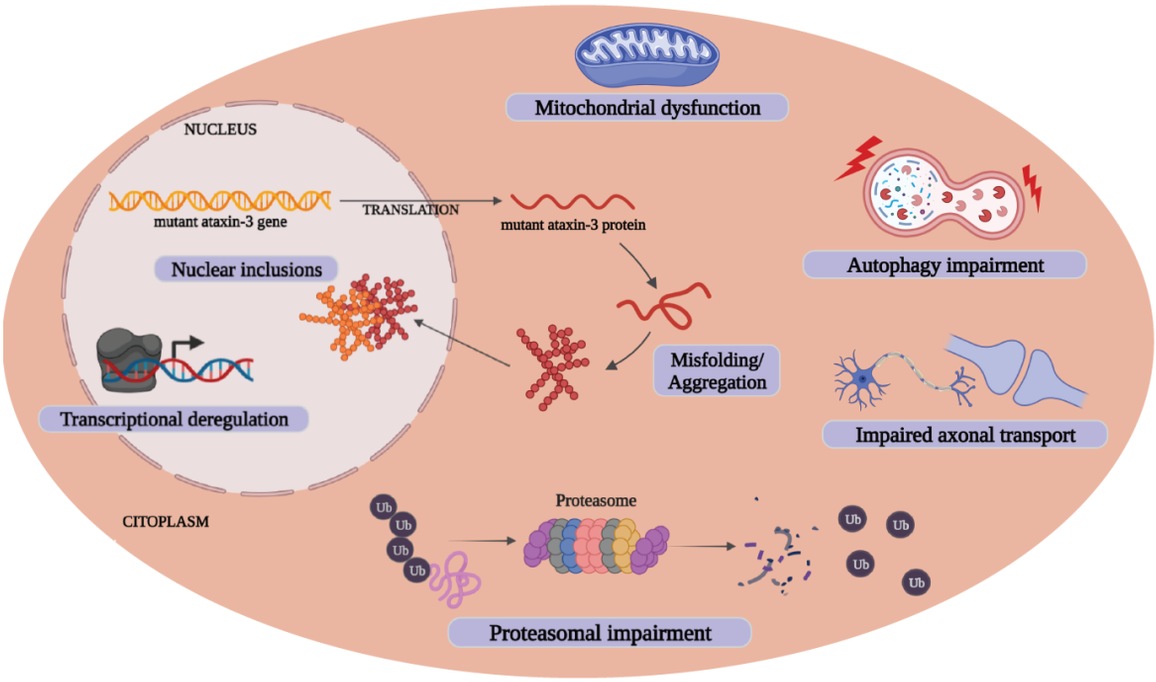

Figure 3. Schematic illustration of some of the pathogenic mechanisms involved in MJD/SCA3.

There is evidence of ATXN3 to be implicated in **transcriptional regulation** through the interaction with several transcriptional activators, repressors and transcription factors. In pathological conditions, it has been observed that several transcription factors are recruited into nuclear inclusions of the mutant ATXN3 protein, such as the TATA-binding protein (TBP), the cAMP response element-binding protein-binding protein (CBP) and the nuclear protein eyes absent protein (EYA) which may contribute to neuronal toxicity[46,86–88].

Furthermore, in vitro studies have shown that mutant ATXN3 also establishes abnormal interactions with several proteins acting as inhibitors or activators of gene transcription[89,90]. For example, it interacts with transcriptional co-activators repressing their function, such as the TAF$_{II}$130, CBP, p300, and p300/CREB-binding protein-associated factor (PCAF)[91,92]. Of note, while both normal and pathological ATXN3 forms interacts with CBP, p300 and PCAF, the mutated form binds strongly to these coactivators, repressing transcription[92]. The transcriptional activation is facilitated by the acetylation of histones whereas transcriptional repression occurs when histones changes to a hypoacetylated state[reviewed in 93]; ATXN3 has also been shown to repress transcription of *MMP-2* gene by interacting with co-transcriptional repressors, namely histone deacetylase 3 (HDAC3) and the nuclear receptor co-repressor (NCoR), which suggests that normal ATXN3 regulates transcriptional repression via histone deacetylation[94]. However, the pathological form of ATXN3 has been shown to display altered DNA and chromatin binding resulting in a gain of function via aberrant activation of *MMP-2* transcription[94] . In a different study, researchers provide evidence that mutant ATXN3 inhibits histone acetylase activity, leading to histone hypoacetylation and, consequently, downregulates gene transcription[95]. It is unclear which effect predominates in which cells and how they may contribute to MJD/SCA3 pathogenesis[95]. In addition, an

altered gene expression induced by pathological ATXN3, either in cell lines and in MJD/SCA3 *post-mortem* patients brains, was associated with an enhanced transcription of several inflammatory genes that includes the metalloproteinase encoding gene *MMP-2*, the amyloid precursor protein (APP), the interleukin 1 receptor-related Fos-inducible transcript (*Fit-1S*), the cytokine stromal cell-derived factor 1α (*SDF1α*), the interleukin-1 receptor antagonist (*IL-1ra*) and interleukin-6 (*IL-6*) genes, which may be associated with an increase in pathogenesis severity[96,97]. Both normal and expanded ATXN3 have been shown to interact with the forkhead box O (FOXO) 4 transcription factor, that is associated with the transcriptional activation of the superoxide dismutase 2 (*SOD2*) gene. However, normal ATXN3 was proposed to function as a transcriptional co-activator, increasing *SOD2* transcription, which is dependent on FOXO4, expanded ATXN3 failing to positively regulate *SOD2* expression and resulting in increased formation of reactive oxygen species and cytotoxicity[98].

Post-translational modifications of proteins have an impact on protein-protein interactions, three-dimensional protein structure, stability, activity, and subcellular localization, regulating a wide variety of cellular pathways[99]. Several post-translational modifications have been shown to play an important role in MJD/SCA3 pathogenesis through the modulation of the expanded disease protein, comprising phosphorylation, ubiquitination and SUMOylation. Consequently, the effect of these modifications is suggested to contribute to neurotoxicity[reviewed in 100]. ATXN3, either in its normal or expanded form, was revealed to be differentially phosphorylated by glycogen synthase kinase 3β (GSK 3β) in studies using cell lines. It has been shown, however, that presence of the polyglutamine expansion prevents phosphorylation leading to an increase in its aggregation and, thus contributing to regulating ATXN3 aggregation[101]. In addition, casein kinase 2 (CK2) has been shown to interact and phosphorylate both normal and expanded ATXN3 with similar efficacy, controlling the nuclear localization, aggregation formation and stability of ATXN3, in a study that was conducted in cells[102,103]. Moreover, CK2 dependent-phosphorylation enhanced the transcriptional repression regulated by normal ATXN3, with possible increased aberrant transcriptional effects upon the presence of an expanded version of ATXN3[103]. Upon pharmacologic inhibition of CK2, not only a reduction in the nuclear levels of ATXN3 were observed but also a decrease of nuclear inclusions formation as well as activation of gene transcription regulated by ATXN3[103]. Additionally, a novel phosphorylation site of ATXN3 at serine 12 (S12) in neurons was identified. At the same time, the authors also observed a loss of dendrites and synapses in cultured rat neurons in the presence of an expanded version of ATXN3[104]. Also, mutating the phosphorylation site at S12 of ATXN3, reduced ATXN3 aggregation and prevented neuronal and synaptic loss *in vivo,* using a MJD/SCA3 rat model, which points to a protective effect in MJD/SCA3 context[104]. In addition, phosphorylation at serine 55 and 236 is enhanced upon the presence of the mutant ATXN3 when compared to the normal ATXN3[105].-Although the functional effect of these alterations has not been yet investigated, it will certainly be relevant for the

understanding of MJD/SCA3 pathogenesis[105].

The cellular function of ATXN3 as a deubiquitinating enzyme was shown to be itself directly modulated through ubiquitination[106]. In fact, ubiquitination similarly activated both normal and pathological versions of ATXN3 in cells[106]. The authors also observed increased ubiquitination of the pathological ATXN3 when compared to the normal ATXN3 in the tissue of a MJD/SCA3 mouse model, suggesting that ubiquitination of the expanded version of the disease protein is contributing to MJD/SCA3 pathogenesis[106]. Lysine 117 was identified as the main site of ubiquitination in both normal and expanded versions of ATXN3, with some differences being detected in the pattern of ubiquitination between the two versions[107]. Ubiquitination at lysine 117 also improved the ability of ataxin-3 to induce aggresome formation in cells[107]. In contrast to what was observed in cells, in *vivo* studies using a Drosophila model of MJD/SCA3 have shown that ubiquitination of ATXN3 prevented eye degeneration by reducing protein aggregation, which points to a neuroprotective role of this modification on ATXN3 in a fly model of MJD/SCA3[108].

CHIP is a ubiquitin ligase that associates with expanded ATXN3 and is responsible for its increased ubiquitination thereby promoting its degradation by proteasome[109]. When overexpressed, CHIP led to the degradation of the pathological ATXN3 and reduced the formation of protein aggregates and cell death mediated by expanded polyglutamine proteins in cell culture[109].

SUMOylation consists in the attachment of a small ubiquitin-related modifier (SUMO) protein to a target substrate to regulate several cellular functions[reviewed in 110]. ATXN3 is also a target of SUMOylation[111]; *In vitro* studies have shown that when SUMOylated at lysine 166, the stability of the mutant ATXN3 is increased, suggesting that SUMOylation could potentially influence aggregation and toxicity of the disease protein and, ultimately, increase the MJD/SCA3 pathogenesis[112]. The impact of these post-translational modifications in the disease protein, ATXN3, needs further investigation *in vivo* to better understand how it affects disease progression.

Mitochondrial function is suggested to be impaired in MJD/SCA3, which may also account for its pathogenesis. *In vitro* studies have shown that the presence of the expanded ATXN3 led to a decrease in the expression levels of Bcl-2 - a protein that suppresses apoptosis - which promoted the release of cytochrome *c* from mitochondria, suggesting that the mutant ATXN3 may be responsible for an enhanced cell death via the activation of mitochondrial apoptotic pathways[113]. Moreover, mutant ATXN3 was also shown to induce neuronal death and activate mitochondrial apoptotic pathways by positively regulating the expression of pro-apoptotic proteins, such as Bax, and negatively regulate the expression of anti-apoptotic proteins, such as Bcl-xL in cultured neurons, again suggesting that the presence of mutant forms of ATXN3 may impact mitochondrial function, highlighting its relevance in the disease context[114]. Also, full-length expanded ATXN3 was

shown to increase oxidative stress by decreasing the activity of anti-oxidant enzymes, and diminishing mitochondrial DNA copy numbers and promoting mitochondrial DNA damage, resulting in mitochondrial dysfunction and induced neuronal cell death both in MJD/SCA3 cell lines, MJD/SCA3 mouse models, and also in MJD/SCA3 patients[115–117]. Conversely, oxidative stress was shown to increase the nuclear accumulation of both normal and expanded ATXN3 in cell studies, leading to a perturbation of protein homeostasis and raising the possibility that frequent oxidative stress during aging may contribute to disease pathogenesis[118]. Additionally, it has been shown that expression of a truncated version of mutant ataxin-3 disrupted the normal morphology of mitochondria, increased the reactive oxygen species and also increased neuronal cell death, further promoting the neurodegeneration process, in both neuroblastoma and MJD/SCA3 mouse model[119].

The two main quality control systems of protein degradation are *i)* the **ubiquitin-proteasome system (UPS)** – the major responsible for protein degradation (80–90%) through the attachment of a ubiquitin molecule to a substrate that mediates degradation by the proteasome, and *ii)* **autophagy** (10–20%) - a mechanism by which intracellular materials are degraded by the lysosome. Several branches of autophagy pathway were identified, being the most well-established (i) *macroautophagy* - double-membrane structures termed as autophagosomes enclose organelles followed by fusion with the lysosome, (ii) *microautophagy* - lysosomal membrane directly engulfs a portion of the cytoplasm, and (iii) *chaperone-mediated autophagy* (CMA) - substrate proteins translocate across the lysosomal membrane[reviewed in 120,121]. These two protein quality control systems seem to have a compensatory mechanism in which inhibition of one pathway requires upregulation of the other[reviewed in 122]. The misfolding and accumulation of polyglutamine-expanded proteins such as ATXN3 into aggregates, which cannot be efficiently degraded by UPS requires autophagy for their degradation[reviewed in 123].

As previously mentioned, in its physiological state, ATXN3 functions as a polyubiquitin binding protein with ubiquitin protease activity[62]. It has been proposed that UPS function may be compromised through the sequestration of proteasome components and chaperones into neuronal intranuclear inclusions formed by the mutant ATXN3 protein[47,124]. Moreover, there is some evidence of an impairment of proteasomal degradation in the disease[47]. In particular, several proteasomal subunits and chaperones have been found to localize in neuronal inclusions in the brains of MJD/SCA3 patients, suggesting that recruitment of these key cellular proteins may be relevant for the pathophysiology of MJD/SCA3[47]. Another evidence of proteasomal dysfunction is the accumulation of an aberrant form of ubiquitin, UBB^{+}, in neuronal inclusions that were found in brains of MJD/SCA3 patients and, it was also observed that UBB^{+} increased the aggregate formation of the mutant disease protein in cells, compromising cellular function and, ultimately, leading to cell death[125]. Interestingly, an overlapping phenotype it was observed between neuronal cells lacking ATXN3 and those overexpressing the expanded version of the protein, that led (in both cases) to increased proteasomal degradation

and deregulation of alpha-5 subunit of integrin, resulting in perturbations in cell adhesion and neuronal cytoskeleton[126]. This indicates that, either the absence or overexpression of ATXN3 leads to a partial loss of function of this protein, thus, assigning a role of ATXN3 in regulating proteasomal degradation through which the mutant protein may be contributing to neurodegeneration[126].

In certain cases, protein degradation is redirected to autophagy, possibly as a compensatory mechanism[reviewed in 122]. The activation of this pathway might promote the removal of intracellular protein aggregates at the initial stages of the disease, thereby preventing their accumulation[reviewed in 127]. However, as the disease progresses, aggregated proteins tend to accumulate, which is thought to contribute to increased toxicity[reviewed in 127]. It was observed that pathological ATXN3 exerts its DUB activity towards parkin, a protein with a neuroprotective function, and promotes its degradation through autophagy, and deregulation of this process was proposed to contribute to MJD/SCA3 pathogenesis[128]. Several reports have described a reduction in beclin-1 protein levels - a key initiator of autophagy that is involved in the autophagosome formation - in tissue from patients and animal models of MJD/SCA3[129–131]. Another study has shown a reduction in beclin-1 levels and the accumulation of autophagy-related gene proteins (ATG), namely ATG7, ATG12, ATG16L2 in *post-mortem* brains of MJD/SCA3 patients, thus suggesting that the autophagy flux is compromised and may account for pathogenesis[131]. Interestingly, overexpression of beclin-1 cleared expanded ATXN3 and was shown to exert a neuroprotective effect in a MJD/SCA3 mouse model, contributing to alleviating disease pathogenesis[129]. Moreover, beclin-1 was also shown to bind and to be deubiquitinated by the normal ATXN3, which protects beclin-1 from degradation mediated by proteasome, and thereby enabling autophagy to occur. Curiously, pathogenic forms of ATXN3 showed to compete with the normal ATXN3 for the binding of beclin-1, resulting in increased degradation of this protein and, consequently, decreased levels of beclin-1, which may contribute to disease as explained above[130]. Besides disease context, and because MJD/SCA3 is a late onset disease with slow progression, age is also a limiting factor in the efficiency of autophagy in the clearance of aggregated proteins and, thus, may be compromised at advanced stages of disease[reviewed in 127].

Calcium signaling plays a crucial role in regulating a wide variety of cellular processes, being particularly important for neuronal function. In neuronal cells, calcium signaling is involved in the control of synaptic activity, neurotransmission, and neuronal energy metabolism[reviewed in 132]. Disruption of calcium homeostasis impairs the ability of neurons to carry out their basic functions and may ultimately lead to cellular dysfunction and degeneration[reviewed in 132,133]. Indeed, impairments of neuronal calcium signaling have been linked to MJD/SCA3, with the pathological ATXN3 (but not the normal ATXN3) being documented to bind to and activate the inositol 1,4,5-trisphosphate receptor type 1 (IP_3R1), favouring the release of intracellular calcium, which results in destabilization in neuronal calcium signaling and, ultimately, contributes to MJD/SCA3

pathogenesis[134].

There is also evidence of an impairment in the **axonal transport** mechanism in MJD/SCA3, supported by some studies conducted in tissue sections of *post-mortem* brains of patients, showing that the presence of a pathological form of ATXN3 in axons, in particular protein aggregates, may contribute to neurodegeneration[135,136].

Despite great efforts in the discovery of the pathogenic mechanisms of MJD/SCA3, they are still largely unknown and require a deeper understanding, especially *in vivo*. The existing data support the view that the presence of a polyglutamine expansion within the disease protein, ATXN3, initiates a sequence of events that are related to transcriptional deregulation, PTM's, mitochondrial and proteasomal impairment, calcium signaling and axonal transport dysregulation, and therefore, contributing to the overall process of MJD/SCA3 neurodegeneration.

1.2.1. Mouse models of MJD/SCA3

The use of animal models is valuable for biomedical research, contributing to increasing the knowledge of the scientific community in several aspects related to human biology. Particularly, mouse models have become widely used in the study of human diseases due to the pathological and physiological similarities shared between mice and humans[137]. The validation of a mouse model encompasses three criteria, as follows: *(i) construct validity*, in which the animal model must resemble the same biological features that are known to cause the human disease (anatomical defects or genetic alterations); *(ii) face validity*, that incorporates a conceptual analogy to the behavioural symptoms of the human disease; and *(iii) predictive validity*, in which the responses to treatments must be similar between humans and the animal model[138].

In the last years, different mouse models of MJD/SCA3 have been created and they have proved to be useful to study certain aspects related to this fatal disorder. It is noteworthy that these models that are described in the literature enabled a clearer understanding of some pathological aspects or molecular mechanisms that were poorly understood until then. Others were very useful for understanding and studying the clinical symptoms associated with the disease[reviewed in 139]. Overall, MJD/SCA3 mouse models have provided valuable information and have enabled the scientific community to be redirected towards new ways to recreate the pathological conditions seen in humans as closely as possible.

In 2014, our laboratory developed a MJD/SCA3 transgenic mouse - the CMVMJD135 mouse model -, which, under the regulation of the CMV promoter (ubiquitous expression), expresses an expanded version of the

human ATXN3 cDNA (the 3 UIMs-containing a variant of ATXN3) at near-endogenous levels and manifests SCA3-like motor symptoms that appear gradually and progress overtime[140]. The symptoms observed in this model include motor incoordination, balance and gait deficits, tremors, loss of limb strength as well as decreased locomotor and exploratory activity (Figure 4). At the neuropathological level, abnormal cell morphology in the pontine nuclei and astrogliosis in the substantia nigra were detected at 24 weeks of age. At a later disease stage, brain weight decrease (42 and 43 weeks of age) was observed and a reduction in the volume of the dentate and pontine nuclei (60 weeks of age), similarly to what occurs in patients, as well as a decreased total cell number in the latter. Ataxin-3 neuronal intranuclear inclusions were detected in cells of affected brain areas, such as the pontine and deep cerebellar nuclei, but also in spared areas, namely, the anterior olfactory nuclei and ventral tenia tecta at 20 weeks of age[140]. A reduction in glucose metabolism was noted in the whole brain (at 43 weeks of age) as was a reduction in cell number and shrunken cell body of surviving neurons in the dentate nucleus (at 56 weeks of age). In addition, a reduction in calbindin staining was observed, a marker for Purkinje cells (at 56 weeks of age). The presence of microglial cells with altered morphology (increased cell body) in the dentate nucleus was also observed, as well as the presence of shrunken cell bodies in the pontine nuclei in the CMVMJD135 mice (at 56 weeks of age). Ubiquitin-positive inclusions located in neurons were present within the pontine nuclei and inferior olivary nucleus (at 56 weeks of age). Moreover, increased levels of proinflammatory cytokines, namely TNF-α, were observed in the brainstem but not in the cerebellum (at 56 weeks of age). A reduced expression of glial glutamate transporters, such as GLT-1 and GLAST was detected (at 32 and 56 weeks of age). A disruption in the endocannabinoid signaling was detected in the Purkinje cell layer as well as in the pontine nuclei (at 56 weeks of age). This model was described to live up to 80 weeks after birth[141]. Neurochemical changes were detected in the cerebellum of this model at an advanced disease stage, particularly, lower levels of N-acetylaspartate, myo-inositol and total choline, myelin basic protein and neurofilament medium, which are indicative of neuronal impairments, disruption of glutamatergic systems, myelin and neurite loss[142].

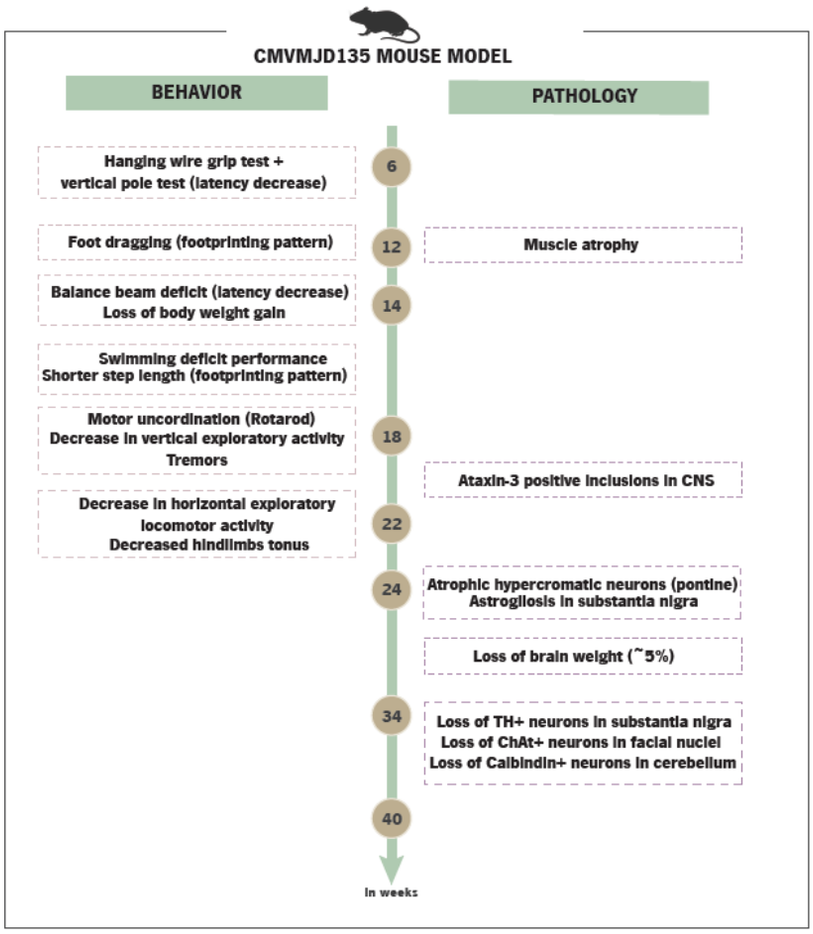

Figure 4. Schematic illustration of CMVMJD135 mice features at phenotypical and pathological levels.

Overall, this model resembles multiple key features of the human disorder, allowing the study of the pathogenic mechanism(s) underlying this disorder, making it a powerful tool for preclinical trials. In fact, this model has been used to test several compounds and therapeutic approaches, some of them with promising results, with potential for translation to the clinical context (Please see Table 2).

Oral treatment with 17-DMAG, an Hsp90 inhibitor, was tested in the CMVMJD135 mouse model. Chronic administration of this compound led to improvements in the motor coordination of this mouse and a reduction of the steady-state levels mutant Ataxin-3 levels and neuronal nuclear aggregates[140]. In contrast, chronic administration, starting one week before the onset of symptoms, of lithium chloride, an autophagy inducer, did not improve the motor impairments of CMVMJD135 mice, despite the confirmed activation of known cellular targets and autophagy biomarkers[143].

Table 2. Pre-clinical trials using the CMVMJD135 mouse model[140].

Compound	Target / Mechanism of action	Route of administration	Treatment duration	Effect		Ref.
				Phenotypic	Neuropathological	
17-DMAG	Autophagy inducer (Hsp90 inhibitor)	Intraperitoneal injections (3 times a week)	Chronic and pre-symptomatic treatment	Motor performance improvement	Reduced mutant Ataxin-3 levels and nuclear aggregates; improved cell morphology in affected brain regions	140
Lithium chloride	Autophagy inducer	Intraperitoneal injections (3 times a week)	Pre-symptomatic treatment (from 4 to 24 weeks of age)	No improvements in motor performance; reduction of tremors at a late-symptomatic age	No changes on mutant Ataxin-3 levels	143
Creatine	Cellular energy buffer	Oral administration (through food supplementation)	Pre-symptomatic treatment	Motor performance improvement	Decreased Ataxin-3-positive nuclear inclusion and astrogliosis; increased calbindin staining in the cerebellum	144

Table 2 (Continued). Pre-clinical trials using the CMVMJD135 mouse model[140].

Compound	Target / Mechanism of action	Route of administration	Treatment duration	Effect		Ref.
				Phenotypic	Neuropathological	
Citalopram	selective serotonin reuptake inhibitor	Oral administration (through drinking water)	Chronic and pre-symptomatic treatment	Motor coordination and balance, gait and body weight improvement	Suppressed the mutant Ataxin-3 aggregation; reduced astrogliosis; increased Calbindin staining in Purkinje cells; increased the number of ChAT+ cells in the substantia nigra and spinal cord	[145]
			Chronic and post-symptomatic treatment	Motor coordination and balance improvement; disease progression attenuation	No impact on ATXN3 aggregation; failed to attenuate reactive astrogliosis; partially prevented cerebellar calbindin staining	[146]
Valproic Acid	HDCA inhibitor	Intraperitoneal injections (during five consecutive days per week)	Pre-symptomatic treatment (from 5 to 30 weeks of age)	Mild and very limited amelioration of motor deficits	No changes in ATXN3 nuclear neuronal inclusions or astrogliosis	[147]
Combined lithium chloride with Temsirolimus	Autophagy inducers	Intraperitoneal injections (3 times a week)	Chronic and pre-symptomatic treatment (from 5 to 24 weeks of age)	No improvements of motor impairments	Reduction of the steady-state protein levels of mutant ATXN3 in the brainstem	[148]

Treatment with creatine, a natural compound present in the daily diet that improves energy production, was assessed as a therapeutic approach for MJD/SCA3 using the CMVMJD135 mouse model[144]. Overall, supplementation with creatine delayed disease progression and ameliorated motor impairments as well as some neuropathological features in this model such as diminished astrogliosis, preserved calbindin-positive cells in the cerebellum and reduced mutant ATXN3 aggregates in affected brain regions, which makes it a promising compound with relevance to be studied in patients[144].

One exploratory study aiming at repurposing drugs conducted in our laboratory, identified citalopram, a selective serotonin reuptake inhibitor, as a promising therapeutic candidate for MJD/SCA3[145]. The beneficial effect of citalopram was tested using the CMVMJD135 mouse model[140]. Chronic and pre-symptomatic treatment with citalopram revealed to improve motor incoordination and lack of balance of transgenic animals, as well as to suppress mutant ATXN3 aggregation and delayed disease progression[145]. To assess the therapeutic efficacy of this compound administered at a post-symptomatic stage, a new trial was conducted using the same transgenic model. The results showed an amelioration of the motor deficits, a slight attenuation of disease progression, and no effects at preventing mutant ATXN3 aggregation[146]. These outcomes revealed that citalopram treatment is still effective at alleviating some behavioural and pathological symptoms, but early treatment initiation seems to be more effective[146]. A few years later, citalopram was tested in a different mouse model, the YACMJD84.2 mice, showing to reduce mutant ATXN3 aggregation and to modulate the levels of some key proteins involved in the cellular protein homeostatic machinery, expected to increase the ability to refold and/or degrade the mutant protein[149].

Despite the existence of several mouse models of MJD/SCA3, few were used in pre-clinical trials to evaluate the therapeutic efficacy of different compounds. In general, the pre-clinical trials carried out to date can be subdivided into two main classes: *(i)* those that target the mutant ATXN3 and, *(ii)* those that act downstream the pathogenic events.

Concerning those that act on the mutant ATXN3, that is, those targeting the synthesis, folding and degradation of the mutant protein, several compounds have been tested, namely: (1) the use of autophagy inducers and (2) the use of Rho-kinase (ROCK) inhibitors.

Regarding point (1), the induction of autophagy in different MJD/SCA3 mouse models seemed to be a promising strategy to modulate ATXN3 aggregation, namely through the use of temsirolimus and cordycepin[150,151]. Temsirolimus, a rapamycin analog, was administered chronically and after the beginning of the symptoms. This compound was able to reduce cytosolic levels of mutant ATXN3, but not the nuclear protein, as well as

the number of aggregates in the motor cortex. Also, it has improved the motor performance[150]. The treatment with cordycepin, led to a decrease in the number and the size of ubiquitinated aggregates and it was also able to reduce mutant ATXN3 protein aggregates and soluble protein levels through the activation of autophagy pathway. Additionally, significant motor improvements were noted upon cordycepin treatment, namely in balance, gait, and motor coordination, suggesting a neuroprotective effect of this compound[151].

Regarding point (2), treatment with H1152, an inhibitor of Rho-kinase (ROCK), led to a significant decrease of mutant ATXN3 protein levels in several brain areas of transgenic mice, including the cerebellum, pontine nuclei and spinal cord[152]. Daily intraperitoneal injections of H1152 beginning at a pre-symptomatic age also ameliorated the motor deficits, suggesting that H1152 is a promising therapeutic agent[152].

Concerning compounds acting downstream the pathogenic events, they include (3) the use of calcium signalling stabilizers, (4) the use of transcriptional regulators, (5) the use of neuroprotective agents, (6) the use of modulators of the serotonergic systems, among others.

Regarding point (3), dantrolene, a stabilizer of intracellular Ca^{2+} signaling, is broadly used for the treatment of malignant hyperthermia and muscle spasticity in patients suffering from this syndrome reviewed in[153]. The treatment in a mouse model of SCA3 was administered orally, through food supplementation, and began after the onset of symptoms. This chronic treatment improved motor coordination and prevented neuronal cell loss in the pontine nuclei and substantia nigra in this transgenic mice of SCA3[134].

Regarding point (4), daily treatment with sodium butyrate, a histone deacetylase inhibitor, in a transgenic mouse model of SCA3 has been shown to improve the motor performance and survival rate and, also, delay the onset of neurological phenotypes. Additionally, sodium butyrate reverted histone hypoacetylation of H3 and H4 histones and transcriptional downregulation (proteins involved in glutamatergic transmission, intracellular Ca^{2+} signaling/mobilization, MAP kinase pathway or regulating neuronal survival/differentiation, GABAA/B receptor subunits and heat shock proteins) in the cerebellum, suggesting that this may be a potential therapeutic agent for MJD/SCA3[154].

Regarding point (5), treatment with resveratrol, an activator of sirtuin-1, was administered to a MJD/SCA3 transgenic mice intraperitoneally and after the development of symptoms. This compound showed a robust improvement of motor and balance impairments and it also restored mRNA levels of sirtuin-1[155]. Despite the beneficial effects of resveratrol as a neuroprotector, its use as a therapeutic agent is limited by its low bioavailability and solubility[156]. Chronic intake of caffeine, an antagonist of adenosine receptors, administered in the drinking water, attenuated motor incoordination as well as the cerebellar atrophy in a SCA3 transgenic

mouse[157]. Nevertheless, the beneficial effects of caffeine still need to be clarified, in particular, the long-term consequences of caffeine consumption especially to understand if the neuroprotection induced by caffeine remains throughout time or if it merely delays rather than abrogate disease progression[157].

Regarding point (6), to assess the beneficial effects of riluzole, an antiglutamatergic drug, a previously characterized inducible mouse model of MJD/SCA3 was used[158]. Post-symptomatic chronic administration of riluzole through the drinking water led to a reduction of the soluble mutant ATXN3 protein levels but failed to improve motor coordination. Besides, increased levels of ATXN3 aggregation and an increase of Purkinje cell damage were unexpectedly observed. This study pinpointed that caution should be taken regarding riluzole treatment as a potential therapeutic agent to be tested in MJD/SCA3 patients, given that the above results may suggest some degree of neurotoxicity in the context of this specific SCA[159].

Despite the beneficial effect of some compounds that underwent these pre-clinical trials, there is still the need of a careful evaluation of their long-term effects and possible associated adverse effects.

1.3. Therapeutic strategies for MJD/SCA3: clinical trials

Given the high complexity of MJD/SCA3 there is still no effective treatment to slow down or halt disease progression. Thus, the existing therapies mainly act on symptomatic relief consisting of pharmacological and non-pharmacological approaches attempting to promote a better quality of life for patients. Concerning the non-pharmacological treatment, physiotherapy, for example by the practice of exercise through the use of video games, was revealed to improve ataxic symptoms[160]. Furthermore, speech therapy for dysarthria and dysphagia may also have a beneficial effect[161]. Occupational therapy was also revealed to have positive effects by ameliorating the depressive symptoms of patients[162].

One of the main challenges of searching for a therapy for MJD/SCA3 is the lack of proper clinical biomarkers for the disease. Few biomarkers are known to be accurate predictors of the disease and include i) imaging - MRI volumetrics, which detects atrophy of certain brain areas such as cerebellar hemispheres, dentate nucleus, brainstem, pons, medulla oblongata, caudate nucleus, parietal, temporal and occipital lobes and also cervical part of spinal cord[163–165]; Magnetic resonance spectroscopy, which measures metabolic ratios, have detected lower levels of NAA/Cr (N-acetyl-aspartate over creatine) in cerebellar hemispheres, vermis and dentate nuclei, which is suggestive of axonal dysfunction[166,167]; and Positron Emission Tomography, which have identified a decreased glucose metabolism in the cerebellum, brainstem, thalamus and putamen[168]; ii)

neurophysiology - peripheral nerve action potentials - through the detection of reduced sural sensory nerve action potential amplitude[169]; and iii) biochemical and molecular biomarkers - increased serum neuron-specific enolase levels[170,171], greater sensitivity to insulin[172], downregulation (miR-29a) or upregulation (miR-34b) of specific microRNAs[173] and upregulation of specific heat-shock proteins such as HSPB1 (HSP27) and decreased DNAJB (HSP40) levels in fibroblasts of MJD/SCA3 patients[174]. Recently, it was identified increased levels of neurofilament light chain (NfL) in the serum of MJD/SCA3 patients, emerging as a potential candidate disease biomarker[175].

The main limitation of conducting clinical trials for MJD/SCA3 is the fact that it is a rare disease, which difficult the recruitment of sufficient patients for an adequate sample size and consequently leads to a decreased statistical power. Nevertheless, some clinical trials have been conducted in the last years (Table 3).

Table 3. Clinical trials in MJD/SCA3 patients conducted in the last years (the clinical trials presented in table 3 concerns trials that are finished and published)

Treatment	Type of Trial	Outcomes	Ref.
Sulfamethoxazole-trimethoprim	Doubled-blinded/n=22/duration=24 weeks	Improved the gait, coordination and spasticity	176,177
Fluoxetine	Open-labeled/n=13/duration=6weeks	No improvements at motor level	178
Mexiletine	Case study/n=8/duration=9weeks	Alleviated muscle cramps	179
Levodopa	Case report/n=1/duration=4years	Ameliorated dystonia and parkinsonism signs	180,181
Tandospirone	Open-labeled/n=10/duration=7weeks	Improved ataxia, depression, insomnia and leg pain	182
Lamotrigine	Open-labeled/n=6/duration=7weeks	Improved gait disturbances	183
Insulin-like growth factor-1	Open-label/n=7/duration=2years	Stabilized disease progression and improved ataxic manifestations	184
Stem cell therapy	Open-label/n=5 to 7/duration=1year	Improved slightly ataxic manifestations	185,186
Varenicline	Doubled-blinded/n=20/duration=8weeks	Improved gait, alternating movements, and stance	187
Lithium carbonate	Doubled-blinded/n=62/duration=48weeks	Ameliorated ataxic manifestations but failed to halt disease progression	188
Valproic acid	Doubled-blinded/n=36/duration=12weeks	Improved locomotor deficits	189

The use of sulfamethoxazole-trimethoprim combination improved gait, coordination and spasticity of MJD/SCA3 patients[176,177]. However, a later study failed to confirm improvement of any of those symptoms, which may compromise the beneficial use of this compound[190]. Treatment with fluoxetine, a serotonin reuptake inhibitor, failed to improve movement deficits 6 weeks after treatment[178]. The oral administration with mexiletine, an anti-arhythmic agent, greatly alleviated patients suffering from muscle cramps[179]. A case study has tested levodopa in a MJD/SCA3 patient and showed to ameliorate parkinsonism signs as well as dystonia[180,181]. The use of tandospirone citrate (5HT1A receptor agonist), a widely used drug for the treatment of anxiety and depression symptoms, remarkably improved ataxia, depression, insomnia and leg pain, which suggests that this might be a useful compound to alleviate these symptoms in MJD/SCA3 patients[182]. Lamotrigine, an anticonvulsant drug commonly used to treat epilepsy[191], exerted a beneficial effect by improving the balance of MJD/SCA3 patients assessed by one leg standing test (OLST) and tandem gait index (TGI), but failed to have a long-term effect. Moreover, treatment of lymphoblastoid cells of a MJD/SCA3 patient with the same compound showed to reduce mutant ATXN3 levels[183]. Subcutaneous treatment with insulin-like growth factor-1 (IGF-1) was revealed to improve the progression of the disease after 8 months of treatment and has been shown to stabilize disease progression in MJD/SCA3 patients[184]. Two clinical trials have tested the efficacy of human umbilical cord stem cell therapy in different spinocerebellar ataxias, including MJD/SCA3[185]. Globally, the treatment with intravenous and intrathecal human umbilical cord mononuclear cells in combination with rehabilitation training significantly improved ataxic manifestations, with great improvements in the quality of life of MJD/SCA3 patients[185]. The use of mesenchymal umbilical cord stem cell therapy by intravenous and intrathecal infusion resulted in symptomatic relief but failed to improve at long-term the symptoms of patients[186]. Treatment with varenicline, a partial agonist of $\alpha 4\beta 2$ neuronal nicotinic receptors and used for the treatment of smoking[192], improved gait, alternating movements, and stance in a small group of patients[187]. Lithium carbonate revealed to be safe and well tolerated in MJD/SCA3 patients though it failed to slow down disease progression, only showing a mild amelioration in the ataxic symptoms after a period of 48 weeks[188]. The use of valproic acid, a histone deacetylase inhibitor, revealed to be safe and improved motor incoordination of MJD/SCA3 patients with some associated adverse effects such as dizziness and loss of appetite[189].

Although the compounds that have been tested exerted some beneficial effects, they did not prove solid results to support their use, and further investigation would be required to understand their safety and effectiveness. It is attractive to think that, in a near future, a possibility could be to test a combinatory therapeutic strategy to study the effectiveness of new agents for MJD/SCA3. Concerning what is mentioned above, several molecular mechanisms are altered in the disease and not all of them are effectively targeted by only one

compound, making it imperative to seek new ways to find an effective treatment to counteract this disorder.

1.4. Targeting MAPT as a therapy for MJD/SCA3: a common ground for different neurodegenerative diseases

Over the last decades, gene therapy has been explored as a powerful therapeutic strategy for a vast array of polyglutamine diseases, including for MJD/SCA3, and has emerged as an alternative to pharmacological approaches. The clarification of some molecular mechanisms underlying MJD/SCA3 has enabled the design of novel therapeutic approaches. A growing body of evidence has demonstrated the use of gene therapy agents for MJD/SCA3 and some of them showing promising results[reviewed in 193].

In fact, gene therapy aims to correct a defective gene or reduce the levels of a harmful defective gene product through the use of sophisticated tools, such as viral vectors[194]. Currently, virus-based vectors are widely used for gene transfer, namely Adeno-Associated Viral Vectors (AAV) because they: *(i)* can transfect dividing and quiescent cells *in vivo*; *(ii)* exhibit no pathogenicity or cytotoxicity and *(iii)* have very mild immunogenicity, which makes them an attractive option for CNS gene therapy[reviewed in 195]

Several pre-clinical studies for MJD/SCA3 have explored the effects of downregulation and upregulation of specific proteins or genes using AAV vectors. One such study demonstrated that overexpression of the calpain inhibitor calpastatin, into the brain of a MJD/SCA3 mouse model, achieved through the use of an AAV vector, led to decreased neuronal dysfunction and neurodegeneration and reduced the size and number of mutant ATXN3 aggregates, suggesting a neuroprotective role of calpastatin[196]. The silencing of mutant ATXN3 was also investigated, through the delivery of AAV encoding artificial micro-RNAs directly into the cerebellum of a MJD/SCA3 mouse model; this led to a reduction of the mutant ATXN3 levels, although it failed to improve motor impairment[197]. Another study also tested the effects of silencing mutant ATXN3 expression by using AAV to deliver an artificial microRNA to the cerebellum of a MJD/SCA3 mouse model. The results showed a reduction in the intranuclear accumulation of the mutant ATXN3 protein, suggesting that this may be an interesting approach to halt the expression of ATXN3 in disease context[198]. A further study tested the intravenous administration of an AAV encoding CRAG, a molecule that facilitates the ubiquitin-proteasome pathway, to a MJD/SCA3 mouse model, in an attempt to reduce mutant ATXN3[199]. This approach successfully reduced the accumulation of mutant ATXN3 aggregates in Purkinje cells and prevented the cerebellum from progressing to severe abnormal phenotypes[199]. The finding of decreased levels of neuropeptide Y (NPY), an amino-acid peptide involved in several physiological functions (cell death inhibitor, autophagy stimulator, among others) in the cerebellum of patients and mouse models of MJD/SCA3 have led scientists to investigate whether NPY overexpression could mitigate motor deficits or neuropathology in a disease mouse model[200]. This study has

taken advantage of an AAV encoding NPY directly injected into the cerebellum of a MJD/SCA3 mouse model, and has shown that NPY overexpression rescues the motor and balance impairments of this mice, and decreases the number of mutant ATXN3 aggregates. Moreover, a significant reduction of neuroinflammation was noted, suggesting NPY as a candidate to modulate the neuropathological and motor deficits in MJD/SCA3[200]. Another example is associated with impairments of brain cholesterol metabolism in MJD/SCA3. A recent study has shown decreased levels of cholesterol 24-hydroxylase (CYP46A1), a neuronal enzyme involved in the cholesterol metabolism pathway, in affected brain areas of MJD/SCA3 patients and mouse models of the disease with potential consequences for the normal function of the cholesterol pathway[201]. Based on this, the authors conducted a pre-clinical trial with two MJD/SCA3 mouse models to evaluate the effects of overexpressing CYP46A1 through the use of an AAV in the brain; the results showed that CYP46A1 overexpression was able to mitigate mutant ATXN3 protein aggregation and to alleviate motor abnormalities, which suggests another interesting approach to slow disease progression[201].

There is evidence suggesting perturbation of alternative splicing triggered by the presence of an expanded version of ATXN3 protein in cells derived from MJD/SCA3 patients[202]. Alternative splicing is a process that enables exons, which are coding sequences, of primary transcripts (pre-mRNAs) to be arranged in different combinations giving rise to structurally and functionally distinct mRNA and protein isoforms[reviewed in 203]. This mechanism plays a key role in the regulation of neuronal development, maturation, and function[reviewed in 204]. Of note, perturbation of alternative splicing regulation is thought to contribute to neurodegeneration in several diseases, such as Spinal Muscular Atrophy, Alzheimer's disease, Amyotrophic Lateral Sclerosis and Frontotemporal Dementia, among others[reviewed in 205].

A recent finding conducted in our laboratory also supports the involvement of ATXN3 in the regulation of alternative splicing in neuronal cells through the modulation of the ubiquitination of splicing factors[206]; this study reported deregulation of the splicing process and suggested the involvement of several splicing factors, seen both in cells silenced for ATXN3 or cells overexpressing the mutant protein. Among these proteins in cells lacking ATXN3 with altered splicing, some were also found to have altered levels of polyubiquitination, namely the serine/arginine-rich splicing factor 7 (SRSF7) or 9G8, a key regulator of Tau splicing[206]. This suggests that SRSF7/9G8 may be a substrate of the DUB activity of ATXN3 and that this protein could be modulating the degradation of SRSF7 through the proteasome. Moreover, a decreased 4R/3R-Tau ratio was also found both in cells expressing the mutant protein and in affected brain areas of the CMVMJD135 mouse model[206]. This finding led us to speculate that this 4R/3R-Tau ratio imbalance may be relevant and that it would be interesting to explore the modulation of such altered protein levels as a therapeutic approach in MJD/SCA3 *in vivo*.

CHAPTER 2 -

OBJECTIVES

CHAPTER 2 – OBJECTIVES

The 4R/3R-Tau ratio imbalance, particularly, the decreased levels of 4R-Tau isoform previously found to be altered in the brain of the CMVMJD135 mouse model of SCA3 (herein designated as SCA3 mouse) and also in SCA3 patients brain samples, requires a better understanding because it was previously proposed that the 4R/3R-Tau ratio disturbance may be contributing for MJD/SCA3 pathogenesis.

Thus, we hypothesized that restoring 4R-Tau protein levels in the brain of the SCA3 mouse could improve the well-established motor dysfunction of SCA3 mice. To accomplish this, we set up a pre-clinical trial taking advantage of the use of an Adeno-associated Viral Vector (AAV) expressing the human 4R-Tau isoform directly injected into the brain and evaluate the effect of the modulation of 4R-Tau protein levels along disease progression by assessment of mice motor performance. Hence, the specific aims of this project were the following:

1. To optimize a viral-based strategy to restore 4R-Tau protein levels using a SCA3 transgenic model (CMVMJD135 mouse model).

2. To conduct a pre-clinical trial to evaluate the therapeutic effect of restoring 4R-Tau protein levels on the phenotype of the SCA3 mice by performing a battery of behavioural tests along disease progression.

3. To assess the transduction efficiency of AAV-CAG-4R-Tau viral vector in mice brain and evaluate 4R-Tau mRNA expression levels in the cerebellum and in the brainstem of SCA3 mice at 20 weeks of age.

CHAPTER 3 -

MATERIALS AND METHODS

CHAPTER 3 – MATERIALS AND METHODS

3.1. *In vivo* experiments

3.1.1. Animals

For the optimization protocols, C57BL/6J mice were used. For the experimental set, SCA3 mouse and WT littermates on a C57BL/6J background were used. Mice were housed in groups of five to six animals in filter-topped polysulfone cages 267 × 207 × 140 mm (370 cm^2 floor area) (Tecniplast, Buguggiate, Italy), with corncob bedding (Scobis Due, Mucedola SRL, Settimo Milanese, Italy) in a conventional animal facility. Environmental enrichment was added to each cage consisting of soft tissue and shredded paper. Animals (Specific Pathogen Free health status) were maintained under standard laboratory conditions with an artificial 12h light/dark cycle (lights on from 8:00 to 20:00h), with an ambient temperature of 21±1 °C and a relative humidity of 50–60 %. The food and water were provided *ad libitum*.

3.1.2. Ethics Statement

All procedures have been approved by the Animal Ethics Committee of the Life and Health Sciences Research Institute (University of Minho) and by the Portuguese regulatory entity for animal research – Direção Geral de Alimentação e Veterinária (DGAV) (DGAV020317 28-09-2016). All the experiments were conducted following European regulations (European Union Directive 2010/63/EU). Health monitoring was performed according to FELASA guidelines, where the Specified Pathogen Free health status was confirmed by sentinel mice maintained in the same animal housing room.

3.1.3. Adeno-associated viral vectors (AAVs)

A human Tau0N4R driven by a CAG promoter, AAV9-CAG-4R-Tau (catalog number: #20110228), with a titter of $1.3x10^{13}$ genome copies (GC) per milliliter (ml) and a control virus, AAV9-CAG-GFP (catalog number: #7076), with a titer of $1.0x10^{13}$ GC/ml were supplied by Vector Biolabs (Malvern, PA). Before being used, AAVs were aliquoted into 25 µl volumes and stored at –80 °C. Aliquots that were thawed for the surgical intervention were kept on ice during the experimental procedure.

3.1.4. Stereotaxic surgeries

One day prior to surgery, animals were weighed and the doses of anesthesia and analgesia were calculated

accordingly. On the surgery day, animals were deeply anesthetized with a mixture of ketamine (Imalgene, Merial, USA) and medetomidine (Dorbene, Zoetis, Spain) [75 mg/kg; 1 mg/kg, intraperitoneally (i.p.)] diluted in saline (NaCl 0.9%) solution. Additionally, it was provided to the animals an appropriate analgesic, the buprenorphine (Richter Pharma AG, Wels, Austria) [0.05 mg/kg, subcutaneously (s.c.)] diluted in NaCl 0.9%. Each animal was positioned in a stereotaxic mouse adaptor (Stoelting, USA). Injections were performed directly into the fourth ventricle [coordinates related to bregma: AP: -6.9; ML: +0.9; DV: 4-3.8] using a 30-gauge needle Hamilton syringe (Hamilton, Switzerland) with either control virus (AAV9-CAG-GFP) and human Tau0N4R virus (AAV9-CAG-4R-Tau) [injection rate = 200 nL/min]. After each injection, the needle was left in place for 2 extra minutes to avoid any backflow up the needle tract and it was slowly withdrawn. After surgery, anaesthesia was reverted with atipamezole hydrochloride (Pfizer Inc., NY, USA), [1 mg/kg; i.p.] diluted in NaCl 0.9%. Mice were monitored daily and buprenorphine (0.05 mg/kg; s.c.) was applied on the first day post-surgery if animals showed visible signs of pain, such as squinting eyes, ears back or contracted skin around the nose and mouth[reviewed in 207].

3.1.4.1. Experimental Groups

To understand the efficacy of the proposed therapeutic approach, the SCA3 mouse model and wild-type littermates were used. This transgenic line was created in our lab and expresses the human ATXN3c cDNA variant under the control of the CMV promoter. The cDNA variant of the ATXN3 gene carries a repeat tract with the sequence $(CAG)_2CAAAAGCAGCAA(CAG)_{129}$, coding for 135 glutamines[140,208]. The experimental groups used were as follows: AAV-CAG-GFP injected SCA3 and WT mice (hereafter called SCA3_GFP and WT_GFP, respectively), and AAV-CAG-4R-Tau injected SCA3 and WT mice (hereafter called SCA3_4R-Tau and WT_4R-Tau, respectively) [n=10 to 15 mice/per group. Please see *3.7. Statistical analyses and sample sizes* section for detailed information]. The mean CAG repeat size (Figure 10B) was not different among SCA3 groups [CAG mean ± SD; $(min–max)_{CAG}$]. SCA3_GFP = 141 ± 4.80; $(132\text{-}149)_{CAG}$. SCA3_4R-Tau = 142 ± 4.85; $(134\text{-}150)_{CAG}$. According to the good practices on animal experimentation, both males and females were used in the present study.

3.1.4.2. Optimization of viral conditions

In the first pilot study conducted the main goal was to determine the best conditions to achieve AAV expression, where three main features were firstly optimized: *(i)* viral concentration, *(ii)* timing for transgene expression, *(iii)* total injection volume. 3-month-old mice (n=1/condition, C57BL/6J wild-type, females) were stereotaxically injected, as previously described, with a total volume of 2 μL into the fourth ventricle on the following

proportions (Figure 5).

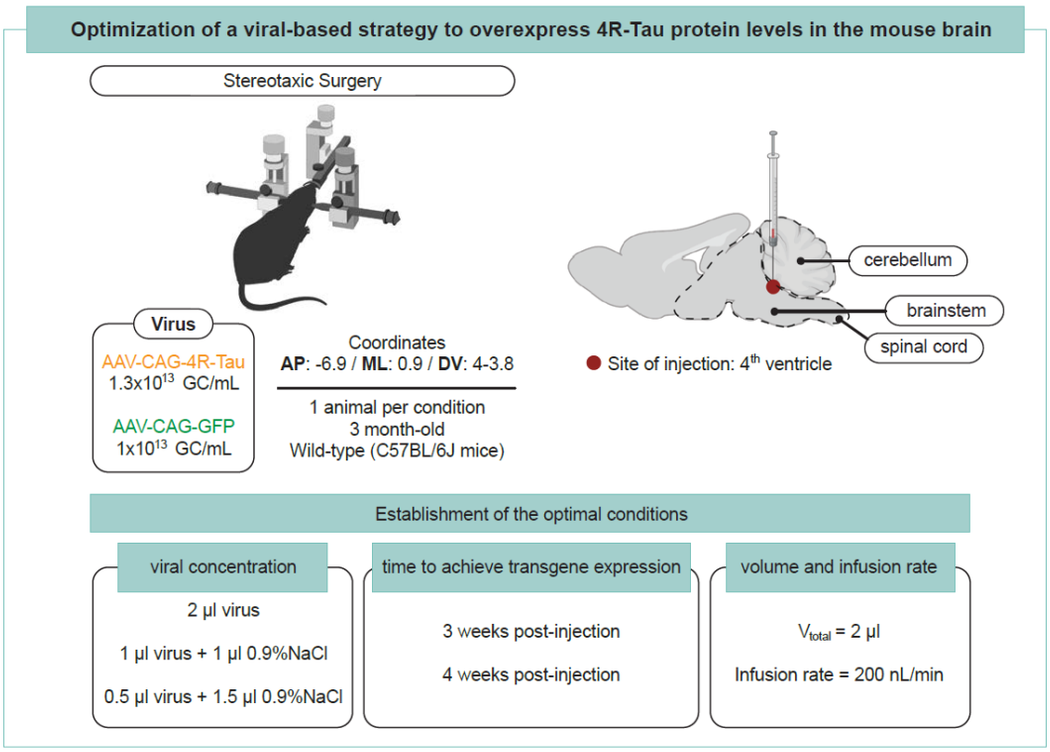

Figure 5. Conditions tested in the first pilot study.

In a second pilot study (Table 4), upon the choice of the best conditions obtained from the first one, and to better mimic the conditions to be used in the larger preclinical trial using SCA3 mice, younger animals (7 weeks of age, SCA3 and WT animals, females, n=3/condition) were used to try to answer the following questions: *i)* is the injected volume sufficient to restore 4R-Tau protein levels in mouse brain? *ii)* does the expression persist or is there a reduction in the 4R-Tau protein levels in the mouse brain, four weeks post-injection?

Table 4. Conditions tested in the second pilot study.

AAV vector	Volume (µL)	Titer	Experimental Groups	Number of animals per condition
AAV-CAG-4R-Tau	3	1.3x10^{13} GC/ml	WT_4R-Tau SCA3_4R-Tau	3 animal / condition
AAV-CAG-GFP		1.0x10^{13} GC/ml	WT_GFP SCA3_GFP	

3.2. Generation of SCA3 mice, genotyping, CAG repeat size and animal identification

SCA3 mice were generated as previously described[140]. DNA extraction, genotype determination of wild-type and transgenic mice as well as CAG repeat size analyses were performed as described previously[208]. At the moment of the weaning (around 3 weeks of age) tail biopsies (2mm) of each mouse were collected for further DNA extraction[208]. The identification of the animals was performed by using an ear clip to ear punch the animals to distinguish them. Determination of genotype was obtained by using the following primers: TR1 (5′-GAAGACACCGGGACCGATCCAG-3′) and TR2 (5′-CCAGAAGGCTGCTGTAAAAACGTGC-3′) to amplify the transgene (454 bp), and the primers mmMJD89 (5′-CAAAGTAGGCTTCTCGTCTCCT-3′) and mmMJD24 (5′-AGTGCTGAGAACACTCCAAG-3′) were used to amplify the mouse endogenous ataxin-3 gene (800 bp) as an internal control for the PCR, as described[208].

3.3. Behavioural Assessment

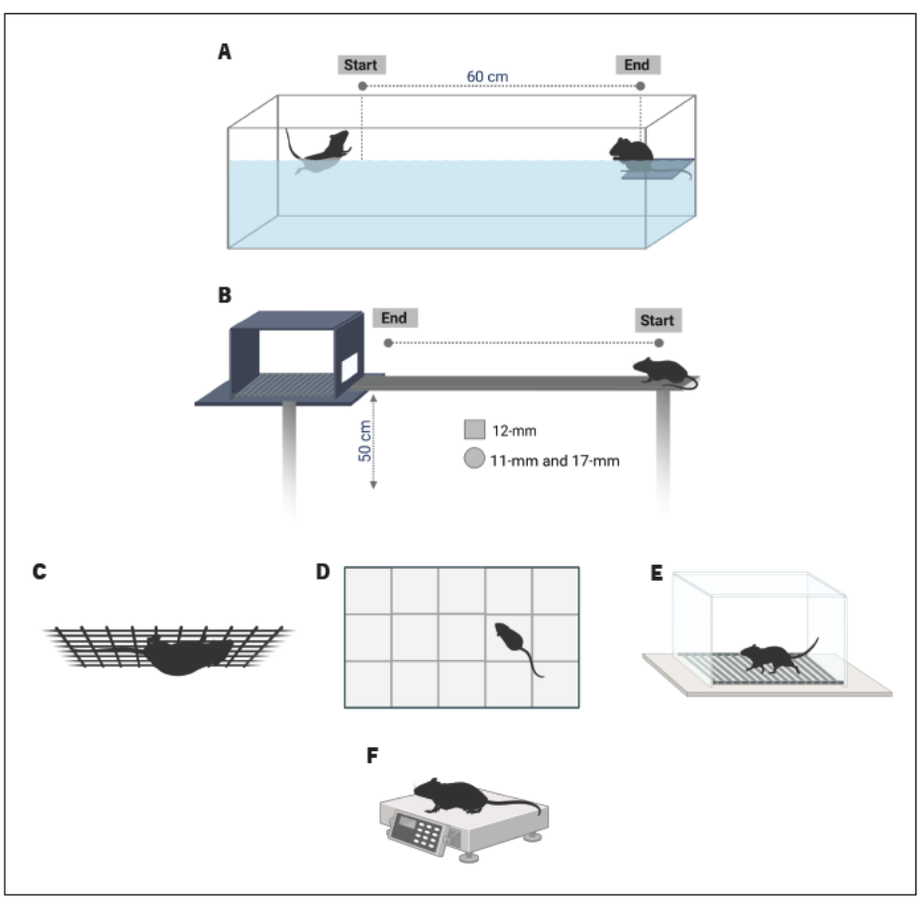

Figure 6. Schematic illustration of behavioural tests conducted in this study. They are as follows: **(A)** Motor swimming test; **(B)** Beam walk balance test; **(C)** Hanging wire grid test; **(D)** Horizontal spontaneous activity test; **(E)** Parallel Rod Floor Test; **(F)** Body weight measurement.

3.3.1. Motor swimming test

The motor swimming test (Figure 6A) was used to assess voluntary locomotion. The latency of each mouse to cross the water tank was measured from a distance of 60 cm – the tank is labelled with a blue line which marks the start point. The water temperature was monitored to 23°C using a thermostat. Mice were trained for 2 consecutive days (3 trials per animal) to traverse a water tank to a visible platform at the end. In the 3 following days (2 trials per animal), they were tested and latency to traverse the tank was registered by the experimenter.

3.3.2. Beam walk balance test

Balance and fine motor coordination (Figure 6B) were assessed by allowing each mouse to cross a graded series of narrow beams until reach an enclosed safety platform as described[209]. Each beam consists of long strips of PVC (1 m) with a 12-mm square or 17-mm and 11-mm round cross-sections that were placed horizontally at 50 cm above the bench surface, with one end mounted on a narrow support and the other end attached to an enclosed black box (20 cm square), into which the mouse could escape. Animals were trained during 3 consecutive days using a square beam (12-mm). In the fourth day, they were tested in the square beam (12-mm) and in round beams (17-mm and 11-mm). When the animal fell or turn around in the beam, it was considered a failed trial. The time the animal took to cross each beam were counted and were discounted if the animal stopped in the beam. Each animal had the opportunity to fail twice in each beam.

3.3.3. Hanging wire grid test

The latency to fall from the grid was recorded as a measure of limb strength (Figure 6C). Each mouse was placed on the top of a metallic grid and inverted 180° towards the surface of the bench. The latency to fall from the grid was registered by the experimenter. The maximum allowed time of the test was 120 seconds.

3.3.4. Horizontal spontaneous activity

Each mouse was transferred to a 15-labeled-squares arena (55 × 33 × 18 cm) and the number of squares travelled in the arena for 1 minute was counted (Figure 6D).

3.3.5. Parallel Rod Floor Test

The parallel rod floor test measures ataxia index and locomotor activity. The floor consists of a series of parallel stainless-steel rods 1.6 mm in diameter with an inter-rod spacing of 6 mm from the edge of one rod to the edge of the next rod. The rods are spaced by drilling through an acrylic frame made from 22.75 x 4-cm^2 side panels, through which they extend 2–3 cm on each side. All rods should be connected outside the acrylic frame by soldering a separate rod perpendicular to the others. The other components are a stainless-steel base plate (21 x 21.5 cm^2) with an acrylic border that is raised 1 cm above the plate, a clear acrylic box (15 x 15 x 20 cm^3) with no bottom. The base plate and the parallel rod floor are connected to electrical clips, one to each component. Mice are placed inside the acrylic box and when the paw of each animal slips through the parallel metal rods and touches the base plate the computer records as a foot slip error (Figure 6E). This test is performed during 3 consecutive days. A period of 1 hour of acclimatization in the testing room is required before mice initiate the test. On the first day, after 1 hour of acclimatization, mice are placed in the parallel rod floor apparatus for 10 minutes to allow them to get used to the apparatus and then transferred back to their home cages. The apparatus is cleaned with 10% isopropyl alcohol between animals. In the second and third days, the parallel rod floor apparatus is connected to the software (ANY-Maze) and number of errors (foot slips) and horizontal distance travelled (in cm) is recorded during a 10 minute period[210].

3.3.6. Body weight

Each mouse was weighed (Figure 6F) one day before the stereotaxic surgeries (5 weeks of age) and then at 6, 10, 12,14 16, 18 and 20 weeks of age.

3.4. Immunofluorescence Analysis

Each animal was deeply anesthetized with a mixture of medetomidine (0.3 mg/kg) and ketamine hydrochloride (150 mg/kg) and transcardially perfused with a saline solution (NaCl 0.9%) followed by 4% paraformaldehyde (PFA). The brains were removed and post-fixed with PFA 4% for 72 h at room temperature on agitation. Then, the brains were cryoprotected in 30% sucrose solution with 0.02% sodium azide at 4 °C. Next, brains were embedded in Optimal Cutting Temperature (OCT) medium using standard procedures. 20-µm thick serial brain sections were sliced with using a cryostat (Leica CM1900) in the sagittal plane and stored at -20 °C in cryopreservation solution (Phosphate buffer 0.1M, pH 7.2, 500 mL; Sucrose, 300 g; Ethylene glycol, 300 mL; 0.02% sodium azide; H_20 for a total volume of 1L) until further processing. Briefly, free-floating sections were subjected to antigen retrieval with citrate buffer, membrane permeabilization with PBS-Triton X-100 0.5%, blocking solution (Ultra V Block, Thermo Scientific), and then incubated with anti-human tau

(HT7, MN1000, Invitrogen, 1:500). Detection was performed using a fluorophore-conjugated anti-mouse IgG 594 (A11039, Invitrogen, 1:1000). 4′,6-diamidio-2-phenylindole (DAPI, 1:1000, Life Technologies, USA) was used to stain the nucleus of cells. The sections were mounted in glass slides using mounting media (Perma-Fluor™ Aqueous Mounting Medium, Thermo Scientific) and were visualized by fluorescence microscopy. Images were acquired using IX81 microscope attached to a XM10 Olympus camera using a 20x magnification. A negative control (no addition of the primary antibody) was used in each experiment.

3.5. RNA Extraction and cDNA synthesis

Total RNA was extracted from cerebellar and brainstem mice tissue using Trizol (Invitrogen, USA). Briefly, tissue containing 1 mL of Trizol was dissociated by mechanical digestion using a 20G needle and 1mL syringe. Then, chloroform was added to each sample to allow phase-separation into distinct layers of the different nuclei acids and protein, upon centrifugation (9000 rpm for 15 min). Then, the upper clear and aqueous phase containing the RNA was carefully transferred to a new sample tube with 100% isopropanol, and the tubes were gently inverted to allow the precipitation of the RNA. After centrifugation (8000 rpm for 15 min), the supernatant was discarded and 1mL of 70% ethanol was added to each sample. After centrifugation (5000 rpm for 5 minutes), the ethanol was discarded and RNAse free water was added to elute RNA pellet and incubated at 65 °C for 10 minutes. Samples were stored at -80 °C until further analysis.

First-strand complementary DNA (cDNA) was synthesized using the iScript™ cDNA Synthesis Kit (Biorad), according to the manufacturer's instructions. For RNA quantification, the Spectrophotometer NanoDrop™ (ThermoFisher Scientific) was used. RNA quality/integrity was verified by the A260/A280 ratio. The volume of nuclease-free water and RNA used for each sample was calculated based on RNA quantification to obtain 0.7 μg of cDNA. Then, 4 μl of 5x iScript Reaction Mix and 1 μl of iScript Reverse Transcriptase (RTase) was added to each reaction tube, followed by the corresponding volume of RNA and nuclease-free water. PCR cycling conditions were as follows: priming at 25°C for 5 minutes, reverse transcription at 46°C for 20 minutes and RT inactivation at 95°C for 1 minute. The synthesized cDNA was stored at -20°C until further use.

3.6. qRT-PCR: Quantitative Real-time Polymerase Chain Reaction

To understand if the 3R- and 4R-Tau protein isoforms are altered in the SCA3 mice at 20 weeks of age (by comparing WT_GFP vs SCA3_GFP experimental groups, n=3 to 4 samples/group, N=2 technical replicates) the mRNA expression levels of both Tau isoforms were measured by qRT-PCR in the cerebellum and brainstem (Please see Table S2-Supplementary Data). Gene expression quantification was performed in a CFX

96TM real-time system instrument (Bio-Rad Laboratories), using SOLIScript® RT-PCR reagent kit (SOLIS BIODYNE) according to the instructions of the manufacturer and using equal amounts of cDNA from each sample. The primers sequence used to evaluate mouse 3R- and 4R-Tau isoforms expression are highlighted in Table 5.

Table 5. Sequence of primers used.

Primer name	Forward (5'-3')	Reverse (5'-3')
Mouse_4R-Tau	TGTCAGGTCGAAGATTGGCTC	CTTATTAATTATCTGCACCTTGCCAC
Mouse_3R-Tau	GTCAGGTCGAAGATTGGCTCTACT	GCTTGTAGACTATTTGCACCTTGC

The beta-2-microglobulin (*B2M*) gene was used as a housekeeping gene. The relative gene expression was determined using the 2-ΔΔCt relative quantification method[211] and it is represented as fold change normalized to the mean of the relative expression of the control group (WT_GFP).

3.7. Statistical analyses and sample sizes

G*Power 3.1.9.4 software was used to calculate the sample size based on a power of 0.95 and a significance level of 0.05 (a priori analysis).

Regarding continuous variables, the assumption of normality was assessed by qualitative analysis of Q-Q plots and frequency distributions (z-score of skewness and kurtosis), as well as by the Kolmogorov-Smirnov and Shapiro-Wilk tests. The assumption of homogeneity of variances was tested by Levene's test for all variables.

For repeated measurements analysis, sphericity was tested using Mauchly's test, and assumed for all tested variables. Values that deviated more than 1.5 interquartile ranges from the mean were considered outliers and excluded from further analyses. For the comparison of means between 2 groups, the two-tailed unpaired Student's t-test or the Mann-Whitney U test was used (when data were normally or non-normally distributed, respectively). All mean comparisons with more than 2 groups were carried out using a one-way ANOVA followed by Tukey's HSD or Dunnett T3's post-hoc test (when data passed on the assumption of homogeneity of variances or when the populations variances were not equal, respectively).

For non-normally distributed data a Kruskal-Wallis test was performed. Regarding the comparison of means with one between and one within-subjects factor, a mixed design ANOVA model was used, followed by Tukey's

HSD post-hoc test for between-subjects variables. For the comparison of medians of discrete variables across time-points, a Friedman's ANOVA was carried out, with pairwise comparisons through the Kruskal-Wallis statistic. Effect size measurements are reported for all analyses (Cohen's d for t-tests and $\eta 2p$ for ANOVAs). GraphPad Prism 8 was used to create graphs. All statistical tests were performed using SPSS 26.0 (SPSS Inc., Chicago, IL) and are reported in Table S1 and Table S2 (Supplementary Data).

CHAPTER 4 -

RESULTS

CHAPTER 4 – RESULTS

AAV-CAG-4R-Tau viral transduction in the brain of C57BL/6J

To assess viral transduction efficacy, we have first conducted a pilot study using a AAV9-CAG-4R-Tau to induce viral-mediated expression of human 4R-Tau protein in the mouse brain, through an intracerebroventricular injection (i.c.v.), into the fourth ventricle because it was previously shown a reduction in the expression levels of 4R-Tau in the brainstem of SCA3 mice, at a late symptomatic age[206]. This choice is related to the fact that the fourth ventricle is close to the regions of interest, which are disease-relevant areas, namely, the cerebellum, the brainstem and the spinal cord. To evaluate the best conditions, namely: *(i)* viral concentration, *(ii)* time to achieve transgene expression and *(iii)* volume and infusion rate, to overexpress human 4R-Tau protein in the mouse brain (wild-type C57BL/6J, 3 months-old, 1 animal per condition), we tested several combinations of these parameters (Table S3-Supplementary Data). Additionally, we used an AAV9-CAG-GFP as a control for the biodistribution of the viral vector.

To confirm the viral transduction and distribution of AAV-CAG-4R-Tau in mice brain, we analysed qualitatively the 4R-Tau protein using a specific antibody for human Tau (HT7). This was assessed 3- and 4-weeks post-injection of the highest viral concentration tested ($1.3x10^{13}$ GC/ml), by immunofluorescence (IF). We detected strong viral transduction near the site of injection at both time-points, namely in the cerebellum and in the brainstem (Figure 7). We have also observed that a 4-weeks incubation period leads to higher human 4R-Tau expression when compared to a 3-weeks incubation time (Figure 7). A negative control (without the addition of primary antibody (HT7)) was used to confirm the specificity of the secondary antibody. A positive control (a transgenic mouse line that expresses mutant human Tau) to confirm that the IF was optimized was also included (Figure S1-Supplementary Data).

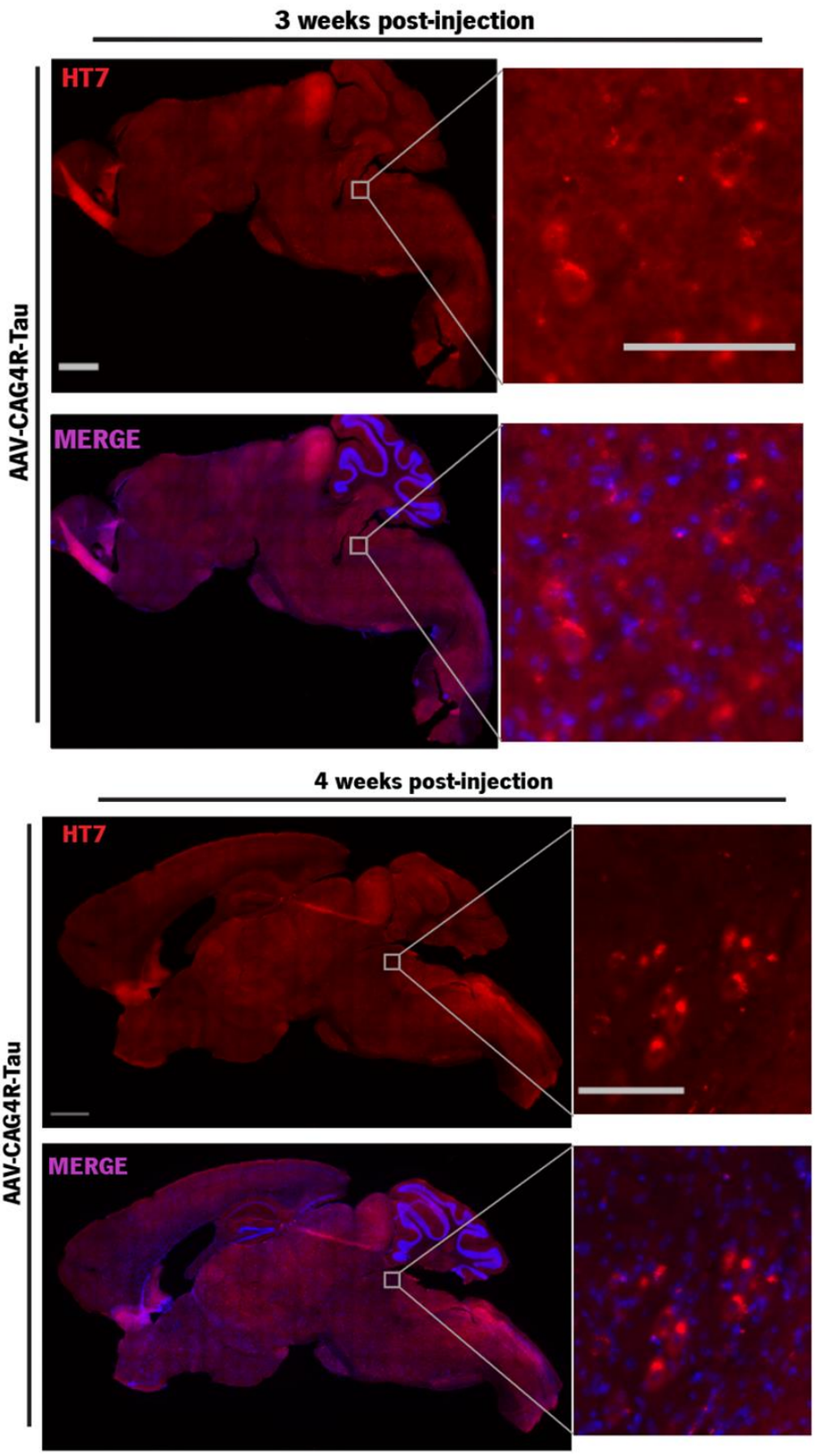

Figure 7. AAV-CAG-4R-Tau viral transduction at 3-weeks and 4-weeks post-injection in the brain of C57BL/6J. Representative images of whole mouse brain sections (20µm-thickness) showing the gradient of viral transduction in wild-type mice (3-month-old, n=1/time-point) at the highest viral concentration tested ($1.3x10^{13}$ GC/ml) using the HT7 antibody (red) which detects the presence of human 4R-Tau. The right panel shows an inset of each mosaic picture. DAPI was used to stain the nucleus of the cells (blue). MERGE represents a superimposed image of HT7 detection and DAPI. 20x magnification. Scale bars of whole mouse brain sections represent 1000 µm. Scale bars of insets of each mosaic picture represent 100 µm. 20x magnification.

We decided to investigate specific areas, which are known to be affected in the disease. Considering that the highest viral transduction was observed 4-weeks post-injection, we further characterized the viral efficacy and expression at this time-point by IF. We observed that AAV-CAG-4R-tau i.c.v administration, successfully transduced some areas around the site of injection (Figure 8). Although some variability was observed between brain regions, the viral expression seemed higher in the pons when qualitatively compared to the other regions of interest, such as, the cerebellum (in the deep cerebellar nuclei), the medulla oblongata, and the cervical portion of the spinal cord, which were transduced to a lesser extent (Figure 8).

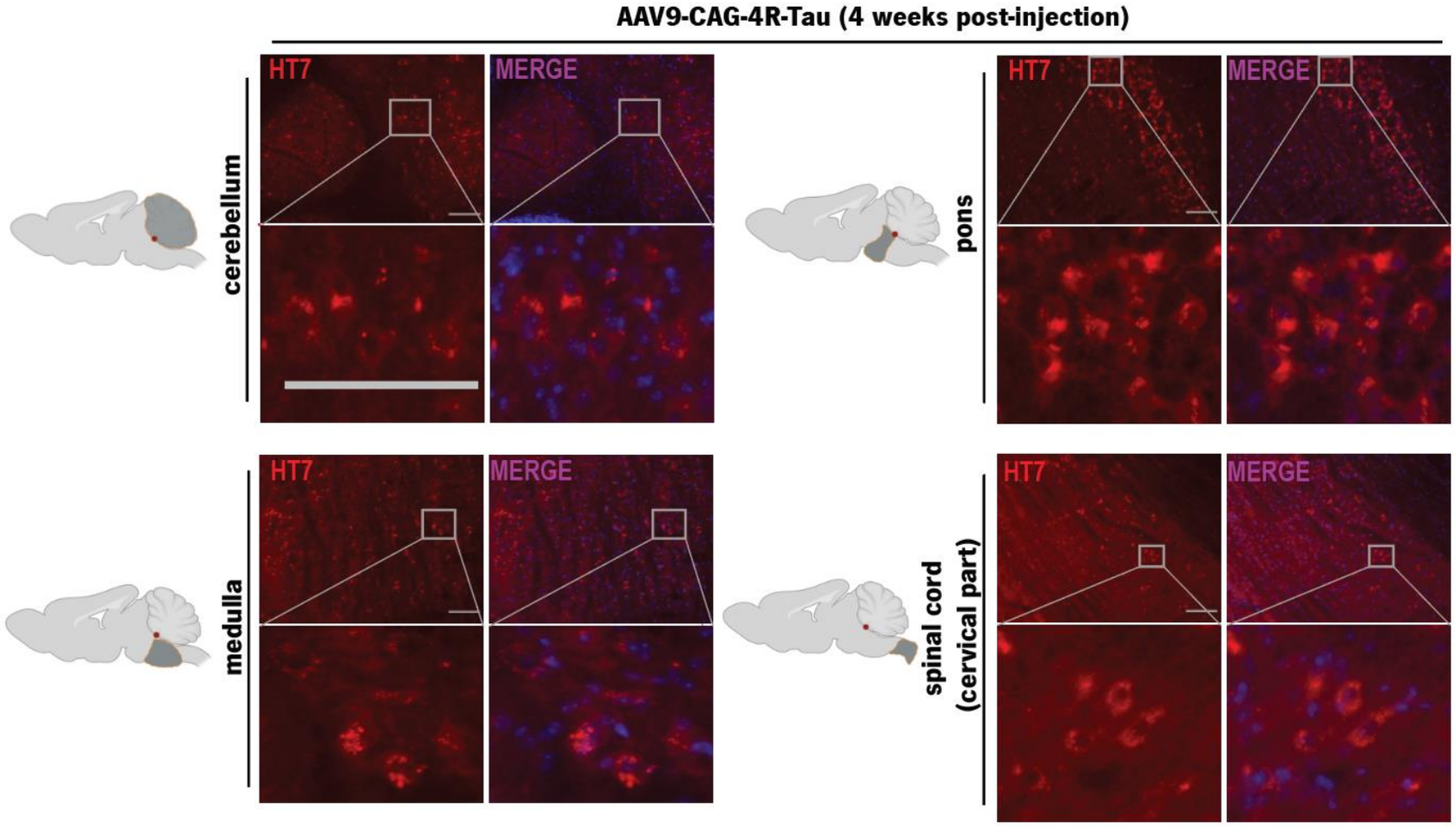

Figure 8. AAV-CAG-4R-Tau stereotaxic injections successfully transduced disease-relevant areas of the CNS. Representative images of the expression of human 4R-Tau in mouse brain sagittal sections (20-µm thickness) 4-weeks post-injection. A representative illustration of the mouse brain area is observed on the left of each panel. The HT7 antibody was used to detect the presence of human Tau (red). DAPI was used to stain the nucleus of the cells (blue). MERGE represents a superimposed image of HT7 and DAPI. n=1/time-point. 20x magnification. Scale bars represent 100 µm.

An additional group, controlling for the infusion setting itself was generated; for this, the control viral vector, AAV-CAG-GFP was injected into mice brain. We observed GFP expression at 3- and 4-weeks post-injection with the highest viral concentration tested ($1.0x10^{13}$ GC/ml) (Figure 9). When compared to AAV-CAG-4R-Tau, we observed that the pattern of GFP expression varies slightly in terms of regions transduced, a widespread expression being detected predominantly in the cerebellum.

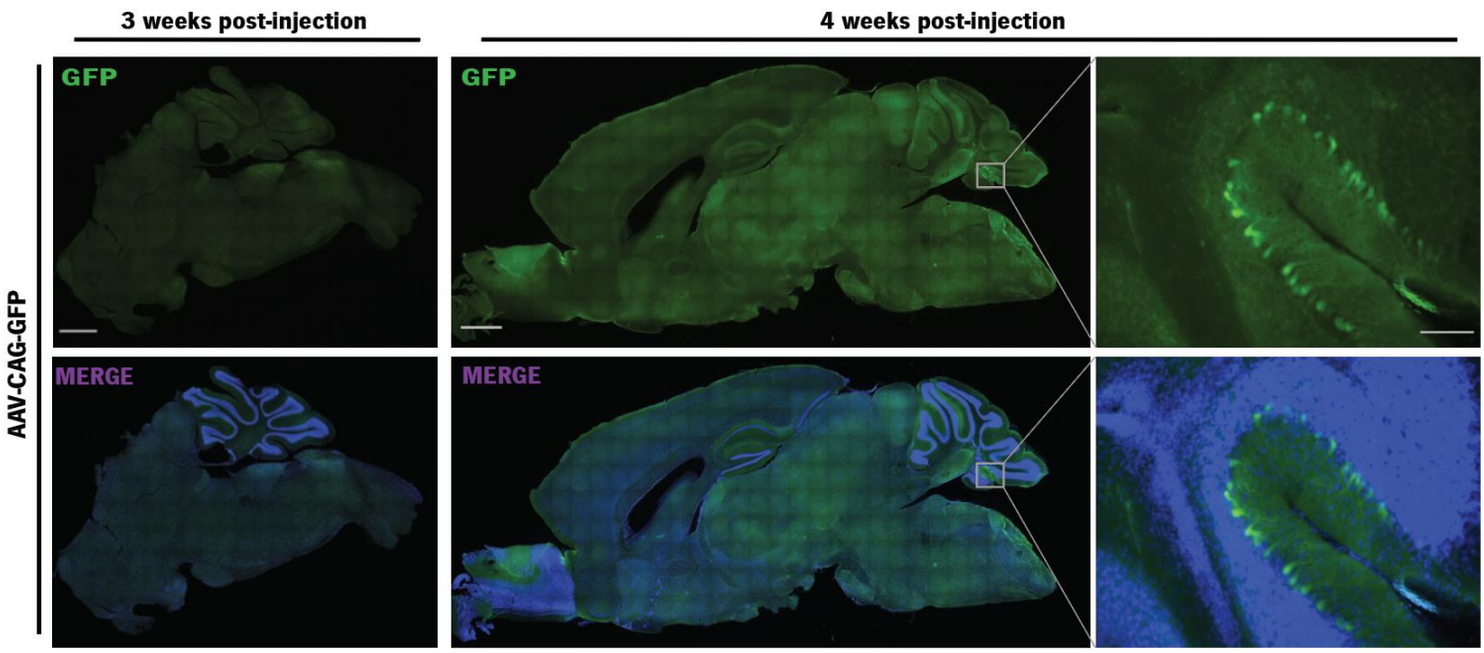

Figure 9. AAV-CAG-GFP stereotaxic injections, showed viral transduction by the observation of GFP signal in wild-type mice at 3 weeks and 4 weeks post-injection. Representative images of GFP fluorescence at both time-points analysed in mice brain sagittal sections (20-µm thickness, n=1/time-point). At right, is an inset of mouse cerebellar region at 4 weeks post-injection. 20x magnification. Scale bars of whole mouse brain sections represent 1000 µm. Scale bars of insets of each mosaic picture represent 100 µm. 20x magnification.

Based on these observations, we consider that we have successfully optimized the conditions for viral transduction and distribution of 4R-Tau protein into the mouse brain, higher at 4-weeks post-injection in the areas of interest as compared to 3-weeks post-injection: *(i)* viral concentration (AAV-CAG-4R-Tau: $1.3x10^{13}$ GC/ml; AAV-CAG-GFP: $1.0x10^{13}$ GC/ml), *(ii)* time to achieve viral transduction (from 3-weeks post-injection) and *(iii)* total injection volume (2 µL). However, it remains to be investigated whether this viral transduction remains robust over time which will be something that we will address in the following experiments.

AAV-CAG-4R-Tau administration into SCA3 mice brain

We have previously shown a decrease in mRNA and protein expression levels of 4R-Tau in the brainstem of SCA3 mice at a late symptomatic age and, importantly, in the pons of *post-mortem* SCA3 patients[206]. These results led us to ask whether modulating 4R-Tau protein levels using a viral-based approach could improve the well-SCA3-related motor dysfunction[140]. We decided to use the CMVMJD135 mouse model (SCA3 mice) developed in our lab because it closely resembles the human disease and because it has been extensively characterized by us and others[140,141]. To test this hypothesis, and after confirming the efficacy of viral transduction (Figure 8 and 9), we stereotaxically administered the AAV-CAG-4R-Tau or AAV-CAG-GFP viral vectors into the fourth ventricle (coordinates: AP: -6.9; ML: +0.9; DV: 4-3.8) of SCA3 and WT-littermates' animals at 5 weeks of age. All groups were assessed for motor function from one week after surgery, until 20 weeks of age as shown in the experimental design (Figure 10).

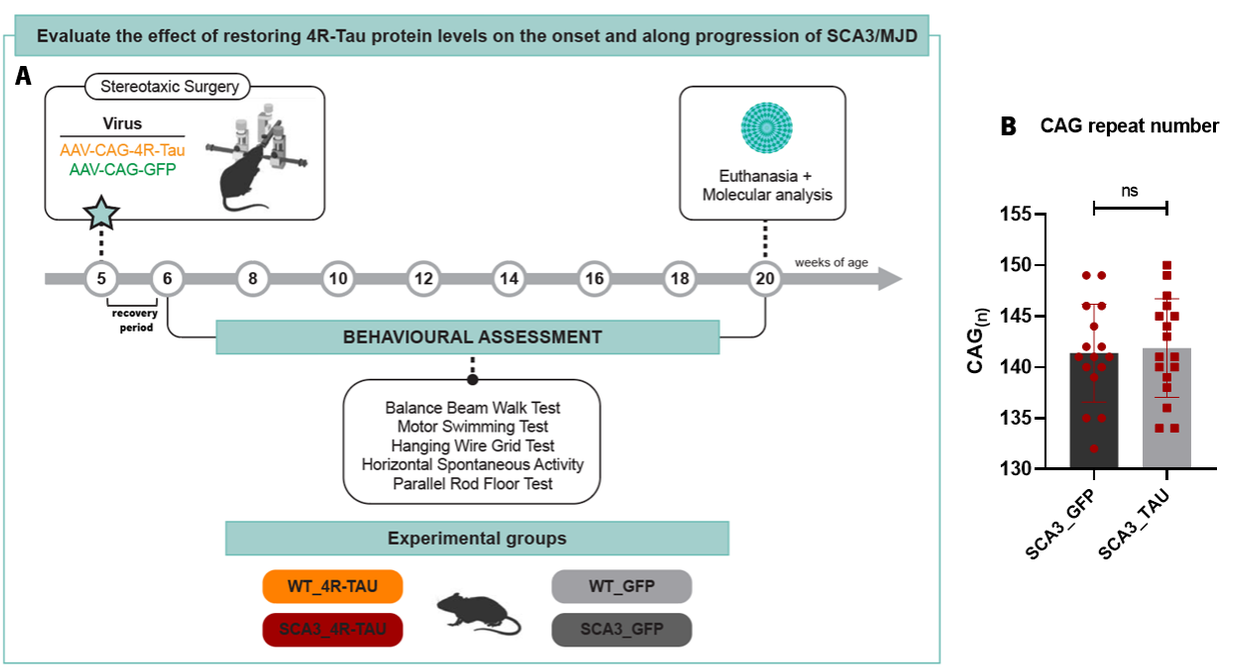

Figure 10. Experimental design. (A) Animals were stereotaxically injected with AAV-CAG-4R-Tau and AAV-CAG-GFP at 5 weeks of age and behavioural assessment was performed from 6 until 20 weeks of age (n= 10 to 15 mice/group). At 20 weeks of age, animals were humanely euthanized and divided accordingly to their final purpose. **(B)** CAG(n) stands for the number of expanded CAG repeats. No significant differences (n.s.) were observed in the mean CAG repeat size (mean±SD) between control (SCA3_GFP, 141±4.80) and treated (SCA3_4R-Tau, 142±4.85) groups (n=16 to 17 mice/group).

Because it is known from previous studies that the onset of the symptoms in our SCA3 mouse model usually occurs at 6 weeks of age with loss of muscular strength[140], we performed the stereotaxic surgeries as early as

possible, to account for viral transduction time (that we showed to occur at 3-weeks post-injection), in an attempt to start the therapy as soon as possible to benefit from the higher therapeutic efficacy window. Thus, we performed the stereotaxic injections, at 5 weeks of age, either with human 4R-Tau or with GFP using the viral conditions previously established, through an i.c.v. injection. To ensure greater homogeneity between the experimental groups, the length of CAG repeat was evaluated, and no differences in the size of the CAG repeat were observed between the SCA3 groups (Figure 10B).

AAV-CAG-4R-Tau administration into SCA3 mice brain did not improve their swimming performance

To evaluate the effect of human 4R-Tau administration in SCA3 mice brain on the disease phenotype, we performed the motor swimming test to assess motor coordination. Intriguingly, we only detected the presence of this phenotype at 20 weeks of age, in which SCA3_GFP animals showed increased latency to traverse the water tank when compared to WT_GFP mice (p_{20w}=0.002) (Figure 11, Table S1–Supplementary Data). This is surprising because differences in the swimming performance between SCA3 and WT mice are usually detected at 16 weeks of age[140]. This lack of difference could be due to the worst performance seen in both treated and non-treated WT mice at initial time-points, from 6 to 10 weeks of age, where they are performing similarly to SCA3 animals. This may arise from the surgery procedure, as the WT and SCA3 performance was not assessed previously in these conditions. Although we did not observe statistically significant differences between genotypes throughout time (p=0.212), we observed that WT_GFP mice require less time to reach the platform when compared to SCA3_GFP mice, especially from 14 weeks of age on, where a clear separation of the curves is observed (Figure 11).

We have also observed that motor deficits appear earlier in SCA3_4R-Tau mice when compared to WT_GFP mice from 18 weeks of age on, suggesting a worse performance of the SCA3_4R-Tau relative to WT_GFP controls (p_{18w}=0.023; p_{20w}=0.042). Additionally, the swimming performance of both WT_4R-Tau and SCA3_4R-Tau mice significantly differed from 14 weeks of age on, as expected (p_{14w}=0.010; p_{16w}=0.023; p_{18w}=0.003; p_{20w}=0.015). No differences in the swimming performance were observed between SCA3_GFP and SCA3_4R-Tau experimental groups throughout time (p=0.996). This suggests that 4R-Tau administration to SCA3 mice failed to improve the swimming performance when compared to the SCA3_GFP mice brain, in all time-points analysed. Importantly, the WT groups performed similarly, suggesting that the virus did not have gross adverse effects.

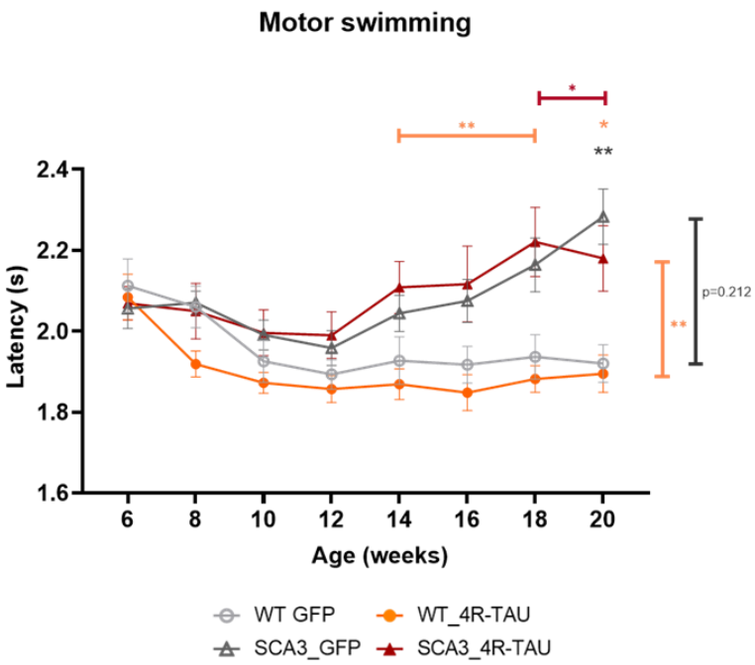

Figure 11. AAV-CAG-4R-Tau administration into SCA3 mice brain did not improve their swimming performance. Motor coordination was assessed by motor swimming test by measuring the latency of each mouse to reach a safe platform during three consecutive days. Statistically significant differences that were detected between the experimental groups (n=10 to 14 mice/group) are represented with distinct colours: *** WT_GFP vs SCA3_GFP comparison** / *** WT_GFP vs SCA3_4R-Tau comparison** / *** WT_4R-Tau vs SCA3_4R-Tau comparison**. One-way ANOVA using Tukey Post-Hoc analysis and Repeated measures ANOVA: Group: $F_{(3, 47)} = 4.733$, $p = 0.006$, $\eta^2_p = 0.232$. Data expressed as group mean ± SEM (* p<0.05, ** p<0.01).

SCA3 mice balance deficits were not improved by AAV-GAG-4R-Tau viral transduction

The balance beam test was used to assess fine motor coordination, in which animals needed to maintain their balance while traversing a set of narrow beams with increased difficulty until reaching a safe dark box. Balance deficits were detected in SCA3_GFP mice in all tested beams from 10 weeks onwards, where SCA3 mice took longer to complete the task when compared to WT_GFP animals (Figure 12A, 12B, 12C). On the opposite, the administration of AAV-CAG-4R-Tau into SCA3 mice brain did not improve and, in some cases, particularly in the 12-mm square (Figure 12A) and 17-mm round beams (Figure 12B), it anticipated the motor phenotype, as it is observed by comparing SCA3_4R-Tau mice with WT_GFP mice ($p_{12\text{-mm}}$=0.001; $p_{17\text{-mm}}$=0.005). Although no statistical differences were observed between the SCA3 experimental groups throughout time (12-mm square: p=0.095; 17-mm round: p=0.737; 11-mm round: p=0.925), SCA3-4R-Tau mice performed worse in all the beams analysed, also suggesting that 4R-Tau administration may be detrimental to SCA3 animals, namely to their balance. This was not a genotype-specific observation, as the WT_4R-Tau mice are also statistically different from the WT_GFP group, a worse performance in the balance being clearly detected

(12-mm square: p=0.002; 17-mm round: p=0.001; 11-mm round: p=0.025); this further suggests a possible toxic effect of 4R-Tau expression on this behavioural feature.

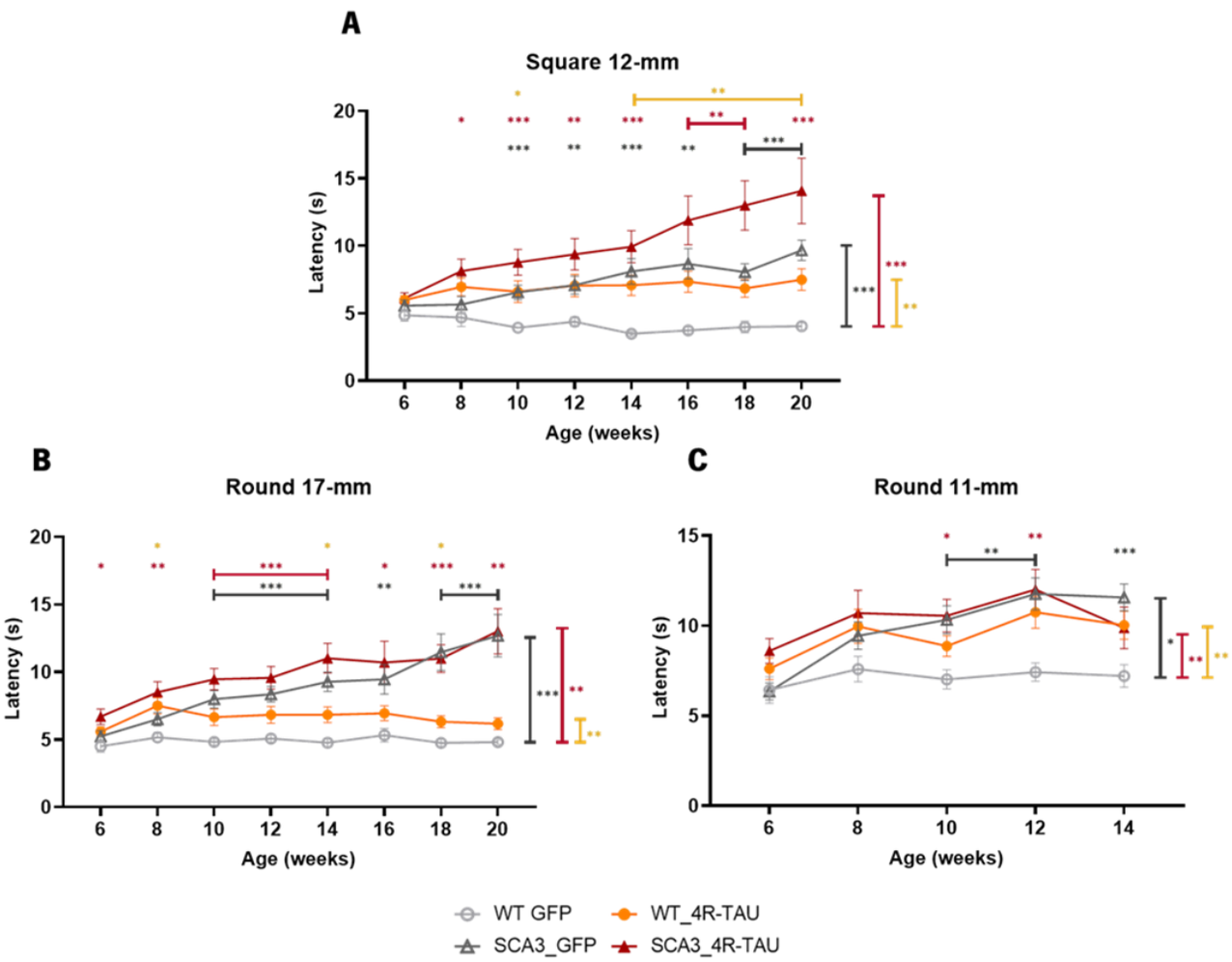

Figure 12. AAV-CAG-4R-Tau administration did not improve SCA3 mice balance deficits. The balance beam walk test was used to evaluate fine motor coordination and balance using a **(A)** 12-mm square beam and two round beams to increase task difficulty with **(B)** 17-mm and **(C)** 11-mm of diameter. The latency to cross each beam was measured. Statistically significant differences that were detected between the experimental groups (n=8 to 14 mice/group) are represented with distinct colours: *** WT_GFP vs SCA3_GFP comparison** / *** WT_GFP vs SCA3_4R-Tau comparison** / *** WT_4R-Tau vs SCA3_4R-Tau comparison** / *** WT_4R-Tau vs WT_GFP comparison**. One-way ANOVA using Tukey Post-Hoc analysis and Repeated measures ANOVA. (A) Group: $F_{(3, 43)} = 8.910$, $p < 0.001$, $\eta^2_p = 0.383$; (B) Group: $F_{(3, 37)} = 10.399$, $p < 0.001$, $\eta^2_p = 0.457$; (C) Group: $F_{(3, 39)} = 4.455$, $p = 0.009$, $\eta^2_p = 0.255$. Data expressed as group mean ± SEM (* p<0.05, ** p<0.01, *** p<0.001).

SCA3_4R-Tau animals showed no amelioration in the ataxia phenotype

The parallel rod floor test was used as a measure of ataxia in mice[210] (ataxia ratio is given by the number of footslips per cm travelled x 100) at three distinct time-points. We started this evaluation at 10 weeks of age (as a baseline) because it was previously shown differences in genotype as early as 12 weeks of age on[212]. As depicted in figure 13, we only detected the presence of the ataxic phenotype at 18 weeks of age, where SCA3_GFP mice committed more footslips than WT_GFP mice, leading to a higher ataxia ratio (given by the number of footslips per cm travelled x 100) when normalized for the distance travelled in a fixed period of time ($p=0.007$). No statistically significant differences were found between SCA3 mice experimental groups ($p_{10w}=0.68$; $p_{14w,20w}=1.00$), suggesting no therapeutic effect of AAV-CAG-4R-Tau administration.

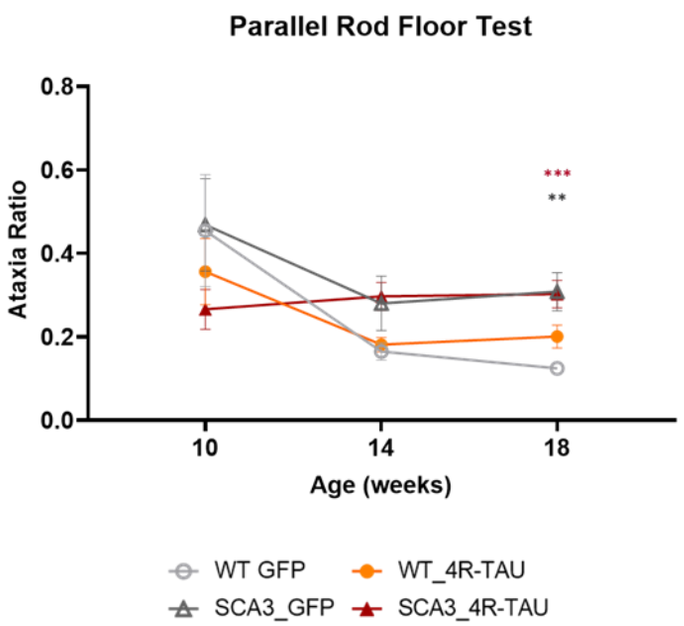

Figure 13. AAV-CAG-4R-Tau administration did not improve ataxia of SCA3 mice. Parallel rod floor test was used as a measure of ataxia at three distinct time-points. Ataxia ratio refers to the number of footslips per cm travelled x 100. Statistically significant differences that were detected between the experimental groups (n=11 to 15 mice/group) are represented with distinct colours: *** WT_GFP vs SCA3_GFP comparison** / *** WT_GFP vs SCA3_4R-Tau comparison**. One-way ANOVA using Tukey Post-Hoc analysis and Repeated measures ANOVA. Group: $F_{(3,48)} = 0.611$, $p = 0.611$, $\eta^2_p = 0.037$. Data expressed as group mean ± SEM (** p<0.01, *** p<0.001).

AAV-CAG-4R-Tau administration did not prevent the lack of body weight gain in SCA3 mice

To understand if the administration of AAV-CAG-4R-Tau and AAV-CAG-GFP viral vectors into mice brain could negatively impact the well-being and/or affect the body weight on this SCA3 model, we weighed the animals every 2 weeks. We analysed body weight separating animals by sex because males usually present higher body weight than females.

As previously described, we observed that SCA3_GFP mice showed a lesser body weight gain than WT_GFP mice throughout time ($p_{females}$=0.008 ;p_{males}=0.040) (Figure 14A and B), which is indicative of disease phenotype[140,141]. SCA3_GFP female mice stopped gaining weight from 10 weeks of age on (Figure 14A), whereas in the case of SCA3_GFP male mice this was only detected from 12 weeks of age on (Figure 14B). On the opposite, both WT groups continued to gain weight until the end of the trial (Figure 14A and B). The lack of gain weight of SCA3 mice goes in line with what is described in the literature for this model[140,141], but the AAV-CAG-4R-Tau administration had no effect on this parameter. Importantly, the viral administration in WT animals showed no toxic effect ($p_{females}$=0.721; p_{males}=0.982), suggesting that 4R-Tau administration might have detrimental effects on the balance of the animals, but not in their well-being assessed by weight measurement.

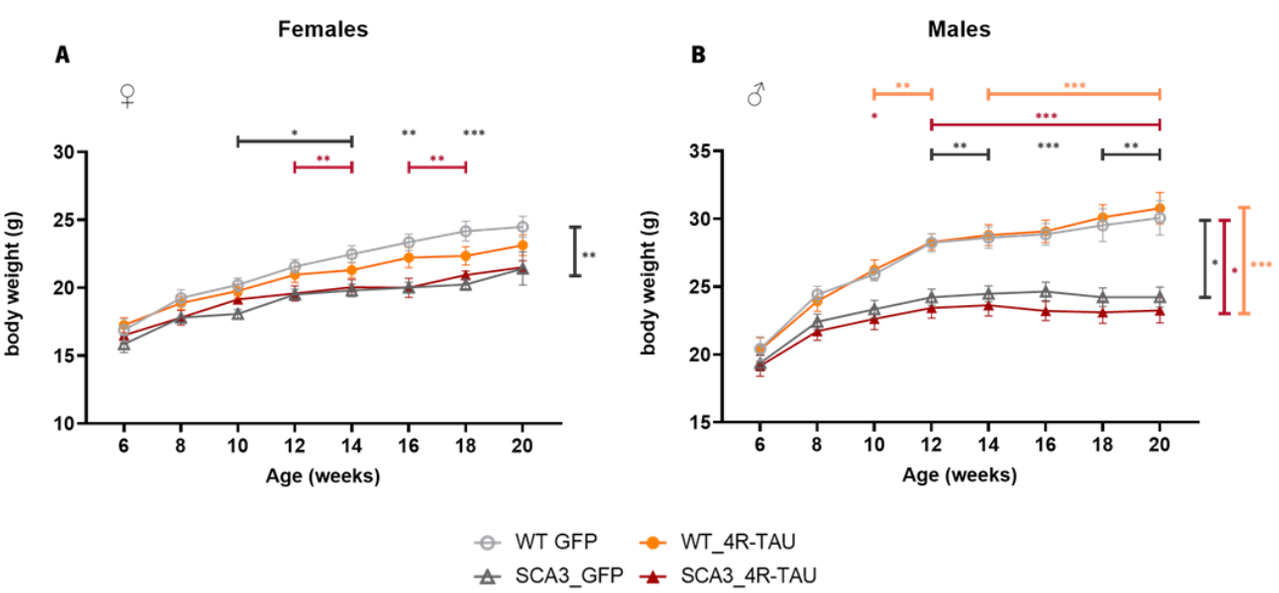

Figure 14. AAV-CAG-4R-Tau administration into mice brain did not improve the lack of body weight gain of SCA3 mice. The body weight of each animal was measured every 2 weeks, from 6 to 20 weeks of age, for **(A)** females and for **(B)** males. Statistically significant differences that were detected between the experimental groups are represented with distinct colours: *** WT_GFP vs SCA3_GFP comparison** / *** WT_GFP vs SCA3_4R-Tau comparison** / *** WT_4R-Tau vs SCA3_4R-Tau comparison**. One-way ANOVA using Tukey Post-Hoc analysis and Repeated measures ANOVA. Females: Group: $F_{(3,20)}$ = 5.128, p = 0.009 , η^2_p = 0.435 (n=5 to 7 mice/group). Males: Group: $F_{(3,23)}$ = 9.458, p < 0.001 , η^2_p = 0.552 (n=4 to 8 mice/group). Data expressed as group mean ± SEM (* p<0.05, ** p<0.01, *** p<0.001).

AAV-CAG-4R-Tau administration into SCA3 mice brain did not alter muscular strength or exploratory deficits

We assessed muscular strength using the hanging wire grid test. We detected that both SCA3_GFP and SCA3_4R-Tau mice showed a decreased latency to fall from the grid at all time-points analysed (Figure 15A), which significantly worsens with age when compared to WT_GFP or WT_4R-TAU mice, as previously described for this model[140,141]. We also observed a tendency for WT_4R-Tau mice to have less strength when compared to WT_GFP, although not statistically significant, which might indicate that 4R-Tau protein levels above the normal threshold in WT brain could impair muscular strength (Figure 15A). No therapeutic effect was observed by the administration of AAV-CAG-4R-Tau.

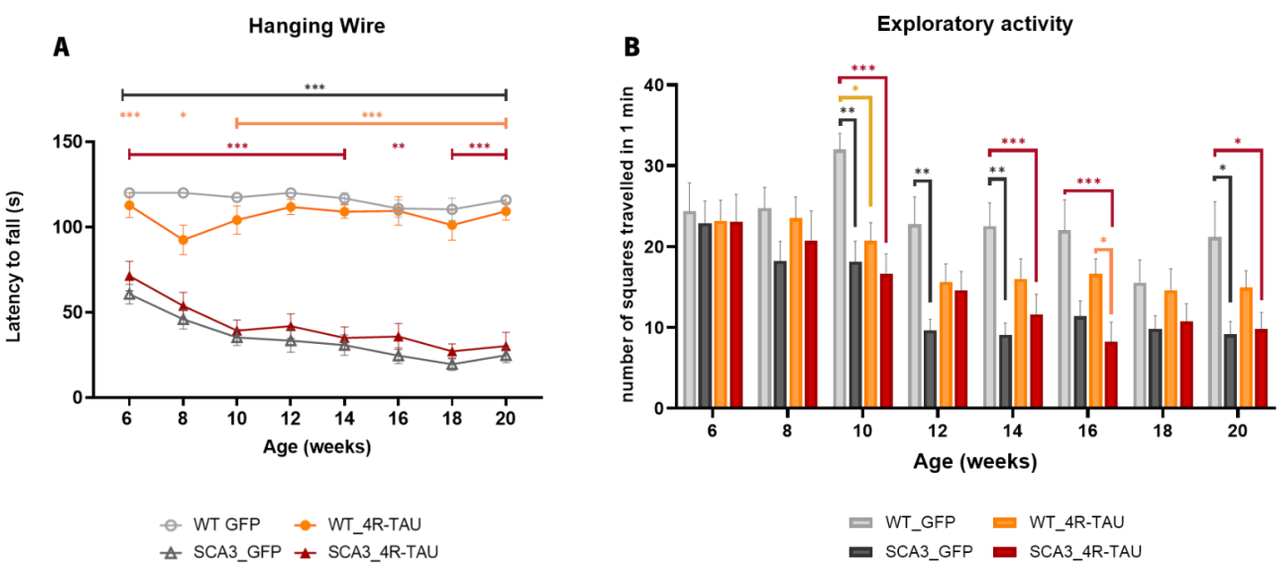

Figure 15. AAV-CAG-4R-Tau administration into SCA3 mice brain did not alter muscular strength deficits or exploratory activity. (A) Mice were placed in a grid that was inverted 180° and muscular strength was evaluated in the four-limbs (n= 11 to 14 mice/group) **(B)** Horizontal spontaneous activity was measured by counting the number of squares each mouse travelled in an open-arena for 1 min (n= 11 to 15 mice/group). Kruskal-Wallis test was used for both tests. Statistically significant differences that were detected between the experimental groups are represented with distinct colours: *** WT_GFP vs SCA3_GFP comparison** / *** WT_GFP vs SCA3_4R-Tau comparison** / *** WT_4R-Tau vs SCA3_4R-Tau comparison** / *** WT_4R-Tau vs WT_GFP comparison**. Data expressed as group mean ± SEM (* p<0.05, ** p<0.01, *** p<0.001).

Finally, we quantitatively assessed horizontal spontaneous activity (Figure 15B) and observed that both SCA3 experimental groups presented a decreased exploratory activity throughout age when compared to both WT animals. Moreover, SCA3_GFP animals presented decreased exploratory activity when compared to WT_GFP animals (p_{10w}=0.003; p_{12w}=0.006; p_{14w}=0.002; p_{20w}=0.019). In agreement with the previous results herein

obtained, we did not observe any beneficial effect of human 4R-Tau administration regarding exploratory activity on SCA3 mice ($p_{6w\text{-}8w\text{-}10w\text{-}14w\text{-}16w\text{-}20w}$=1.000; p_{12w}=0.653). Altogether, these results suggest that administration of AAV-CAG-4R-Tau in SCA3 mice brain was not able to improve the behavioural deficits of the SCA3 mice tested, at least using the experimental design here proposed.

Wide and strong AAV-CAG-4R-Tau viral transduction was found in mice brain 9-weeks post-injection

To evaluate if human 4R-Tau expression remained stable throughout time in the brain of mice that underwent behavioural assessment, we euthanized some animals (n=2 mice/group) at a mid-time point (at 14 weeks of age, *i.e.*, 9-weeks post-injection). By performing an IF technique as previously described (results section: *AAV-CAG-4R-Tau viral transduction in the brain of C57BL/6J*), we also confirmed the presence of viral transduction using both viral vectors (4R-Tau and the control GFP) in the mouse brain with 14 weeks of age (Figure 16A and B, negative control: Figure S2-Supplementary Data).

We detected the presence of 4R-Tau expression (sagittal sections, 20-µm thickness, n=2 mice/group) of both WT and SCA3 mice in several disease-relevant brain areas, namely in the cerebellum, the pons, the medulla oblongata and in the cervical portion of the spinal cord (Figure 16A). We also noticed that the pattern of distribution of the human 4R-Tau varies in these areas, as assessed qualitatively. In fact, we noticed a robust human 4R-Tau protein expression in the cerebellum, for both WT and SCA3 mice (Figure 16A), which is not surprising because it is the closest area near the site of injection (fourth ventricle). When observing in more detail other brain areas proximal to the injection site, we observed a lower transduction coverage when compared to the cerebellum that was widely transduced by the virus (Figure 16A).

Nevertheless, we could conclude that both WT and SCA3 mice, either injected with AAV-CAG-4R-Tau (Figure 16A) or AAV-CAG-GFP (Figure 16B), showed viral transduction 9-weeks post-injection in the same brain areas of the CNS despite presenting slight variations in the pattern of expression and distribution between individual animals.

This finding gives us more confidence that any change observed in the behavioural phenotype, at least until the animals reached 14 weeks of age, may be related to the presence of the human 4R-Tau protein expression in mice brain.

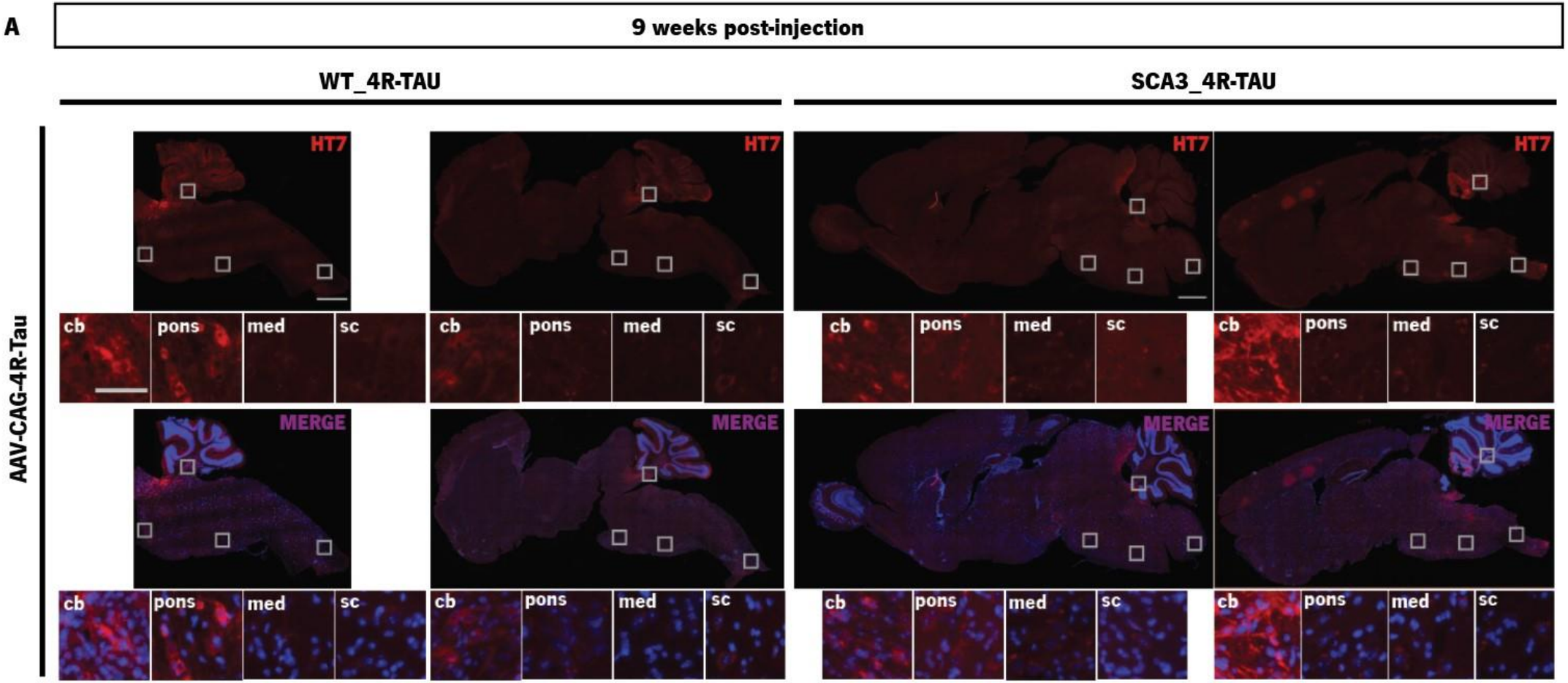
A
9 weeks post-injection
WT_4R-TAU
SCA3_4R-TAU
AAV-CAG-4R-Tau
HT7
MERGE
cb
pons
med
sc

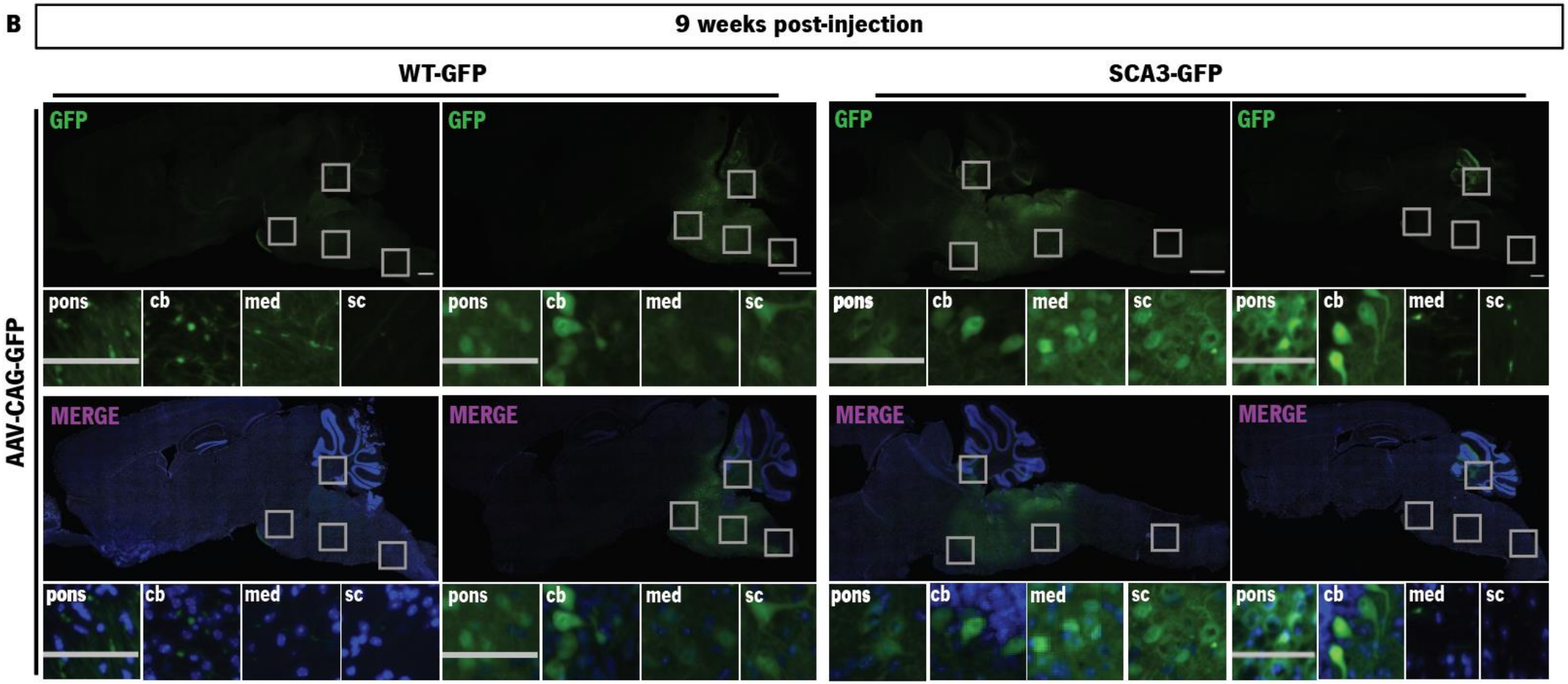
B
9 weeks post-injection
WT-GFP
SCA3-GFP
AAV-CAG-GFP
GFP
MERGE
pons
cb
med
sc

Figure 16. Viral transduction and transgene expression coverage 9-weeks post-injection. (A) Representative images of mice brain sagittal sections (20-µm thickness) of both wild-type and transgenic mice injected with AAV-CAG-4R-Tau, 9 weeks post-injection, injected with a total volume of 3 µL, showing the human 4R-Tau expression in several brain areas, including cerebellum (cb), pons, medulla oblongata (med) and spinal cord (sc). The HT7 antibody detects the presence of human Tau (red). Cell nuclei were counterstained with DAPI (blue). **(B)** Representative images of mice brain sagittal sections (20-µm thickness) of both wild-type and transgenic mice injected with AAV-CAG-GFP, 9-weeks post-injection, showing GFP expression in several brain areas, including cerebellum (cb), pons, medulla oblongata (med) and spinal cord (sc). Cell nuclei were counterstained with DAPI (blue). 20x magnification. Scale bars of whole mouse brain sections represent 1000 µm. Scale bars of insets of each mosaic picture represent 100 µm. 20x magnification.

AAV-CAG-4R-Tau administration into mice brain still shows transduction 15 weeks post-injection

At the end of the trial, at 20 weeks of age (*i.e.* 15 weeks post-surgery), it was important to confirm if the human 4R-Tau expression driven by AAV-CAG-4R-Tau was still present in the mouse brains. To answer this, we used a set of animals (n=4 to 5 mice/group) that underwent the behavioural assessment to evaluate if the DNA transduced through the virus was still being expressed in the mouse brain and, if so, if the pattern of expression and distribution was similar to that observed at 9-weeks post-injection.

Indeed, immunofluorescence analysis revealed that human 4R-Tau expression driven by AAV-CAG-4R-Tau was still present in the mice brain 15-weeks post-injection (Figure 17A). Appropriate controls were used for this experiment (Figure S4-Supplementary Data). Concerning the pattern of both human 4R-Tau expression driven by AAV-CAG-4R-Tau (Figure 17A, Figure S3-Supplementary Data) and GFP expression driven by AAV-CAG-GFP (Figure 17B, Figure S3-Supplementary Data), we also observed that expression was limited to areas surrounding the injection site, namely the cerebellum (cb), the pons, the medulla oblongata (med) and the cervical portion of the spinal cord (sc). When comparing WT and SCA3 mice subjected to both AAV-CAG-4R-Tau and AAV-CAG-GFP administration, the pattern of viral distribution was somehow heterogeneous between brain regions and, thus, the degree of fluorescence intensity varied substantially in the different areas analysed, as assessed qualitatively (Figure 17A and B, Figure S3-Supplementary Data). For the majority of the brain sections analysed, we detected a higher viral expression around the cerebellar area when compared to the above-mentioned regions (Figure 17A and B, Figure S3-Supplementary Data).

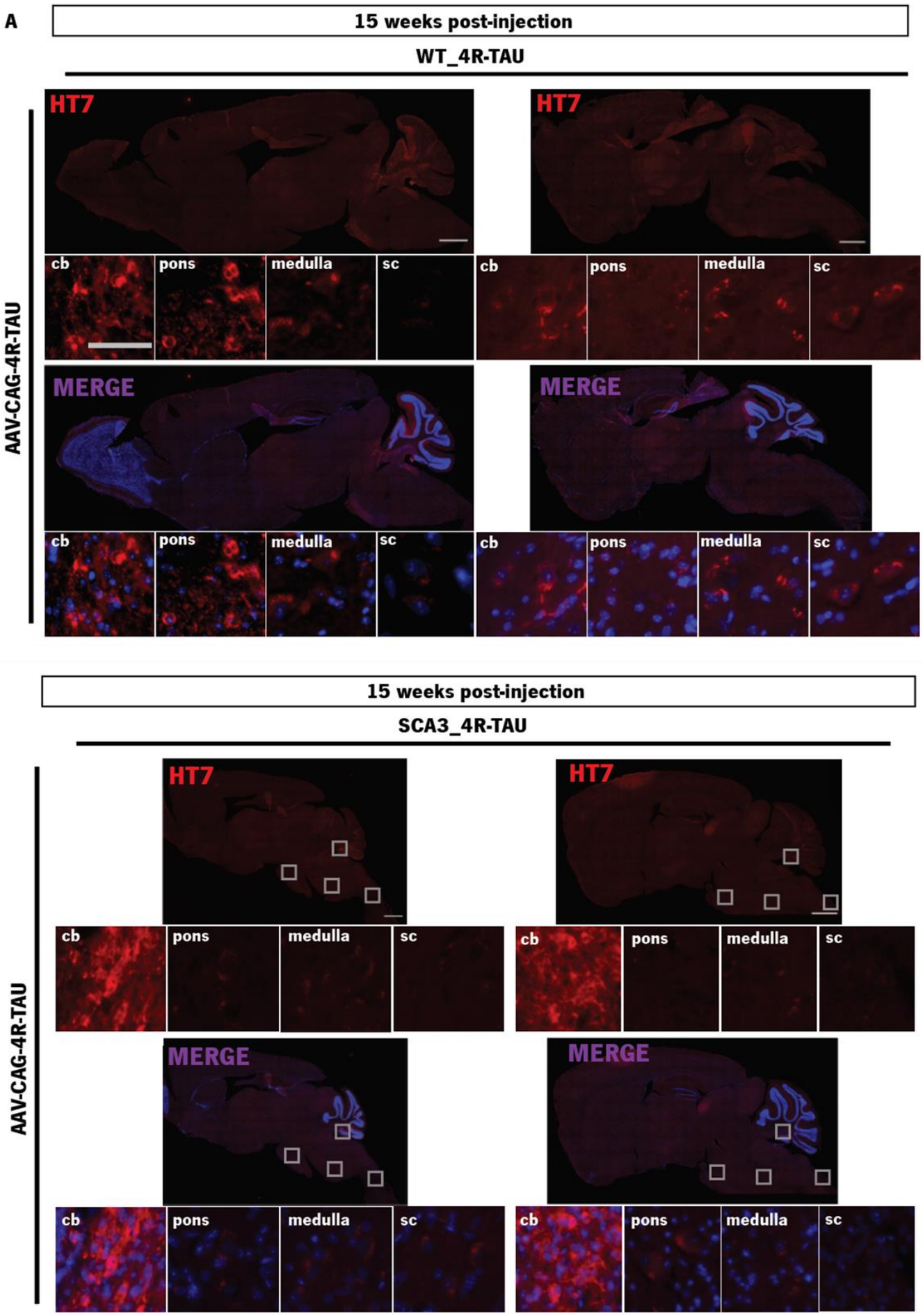
A
15 weeks post-injection
WT_4R-TAU
AAV-CAG-4R-TAU
HT7
HT7
cb
pons
medulla
sc
cb
pons
medulla
sc
MERGE
MERGE
cb
pons
medulla
sc
cb
pons
medulla
sc
15 weeks post-injection
SCA3_4R-TAU
AAV-CAG-4R-TAU
HT7
HT7
cb
pons
medulla
sc
cb
pons
medulla
sc
MERGE
MERGE
cb
pons
medulla
sc
cb
pons
medulla
sc

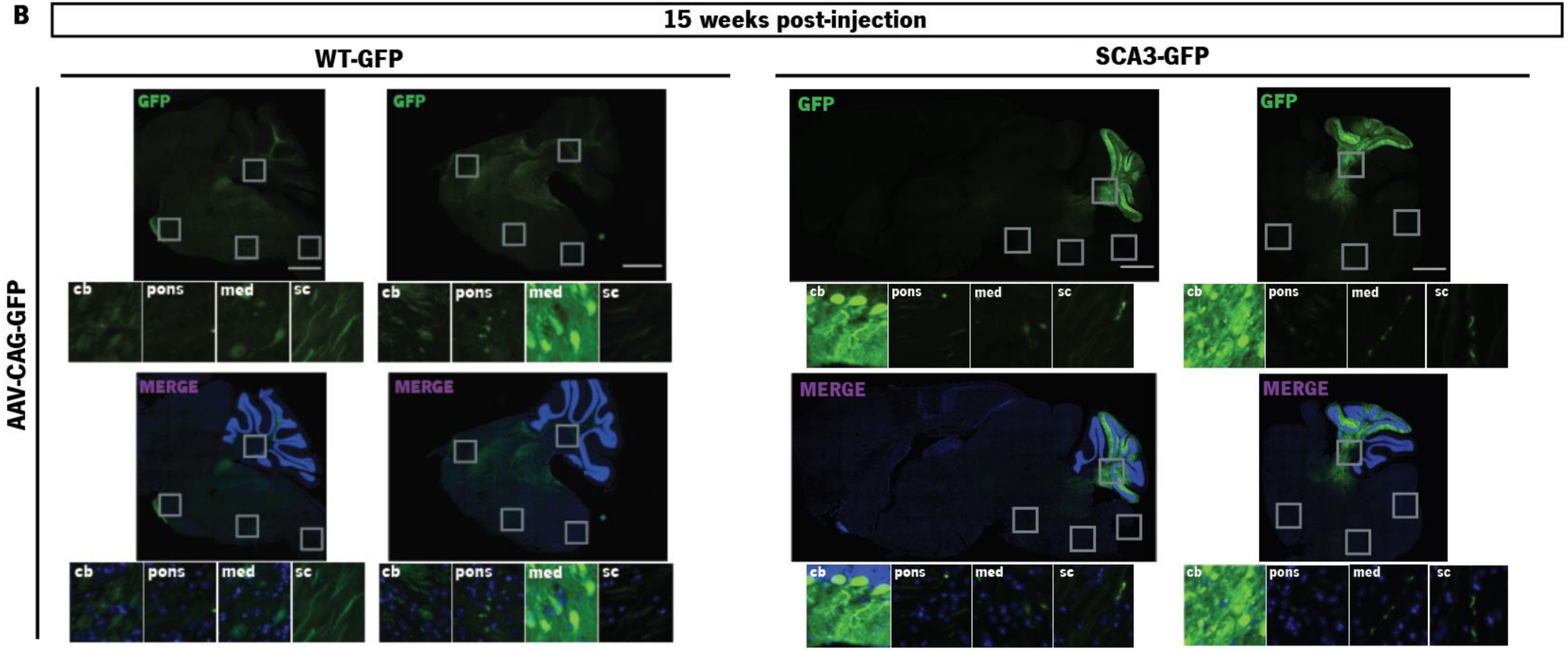
B
15 weeks post-injection
WT-GFP
SCA3-GFP
AAV-CAG-GFP
GFP
MERGE
cb
pons
med
sc

Figure 17. AAV-CAG-4R-Tau and AAV-CAG-GFP administration into mouse brain leads to strong human 4R-Tau and GFP expression observed at 15-weeks post-injection. Representative mouse brain sagittal sections (20 µm-thickness) of both WT and SCA3 mice, injected with a total volume of 3 µL of **(A)** AAV-CAG-4R-Tau (n= 4 to 5 mice/group) or **(B)** AAV-CAG-GFP (n=4 mice/group) showing expression in several brain areas, including the cerebellum (cb), pons, medulla oblongata (med) and spinal cord (sc) at 15-weeks post-injection. The HT7 antibody detects the presence of human Tau (red). Cell nuclei were counterstained with DAPI (blue). 20x magnification. Scale bars of whole mouse brain sections represent 1000 µm. Scale bars of insets of each mosaic picture represent 100 µm. 20x magnification.

4R-Tau isoform mRNA levels are not altered in the cerebellum and brainstem of SCA3 mice at 20 weeks of age

The main motivation for this study was the previous observation that 4R-Tau isoform was under-expressed in the brain of SCA3 mice at advanced disease stages (34 weeks of age)[206]. Next, we aimed to address if 3R- and 4R-Tau protein isoforms would already be altered in SCA3 mice at an earlier stage of disease – at 20 weeks of age. For this, the expression levels of 3R- and 4R-Tau protein isoforms in WT and SCA3 mice (n=3 to 4 samples/group) in two disease-relevant brain areas of the CNS, the cerebellum and the brainstem, were examined by quantitative RT-PCR analysis (Figure 18 and 19, Table S2-Supplementary Data).

Regarding the cerebellum, we did not observe statistically significant differences in the expression of 3R-Tau (p=0.558, Cohen's d=0.480) (Figure 18A) and 4R-Tau (p=0.293, Cohen's d=0.898) (Figure 18B) between WT and SCA3 mice. Moreover, no statistically significant differences were detected regarding 4R/3R-Tau ratio (Figure 18C) in this brain area.

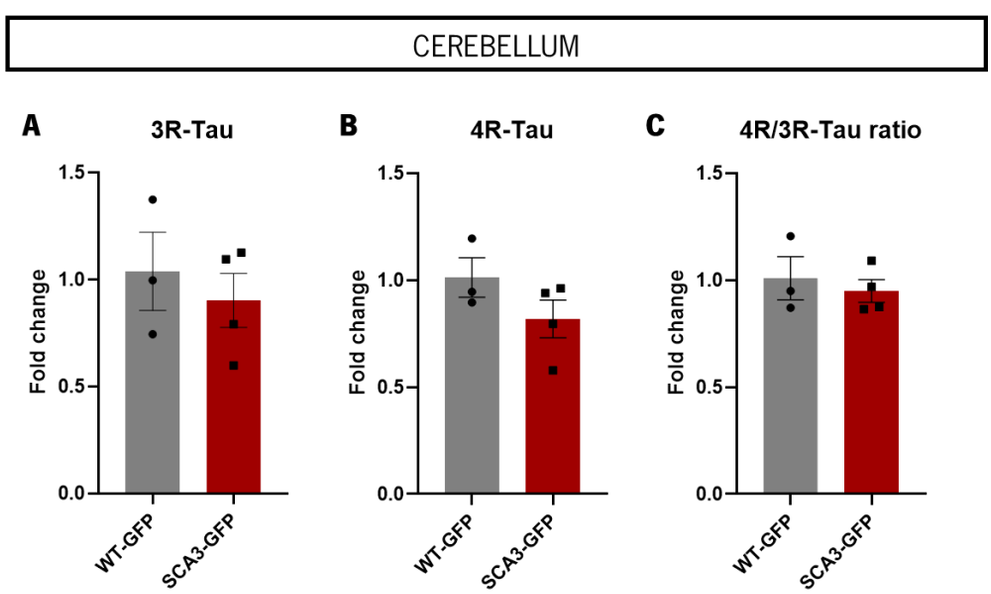

Figure 18. No alterations were found in 3R- and 4R-Tau expression mRNA levels in the cerebellum of SCA3 mice at 20 weeks of age. qRT-PCR analysis of mRNA 3R-Tau, 4R-Tau expression levels in the cerebellum of WT and SCA3 mice. No statistically significant differences were observed in relative expression of **(A)** 3R- Tau, **(B)** 4R-Tau and **(C)** 4R/3R-Tau ratio (n=3 to 4 samples/group; N=2 technical replicates). *B2M* was used as a housekeeping gene. Relative gene expression was calculated using the 2-ΔΔCt relative quantification method and is represented as fold change of gene expression (relative to control WT group). Data expressed as group mean ± SEM.

In the brainstem, SCA3 mice displayed similar 3R-Tau (p=0.192, Cohen's d=1.151) and 4R-Tau (p=0.089, Cohen's d=1.608) expression when compared to WT mice (Figure 19A and B, respectively, Table S2-Supplementary Data). Nevertheless, a strong tendency towards a decrease in the mRNA expression levels of 4R-Tau isoform was observed (p=0.089; Cohen's d = 1.608), in accordance with what had been observed at 34 weeks of age[206]. Similarly, as it has been observed in the cerebellum, no statistically significant differences were detected in the 4R/3R-Tau ratio in the brainstem (Figure 19C).

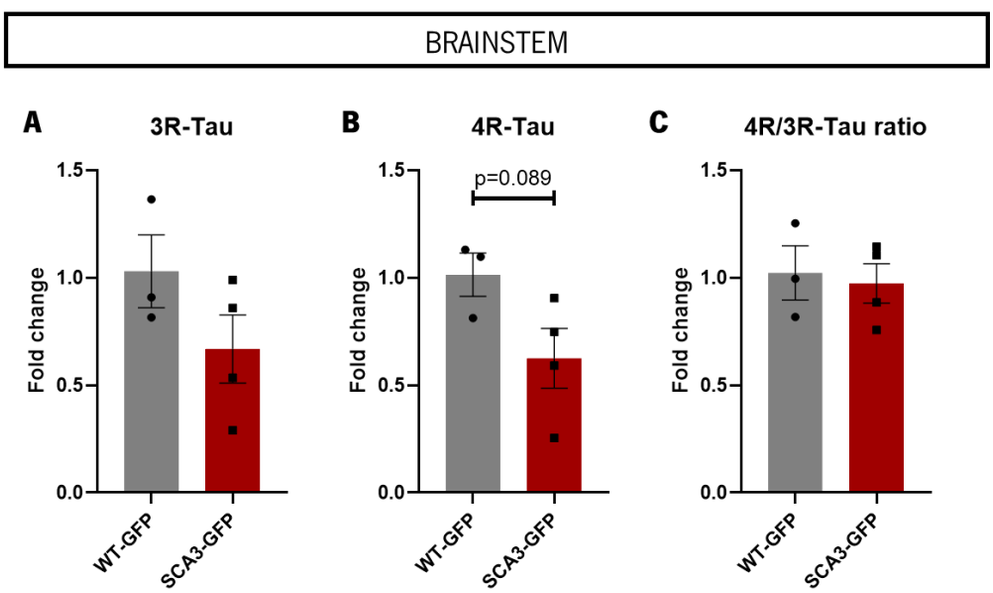

Figure 19. No alterations were found in 3R- and 4R-Tau expression mRNA levels in the brainstem of SCA3 mice at 20 weeks of age. qRT-PCR analysis of mRNA 3R-Tau, 4R-Tau expression levels in the brainstem of WT and SCA3 mice. No statistically significant differences were observed in relative expression of **(A)** 3R- Tau, **(B)** 4R-Tau and **(C)** 4R/3R-Tau ratio (n=3 to 4 samples/group; N=2 technical replicates). *B2M* was used as a housekeeping gene. Relative gene expression was calculated using the 2-ΔΔCt relative quantification method and is represented as fold change of gene expression. Data expressed as group mean ± SEM.

CHAPTER 5 -

DISCUSSION

CHAPTER 5 – DISCUSSION

In the present study we sought to evaluate if modulation of 4R-Tau expression could be a strategy to alleviate motor deficits in the CMVMJD135 mouse model (the SCA3 mice), the rationale being that we previously found in a recent study conducted in our laboratory, decreased 4R-Tau protein levels in the brainstem of SCA3 mice at a late symptomatic age (34 weeks of age) and in *post-mortem* brain samples of MJD/SCA3 patients[206]. The reduction of 4R-Tau, in parallel with no alterations in 3R-Tau protein, yield an imbalance of the 4R/3R-Tau isoforms ratio[206]. This molecular finding point to an involvement of Tau in MJD/SCA3 suggestive to contribute to disease pathogenesis[206]. This supports the idea that a strict balance of Tau isoforms is highly important for normal brain function. Moreover, the normal adult brain expresses 3R-Tau and 4R-Tau isoforms that are present in equal proportions in the human brain, thus being critical to maintaining the proper neuronal physiology of the brain[213]. Tau isoform imbalance was also observed in other polyglutamine diseases, particularly, in the brains of subjects with Huntington's disease (HD), where an increased 4R/3R-Tau ratio was found in the cortex and striatum, caused by increased 4R-Tau protein levels[214,215]. The Tau isoform imbalance observed in MJD/SCA3 mice and brain samples of patients as well as in the brains of HD patients, suggests that deregulation of Tau protein could be a shared element of the pathogenic process of these polyQ disorders. For instance, apart from the elevated total Tau levels due to increased 4R-Tau levels observed in HD, some studies have reported the presence of hyperphosphorylated Tau and Tau-positive cytoplasmic aggregates in patients and mouse models of HD[216]. Thus, this raises the question of whether this may also be relevant in the context of MJD/SCA3 pathogenesis, highlighting the relevance of investigating pathological findings associated with Tau in the MJD/SCA3 context in future experiments. Interestingly, reduced 4R-Tau protein levels were also found in the brain of a mouse model of Down syndrome, causing an imbalance in the 4R/3R-Tau ratio at both mRNA and protein levels[217]. Moreover, there is evidence in the literature of alternative splicing deregulation in several neurodegenerative disorders, such as Alzheimer's disease, Huntington's disease and Parkinson disease, that may account for the process of neurodegeneration[reviewed in203].

The fact that a functional interaction was found between ATXN3 and the splicing factor SRSF7, a key regulator of MAPT (Tau) exon 10 splicing, namely, that protein levels of SRSF7 decrease upon silencing ATXN3, suggests a role for ATXN3 in splicing regulation[206], particularly of the Tau mRNA. Additionally, it was also found that ATXN3 is in physical proximity with SRSF7 in neuronal cells given by protein ligation assay[206], suggesting that these proteins may interact, putting them in the same cellular path. All these findings suggest a potential imbalance of Tau isoforms in the brain of SCA3 mice and patients that may be contributing to MJD/SCA3 pathogenesis.

Based on this, we evaluated if modulating 4R-Tau levels would alleviate motor deficits in the SCA3 mice using Adeno-Associated-Viral Vectors (AAV) for transduction of the relevant cDNA. AAVs are a suitable tool for gene therapy due to their safety profile and efficiency in transducing a wide range of cellular types. Moreover, in the past few years, their use has been growing for the treatment of CNS disorders, such as Alzheimer's disease, Parkinson's disease, Huntington's disease, Amyotrophic lateral sclerosis and Spinal muscular atrophy[reviewed in 218]. The development of efficient gene therapy strategies for the treatment of CNS disorders is quite challenging and requires the gene of interest to be effectively and safely delivered to the target area. This becomes a bigger issue regarding CNS disorders characterized by highly complex neuropathology in which several brain areas are affected. In these cases, less effective the delivery of the genetic material to a restricted area will be in ameliorating disease. A possible approach to delivering genes of interest into the CNS is through the cerebrospinal fluid (CSF)[219]. This can be achieved by an intracerebroventricular (i.c.v.) injection, which has been shown to yield a successful induction of transgene expression in mice[220,221]. For instance, repeated i.c.v. injections of antisense oligonucleotides (ASO) in a SCA3 mouse model led to a reduction in insoluble disease protein, ataxin-3, and in its nuclear accumulation, in the cerebellum and brainstem. Unfortunately, the effects at the motor level were not investigated[222]. A posterior study was conducted using ASO targeting the mutant ataxin-3 through an i.c.v. injection in a different MJD/SCA3 transgenic mouse model[223]. This approach induced a widespread CNS distribution of ASO and, at motor level, proved to fully rescue the locomotor impairments of these mice[223]. The rescue on motor defects was associated with a recovery of defects in the firing frequency of Purkinje neuron function. Also, ASO therapy prevented nuclear accumulation of disease protein up to at least 14 weeks post-treatment. However, the treatment and evaluation were not extended beyond 29 weeks[223]. A recent study has tested an AAV carrying an artificial miRNA capable of downregulating the mutant ataxin-3, injected in the cisterna magma of an MJD/SCA3 mouse model, and proved to significantly reduce ataxin-3 aggregates, thus ameliorating the neurotoxicity induced by the disease protein[224].

The most common approach to delivering AAV vectors to the CNS is through direct infusion into the brain using a stereotaxic device, since the blood-brain barrier represents a key obstacle to gene delivery to the CNS[219]. Concerning the serotype choice, we used AAV9 due to its efficient transduction of both neurons and glia cells as reported elsewhere[225,226]. As a promoter, we used the CAG (chicken beta-actin promoter) which is known for its high-level ubiquitous expression properties[225]. Considering the heterogeneity of SCA3 neuropathology, spanning multiple brain regions, a region-targeting therapeutic approach may not be sufficient to reach the expected maximum therapeutic potential. Therefore, in this work, we have designed a preclinical trial by administering the human 4R-Tau onto an AAV9 under the ubiquitous expression of the CAG promoter. To reach maximal therapeutic effect and broad virus transduction coverage, we aimed to perform the

stereotaxic injections into the fourth ventricle, hoping for wider and strong human 4R-Tau transduction as in our pilot studies. The main goal was to achieve viral distribution near regions surrounding the injection site in mice brain, especially, the brainstem, where it was previously shown to have diminished 4R-Tau protein expression levels at a late symptomatic age[206]. Some studies have also demonstrated efficient viral transduction through this route of administration (i.c.v injection) in mice[220,227]. Our data tell us that delivery of AAV-CAG-4R-Tau by i.c.v. injection in mice brain is an efficient delivery route for widespread transduction of these brain regions. This was also shown previously in different contexts, where the same serotype and promoter showed to be efficient in transducing an AAV expressing the N-acetylglucosamine 6-sulfatase, a deficient lysosomal enzyme, administered into the CSF of a disease mouse model. This approach led to a restoration of normal behaviour and extended lifespan of treated mice[228]. Similar studies, but using different serotypes and the same promoter, showed that AAV encoding acid β-galactosidase, a deficiency enzyme, when introduced directly in the thalamus and in the deep cerebellar nuclei of a mouse model of a particular type of lysosomal storage disease, was able to restore protein levels to nearly normal in the brain. Although motor impairments were not ameliorated, the survival rate was extended in this model[229]. Another study tested the efficacy of AAV1 expressing fibroblast growth factor 14 (FGF14) administration, which is highly expressed in the CNS, into adult murine Purkinje neurons. The results showed efficient viral transduction, thus validating the expression of this protein in neurons *in vivo*[230]. Our first results indicate that AAV-CAG-4R-Tau (titer: $1.3x10^{13}$ GC/ml) administration through i.c.v. delivery into mice brain (WT, 3-month-old) led to good diffusion within the CNS and transgene expression 3- and 4-weeks post-injection, the highest expression being detected 4-weeks after injection when compared to 3-weeks post-injection. We selected this time window (3- and 4-weeks post-injection) to assess if the human 4R-Tau was efficiently expressed in the mouse brains under the conditions tested. The pattern of human 4R-Tau expression was detected in the cerebellum, the pons, the medulla oblongata and the cervical portion of the spinal cord (Figure 8).

Next, upon the establishment of the optimal conditions to induce human 4R-Tau expression in healthy adult mice brain, we sought to validate these conditions in younger animals (7 weeks of age) to more closely mimic the conditions of the proposed preclinical trial in this study. In this second pilot experiment, we used the same conditions as before, but testing a larger volume of virus (3 µl) to increase the expression of the previously transduced regions. Moreover, at this stage of the work, we were still uncertain if the amount of virus that was introduced in mice brain was sufficient to restore the 4R-Tau protein levels to normal levels. Understanding this is of extreme importance because it is widely reported in the literature that increased levels of 4R-Tau isoform are, on the other hand, associated with other neurodegenerative disorders, such as Progressive supranuclear palsy (PSP), Corticobasal degeneration (CBD) and frontotemporal dementia with parkinsonism

linked to chromosome 17 (FTDP-17)[reviewed in 231]. Therefore, the ultimate goal of this approach would be to restore the expression levels of 4R-Tau protein, and not upregulate its levels excessively, in SCA3 mice brain. Unfortunately, we were not able to successfully optimize the antibody to detect 4R-Tau protein by western blot analysis for this thesis. This experiment would answer two important questions: (1) Are 4R-Tau protein expression levels altered in the cerebellum and brainstem at 11 and 20 weeks of age in SCA3 mouse brains? (2) Is the injected volume and viral concentration sufficient to restore 4R-Tau protein levels in the mouse brains?

Another difficulty that we faced was the adjustment of stereotaxic coordinates in younger animals. The stereotaxic coordinates we used were obtained from adult brains atlases [232]. Therefore, they are not accurate for younger mice which led us to think that we might not be injecting precisely into the fourth ventricle. Also, animals at this age present considerable differences in brain size and in body weight, which imposes more difficulties in reaching precisely the same spot, in all individuals, in the brain when performing the stereotaxic injections.

In this study, we have used the CMVMJD135 mouse model (SCA3 mice) because it exhibits phenotypic and neuropathological similarities with the human disorder and presents an early disease onset, usually at 6 weeks of age[140,141]. This makes this SCA3 mice a valuable model to study molecular mechanisms underlying SCA3 as well as for therapy testing, as it presents multiple quantifiable measures. As an example, this model was used to test the effect of citalopram, a selective serotonin reuptake inhibitor; this compound proved to have a marked therapeutic effect improving balance and motor coordination and leading to a marked suppression of mutant ATXN3 aggregation and neuronal loss[146]. Additionally, creatine, a cellular energy buffer, also showed to be a promising compound for SCA3 therapy as it significantly improved motor dysfunction and neuropathology[144]. In contrast, lithium chloride treatment failed to rescue the motor phenotype, excluding this compound as a good candidate for the treatment of MJD/SCA3[143]. Based on these previous studies, in this work, we used the SCA3 mice to investigate if AAV-CAG-4R-tau administration into mice brain would alleviate the behavioural deficits. The initiation of a treatment pre-symptomatically is usually desirable because after the onset of the symptoms it is more difficult to revert the phenotype. This is corroborated by previous studies, in which treatment with citalopram initiated at a post-symptomatic age led to an improvement in motor coordination and balance to a lesser extent than when initiating the treatment earlier[146]. Besides, it failed to counteract ATXN3 aggregation when compared to the treatment initiated at a pre-symptomatic age[145]. Moreover, the existence of a genetic test for MJD/SCA3 allows the detection of the disease-causing allele before symptoms onset in humans[52], hence a pre-symptomatic treatment is a more feasible strategy. Here, despite administering the virus pre-symptomatically (5 weeks of age), the peak of the viral transduction only

occurs at an early symptomatic age (8 to 9 weeks of age) in SCA3 mice, thus our approach may be considered an early symptomatic treatment. In fact, the timing of treatment initiation may be critical. Based on this, it would be valuable to investigate if treatment would be effective at improving motor deficits if initiated post-symptomatically, to better mimic what usually occurs in the clinics.

We performed the stereotaxic injections either with AAV9 encoding human 4R-Tau or GFP into the fourth ventricle of mice brain at 5 weeks of age. The behavioural assessment started one week after surgery (6 weeks of age) until animals reached 20 weeks of age. We selected a set of behavioural tests to assess motor performance that were already extensively characterized in this SCA3 mice[140,141]. The analysis of the behavioural data considered three main aspects: *(i)* the detection of motor phenotype between non-treated animals *(ii)* the evaluation of the therapeutic potential of the human 4R-Tau administration by comparing the SCA3 groups and *(iii)* the assessment of the potential adverse impact on well-being that might be associated with exposure to this viral vector by comparing the "treatment" and "control" WT groups. Taking into consideration that we observed a high viral expression at 4-weeks when compared to 3-weeks post-injection, any changes in the behaviour that we observed at 10 weeks of age may be due to the presence of the human 4R-Tau expression in mice brain. In fact, it is documented that gene expression mediated by AAVs has a peak of expression within 2 to 3 weeks in mice[233], which we also corroborated in the present study.

WT_GFP mice performed significantly better than SCA3_GFP mice for almost all the behavioural tests conducted, confirming that SCA3 mice exhibited the expected motor impairments, as previously described, and thus, confirming the phenotype already established for this mouse model[140,141]. Nevertheless, differences in age of motor dysfunction onset were detected when compared with previous groups, most likely due to the surgical procedure that these animals were subjected (both WT and SCA3 mice). Balance and motor coordination were assessed by the balance beam walk and motor swimming tests, respectively, both measuring two key aspects related to SCA3 phenotype. Regarding swimming performance, SCA3 mice only started to exhibit swimming defects at 20 weeks of age (Figure 11). Moreover, we have also observed in our study an abnormal posture and unsynchronised movements of the SCA3 mice, as compared to what is described[140]. Regarding fine motor coordination, SCA3_GFP mice started to display balance deficits already at 10 weeks of age as assessed by balance walk beam test (Figure 12) and worsen throughout time using the 12-mm square beam, being even more prominent when the task difficulty was increased by using round beams. This result are in accordance with previous studies, where SCA3 mice have a significantly higher latency than WT animals detected at the same age[140]. Muscular strength deficits are the first manifestation in this model starting already at 6 weeks of age. Here, the SCA3 mice also exhibited less strength throughout age (Figure 15A) and lack of body weight gain (Figure 14) when compared to WT mice, as described[140]. Intriguingly, the mean

of CAG repeat length reported here (Figure 10B) does not explain the later onset of disease symptoms observed. It is widely reported that repeat length positively correlates with disease severity, as observed in MJD/SCA3 mice and patients[51,208]. Conversely, we would expect to observe anticipation of the motor phenotype when compared to previous studies[140], since SCA3 mice herein used present a higher CAG repeat number.

A limitation of the present study is that we might have started to treat SCA3 animals too early, where no alterations in the 3R/4R-Tau ratio yet occur at the point where the treatment is initiated. Therefore, we assessed mRNA expression levels of Tau isoforms in SCA3 mice in the cerebellum and brainstem at 20 weeks of age to investigate if they were altered or not. By conducting qRT-PCR we did not observe significant differences in the 3R-Tau, 4R- Tau, and 4R/3R-Tau ratio expression levels in these both well-known affected brain regions, at least at the mRNA level (Figure 18 and 19). Nevertheless, taking our results regarding 4R-Tau relative expression in the brainstem (Figure 19B), we observed a tendency for a decreased 4R-Tau expression in this region (non-significant) that might be in line with what was previously observed in older animals[206], thus supporting that normalizing 4R-Tau levels in SCA3 mice brain might be important. Regarding the 4R-Tau mRNA relative expression in the cerebellum, there might be an explanation for the lack of significant differences. In the MJD/SCA3 context, the cerebellar cortex or granular layer are apparently unaffected, but within the deep cerebellar nuclei, namely, in the dentate nucleus, neuronal loss usually occurs[30,234]. Thus, when analysing a sample from the whole cerebellum a dilution effect will occur, masking our results. Moreover, it is important to highlight that these differences were not addressed in treated mice because they were injected with human 4R-Tau protein and a close homology in the sequence exists between human and mouse Tau isoforms (89%) [235], which did not allow us to distinguish between 4R-Tau endogenous mRNA levels versus levels of the mRNA introduced by the virus.

Administration of AAV-encoding human 4R-Tau in SCA3 mice did not lead to any beneficial changes in their motor performance for any of the tests performed. Indeed, we observed that treated SCA3 mice seemed to have a worse swimming performance than non-treated SCA3 mice (although non-significant) during a time window that comprises 14 and 18 weeks of age, which might point to a negative effect of human 4R-Tau administration (Figure 11). In addition, when motor coordination was assessed by the balance beam walk test, treated SCA3 mice exhibited more marked balance deficits than non-treated SCA3 mice (albeit the differences were non-significant), as seen by the increased latency to cross the 12-mm square and 17-mm round beams (Figure 12). This suggests that AAV-CAG-4R-Tau administration failed to improve motor phenotype. Regarding muscular strength deficits, assessed by hanging wire grid test, and although the difference was not statistically significant, treated SCA3 mice showed higher latency to fall off the grid when compared to SCA3_GFP mice (Figure 15A).

Regarding WT mice, AVV-CAG-4R-Tau administration led to balance impairments when compared to WT_GFP-injected animals throughout time in all the beams used (Figure 12). Moreover, we also observed a tendency for a decrease in muscular strength in treated when compared to non-treated WT mice (Figure 15A) (although not statistically significant). Therefore, human 4R-Tau protein expression might be negatively impacting the motor performance of treated WT mice. In this regard, it would be interesting to screen the effects of the presence of 4R-Tau protein levels above the normal threshold in mice by evaluating learning and memory deficits using cognitive tests such as Y-Maze, for example[reviewed in 236], since it is described that increased 4R-Tau protein levels are associated with other neurodegenerative disorders, such as PSP, CBP and FTDP-17 associated with cognitive impairments, as mentioned above[reviewed in 231]. At the molecular level, protein aggregation assays could be performed to monitor Tau protein aggregation in the MJD/SCA3 context and upon viral transduction of human 4R-Tau. This observation regarding treated and non-treated WT mice might support the concept of a deleterious effect of 4R-Tau protein administration in healthy mice. This is not surprising because it is known that there are diseases caused by overexpression of 4R-Tau[eviewed in 237]. Indeed, there is a significant lack of information in the literature regarding the effects of overexpression of Tau isoforms at the motor function level. The existing studies mainly focused on cognitive behavioural tests[238,239]. In the present study, we found that human 4R-Tau expression in WT mice might have an impact on their motor performance, namely, in motor coordination (given by the balance beam walking test, Figure 12), but not in SCA3 mice. However, it remains to be clarified at which age SCA3 animals start to present reduced 4R-Tau protein levels, which ultimately will have implications for the potential therapeutic effect of 4R-Tau administration. Body weight measurement is a good indicator of mouse well-being[240]. Because we did not detect significant alterations in the body weight of mice injected with AVV-CAG-4R-Tau, it is reasonable to infer that the toxicity observed at the level of the motor performance may not be related to a systemic toxicity, but rather to a direct effect in the brain. Additionally, daily observation of the mice showed that their appearance and general welfare were preserved.

Next, we aimed to determine if the expression of the transduced vectors would still be present in mouse brains 9-weeks post injection. Using a specific antibody to detect the presence of human Tau (HT7) and not the endogenous murine Tau, we have confirmed that the virus was able to transduce the regions surrounding the injection site (Figure 16A). Because the control virus encodes for GFP, we could easily observe that transduction of GFP also led to a good coverage of our target regions (Figure 16B). Several studies of AAV-mediated expression have reported that expression of cDNAs transduced remains stable over a long time. For instance, the use of an AAV-expressing human *SLC2A1*, the gene encoding GLUT1, was administered to GLUT1-deficient mice through i.c.v. injection and the encode transporter revealed to be strongly expressed

up to 3-months post-injection[241]. This is also corroborated by other studies, where viral expression was found to be stable up to 6-months post-injection[242,243]. In the context of Niemann-Pick disease type A, a lysosomal storage disorder, a recent study has shown that viral expression remained robust 3-months post-injection when compared to 1-month post-injection by administering AAV-expressing human ASM, the disease-causing protein[244]. At the end of the behavioural assessment, we evaluated if the viral expression was still present (15-weeks post-injection) and, indeed, we detected the presence of both human 4R-Tau and GFP. The pattern of distribution at 15-weeks post-injection (Figure 17) was similar to what observed at 9-weeks post-injection (Figure 16).

The pattern of viral distribution was quite heterogeneous between animals, either by comparing the vectors with each other (AAV-CAG-4R-Tau vs AAV-CAG-GFP) or by comparing the animals that were injected with the same vector. This may be because surgeries were performed on very young animals when compared to the first pilot study that we performed (5 weeks of age versus 13 weeks of age) and differences in brain size at these ages are expected**,** which makes the stereotaxic coordinates used to slightly deviated from the expected injection site - the fourth ventricle. At 5 weeks of age, we observed a noticeable difference in terms of brain size, especially between males and females, affecting the accuracy of the injection site. Actually, is reported that the size of the target brain region considerably differs between young versus adult animals[245], which may be the reason why we observed such differences in the pattern of human 4R-Tau and GFP distribution between the younger and older animals. Concerning mouse brain volume, it is reported that is almost stable already at 3-weeks of age, although some variations occur during the development and as mice age[246]. Hence, for future studies, mice with older age might be better to perform the viral injections, even though this would only allow testing of a post-symptomatic intervention.

Despite these constraints, we observed that the transduced areas within the CNS were quite similar between animals with slight variations between individual animals, either injected with AAV-expressing human 4R-Tau or AAV-expressing GFP (Figure 16, Figure 17, Figure S3-Supplementary Data). The brain areas transduced within the CNS comprise mainly the cerebellum, the brainstem and the spinal cord (cervical portion). When translating this observation into the disease context, these are disease-relevant brain areas and some nuclei within these regions proved to exhibit ataxin-3 intranuclear inclusions at late symptomatic ages in SCA3 mice, namely the dentate nuclei (cerebellum), pontine nuclei, locus coeruleus and reticulotegmental nucleus of the pons (pons), inferior olive, cuneate nuclei and facial nuclei (medulla oblongata)[140]. Interestingly, we have shown that neuronal loss and the presence of ataxin-3 nuclear inclusions in the spinal cord occurs at earlier stages of the disease, starting as early as 11 weeks of age (unpublished observations). As future work, it would be interesting to study the impact of this approach from a neuropathological point of view and try to

understand the possible alterations caused by viral administration into the SCA3 mouse brains at these specific regions, particularly in the spinal cord, where neuropathology signs are observed early in the disease progression.

Altogether, these results suggest that in order to achieve the desired levels of a therapeutic protein, it is of extreme importance to evaluate the viral conditions tested, particularly, the type (and serotype) of virus being used, the delivery route, and the timing for viral transduction. The currently available pre-clinical data support the use of AAV-mediated gene therapy as an attractive approach for the treatment of neurodegenerative disorders, particularly, for MJD/SCA3. As an example, the application of AAV vectors for the treatment of CNS disorders has been used in clinical trials for other neurodegenerative diseases, such as Alzheimer's disease[247], Parkinson disease[248] and Spinal muscular atrophy[249], among others, where it was shown to be safe. Our data indicate that we successfully induced viral transduction in mice brain using a human 4R-Tau encoding AAV and we achieved a widespread distribution to surrounding areas near the injected site, and an expression that remained stable throughout time. However, from a therapeutic perspective, the observations of a lack of a beneficial effect on motor behavior raise the question of when should the AAV-CAG-4R-Tau vector start to be administered to SCA3 mice. Next time, to better assess the therapeutic value of this therapeutic approach, a deeper optimization of viral conditions and treatment initiation should be performed. Although we did not observe improvements in motor deficits of SCA3 mice upon AAV-CAG-4R-Tau administration, in the conditions tested here, the rationale of rescuing 4R-Tau still holds, and we can, in the future, devise an optimized strategy for delivery and balanced expression of this protein. Additionally, and since the basis for 4R/3R-Tau ratio imbalance is the decrease of the 9G8 splicing factor[206], Tau mRNA being only one of its targets, another approach could be to use similar viral vectors to rescue 9G8 levels in SCA3 mice.

CHAPTER 6 -

CONCLUDING REMARKS AND FUTURE PERSPECTIVES

CHAPTER 6 – CONCLUDING REMARKS AND FUTURE PERSPECTIVES

The work performed during this dissertation provided important insights about the potential therapeutic effects of human 4R-Tau administration and modulation in SCA3 mice. Despite the observed lack of therapeutic effect, several questions arose during the development of this work that may be helpful to clarify the precise effect of 4R-Tau administration in SCA3 mice brain. First, it is important to address the precise period when a decreased 4R-Tau levels are altered in the brain of SCA3 mice. So, as a future perspective, it would be interesting to:

(1) **Assess 4R-Tau expression levels throughout time in SCA3 mice**. For that, a longitudinal study to determine the Tau isoforms protein and mRNA levels in different CNS regions would be essential.

(2) **Conduct a post-symptomatic treatment based on the results obtained in (1)**. Investigate the effects of initiating the treatment only at the age at which the levels of 4R-Tau are confirmed to be altered in the brain of SCA3 mice, most likely at a post-symptomatic age, that is, after the development of some motor symptoms, starting 4R-Tau administration from the period when diminished 4R-Tau protein levels are detected, particularly, at the specific regions where the Tau isoform imbalance is present.

(3) **Analyse the effects of AAV-CAG-4R-Tau administration on neuropathology.** The relevant neuropathological features of this model are described to appear between 20 to 35 weeks of age. Because we did not detect any beneficial effects of human 4R-Tau expression at the motor level, we did not investigate possible neuropathological changes; nevertheless, it would be interesting to evaluate the effects of this treatment on pathological features, mainly in the spinal cord, where those findings are more evident at 20 weeks of age. To evaluate the possible relationship between Ataxin-3 and Tau in the neuropathological process, an immunofluorescence analysis can be performed to detect whether there is a colocalization of normal or hyperphosphorylated Tau protein with ATXN3 aggregates/inclusions in the SCA3 mouse brains.

In summary, our results did not exclude the therapeutic potential of AAV-CAG-4R-Tau administration in SCA3 mice brain. Investigating deeper these questions would certainly help to redefine a new and more accurate strategy to evaluate the effects of this approach for reduction of MJD/SCA3 pathogenesis.

REFERENCES

1. Twist, E. C. et al. Machado Joseph disease maps to the same region of chromosome 14 as the spinocerebellar ataxia type 3 locus. 7.
2. Schöls, L., Bauer, P., Schmidt, T., Schulte, T. & Riess, O. Autosomal dominant cerebellar ataxias: clinical features, genetics, and pathogenesis. The Lancet Neurology 3, 291–304 (2004).
3. Margolis, R. L. The spinocerebellar ataxias: Order emerges from chaos. Curr Neurol Neurosci Rep 2, 447–456 (2002).
4. Paulson, H. Dominantly Inherited Ataxias: Lessons Learned from Machado-Joseph Disease/Spinocerebellar Ataxia Type 3. Semin Neurol 27, 133–142 (2007).
5. Paulson, H. Machado–Joseph disease/spinocerebellar ataxia type 3. in Handbook of Clinical Neurology vol. 103 437–449 (Elsevier, 2012).
6. Nakano, K. K., Dawson, D. M. & Spence, A. Machado disease: A hereditary ataxia in Portuguese emigrants to Massachusetts. Neurology 22, 49–49 (1972).
7. Woods, B. T. Nigro-spino-dentatal Degeneration with Nuclear Ophthalmoplegia A Unique and Partially Treatable Clinico-pathologicalEntity. 18.
8. Rosenberg, R. N., Nyhan, W. L., Bay, C. & Shore, P. Autosomal dominant striatonigral degeneration: A clinical, pathologic, and biochemical study of a new genetic disorder. Neurology 26, 703–703 (1976).
9. Romanul, F. C. A., Fowler, H. L., Radvany, J., Feldman, R. G. & Feingold, M. Azorean Disease of the Nervous System. New England Journal of Medicine 296, 1505–1508 (1977).
10. Coutinho, P. & Andrade, C. Autosomal dominant system degeneration in Portuguese families of the Azores Islands: A new genetic disorder involving cerebellar, pyramidal, extrapyramidal and spinal cord motor functions. Neurology 28, 703–703 (1978).
11. Lima, L. & Coutinho, P. Clinical criteria for diagnosis of Machado-Joseph disease: report of a non-Azorena Portuguese family. Neurology 30, 319–322 (1980).
12. Vale, J. et al. Autosomal dominant cerebellar ataxia: frequency analysis and clinical characterization of 45 families from Portugal: Autosomal dominant cerebellar ataxia: characterization of 45 Portuguese families. European Journal of Neurology 17, 124–128 (2010).
13. Boonkongchuen, P. et al. Clinical analysis of adult-onset spinocerebellar ataxias in Thailand. BMC Neurol 14, 75 (2014).
14. Schöls, L. et al. Autosomal dominant cerebellar ataxia: Phenotypic differences in genetically defined subtypes?: Phenotypes in Dominant Ataxias. Ann Neurol. 42, 924–932 (1997).
15. Zhao, Y. et al. Prevalence and ethnic differences of autosomal-dominant cerebellar ataxia in Singapore: Autosomal-dominant cerebellar ataxia in Singapore. Clinical Genetics 62, 478–481 (2002).

16. Tsai, H.-F. et al. Analysis of trinucleotide repeats in different SCA loci in spinocerebellar ataxia patients and in normal population of Taiwan. Acta Neurol Scand 109, 355–360 (2004).
17. Stevanin, G. et al. Clinical and molecular features of spinocerebellar ataxia type 6. Neurology 49, 1243–1246 (1997).
18. van de Warrenburg, B. P. C. et al. Spinocerebellar ataxias in the Netherlands: Prevalence and age at onset variance analysis. Neurology 58, 702–708 (2002).
19. Maruyama, H. et al. Difference in disease-free survival curve and regional distribution according to subtype of spinocerebellar ataxia: A study of 1,286 Japanese patients. Am. J. Med. Genet. 114, 578–583 (2002).
20. Paradisi, I., Ikonomu, V. & Arias, S. Spinocerebellar ataxias in Venezuela: genetic epidemiology and their most likely ethnic descent. J Hum Genet 61, 215–222 (2016).
21. Moseley, M. L. et al. Incidence of dominant spinocerebellar and Friedreich triplet repeats among 361 ataxia families. Neurology 51, 1666–1671 (1998).
22. Pujana, M. A. et al. Spinocerebellar ataxias in Spanish patients: genetic analysis of familial and sporadic cases. Human Genetics 104, 516–522 (1999).
23. Barbeau, A. et al. The natural history of Machado-Joseph disease: An analysis of 138 personally examined cases. Canadian Journal of Neurological Sciences 11, 510–525 (1984).
24. Rosenberg, R. N. Machado-Joseph disease: An autosomal dominant motor system degeneration. Mov Disord. 7, 193–203 (1992).
25. Kieling, C., Prestes, P., Saraiva-Pereira, M. & Jardim, L. Survival estimates for patients with Machado-Joseph disease (SCA3). Clinical Genetics 72, 543–545 (2007).
26. Gwinn-Hardy, K. et al. Spinocerebellar Ataxia Type 3 Phenotypically Resembling Parkinson Disease in a Black Family. Arch Neurol 58, 296 (2001).
27. Moro, A. et al. Nonmotor symptoms in spinocerebellar ataxias (SCAs). cerebellum ataxias 6, 12 (2019).
28. What is Ataxia? - National Ataxia Foundation. https://www.ataxia.org/what-is-ataxia/.
29. Takiyama, Y. et al. A clinical and pathologic study of a large Japanese family with Machado- Joseph disease tightly linked to the DNA markers on chromosome 14q. Neurology 44, 1302–1302 (1994).
30. Durr, A. et al. Spinocerebellar ataxia 3 and machado-joseph disease: Clinical, molecular, and neuropathological features. Ann Neurol. 39, 490–499 (1996).
31. Muñoz, E. et al. Intranuclear inclusions, neuronal loss and CAG mosaicism in two patients with Machado–Joseph disease. Journal of the Neurological Sciences 200, 19–25 (2002).

32. Rüb, U. et al. Degeneration of the external cuneate nucleus in spinocerebellar ataxia type 3 (Machado–Joseph disease). Brain Research 953, 126–134 (2002).

33. Yamada, M., Sato, T., Tsuji, S. & Takahashi, H. CAG repeat disorder models and human neuropathology: similarities and differences. Acta Neuropathol 115, 71–86 (2007).

34. Ross, C. A. When more is less: Pathogenesis of glutamine repeat neurodegenerative diseases. Neuron 15, 493–496 (1995).

35. Klockgether, T. et al. Autosomal dominant cerebellar ataxia type I. 7.

36. Lopes-Cendes, I. et al. Limits of Clinical Assessment in the Accurate Diagnosis of Machado-Joseph Disease. Archives of Neurology 53, 1168–1174 (1996).

37. Murata, Y. et al. Characteristic Magnetic Resonance Imaging Findings in Machado-Joseph Disease. Arch Neurol 55, 33 (1998).

38. Onodera, O. et al. Progressive atrophy of cerebellum and brainstem as a function of age and the size of the expanded CAG repeats in theMJD1 gene in Machado-Joseph disease. Ann Neurol. 43, 288–296 (1998).

39. Schulz, J. B. et al. Visualization, quantification and correlation of brain atrophy with clinical symptoms in spinocerebellar ataxia types 1, 3 and 6. NeuroImage 49, 158–168 (2010).

40. Tokumaru, A. M. et al. Magnetic Resonance Imaging Findings of Machado–Joseph Disease: Histopathologic Correlation: Journal of Computer Assisted Tomography 27, 241–248 (2003).

41. Biirk, K. et al. Autosomal dominant cerebellar ataxia type I. 9.

42. Iwabuchi, K., Tsuchiya, K., Uchihara, T. & Yagishita, S. Autosomal dominant spinocerebellar degenerations. Clinical, pathological, and genetic correlations. Rev Neurol (Paris) 155, 255–270 (1999).

43. Abe, Y. et al. CAG repeat number correlates with the rate of brainstem and cerebellar atrophy in Machado-Joseph disease. Neurology 51, 882–884 (1998).

44. Rüb, U., Brunt, E. R. & Deller, T. New insights into the pathoanatomy of spinocerebellar ataxia type 3 (Machado–Joseph disease): Current Opinion in Neurology 21, 111–116 (2008).

45. Paulson, H. L. et al. Intranuclear Inclusions of Expanded Polyglutamine Protein in Spinocerebellar Ataxia Type 3. Neuron 19, 333–344 (1997).

46. Perez, M. K. et al. Recruitment and the Role of Nuclear Localization in Polyglutamine-mediated Aggregation. The Journal of Cell Biology 143, 14 (1998).

47. Schmidt, T. et al. Protein surveillance machinery in brains with spinocerebellar ataxia type 3: Redistribution and differential recruitment of 26S proteasome subunits and chaperones to neuronal intranuclear inclusions: Proteasome and Chaperones in SCA3. Ann Neurol. 51, 302–310 (2002).

48. Takiyama, Y. et al. The gene for Machado–Joseph disease maps to human chromosome 14q. Nat Genet 4, 300–304 (1993).

49. Kawaguchi, Y. et al. CAG expansions in a novel gene for Machado-Joseph disease at chromosome 14q32.1. Nat. Genet. 8, 221–228 (1994).

50. Maruyama, H. et al. Molecular features of the CAG repeats and clinical manifestation of Machado–Joseph disease. Human Molecular Genetics 4, 807–812 (1995).

51. Maciel, P. et al. Correlation between CAG Repeat Length and Clinical Features in Machado-Joseph Disease. Am. J. Hum. Genet. 8 (1995).

52. Maciel, P. Improvement in the Molecular Diagnosis of Machado-Joseph Disease. Arch Neurol 58, 1821 (2001).

53. Takiyama, Y. et al. Evidence for inter-generational instability in the CAG repeat in the MJD1 gene and for conserved haplotypes at flanking markers amongst Japanese and Caucasian subjects with Machado-Joseph disease. Human Molecular Genetics 4, 1137–1146 (1995).

54. Sasaki, H. et al. CAG repeat expansion of Machado-Joseph disease in the Japanese: analysis of the repeat instability for parental transmission, and correlation with disease phenotype. Journal of the Neurological Sciences 133, 128–133 (1995).

55. Igarashi, S. Intergenerational instability of the CAG repeat of the gene for Machado- Joseph disease (MJD1) is affected by the genotype of the normal chromosome: implications for the molecular mechanisms of the instability of the CAG repeat. Human Molecular Genetics 5, 923–932 (1996).

56. Carvalho, D. R., La Rocque-Ferreira, A., Rizzo, I. M., Imamura, E. U. & Speck-Martins, C. E. Homozygosity Enhances Severity in Spinocerebellar Ataxia Type 3. Pediatric Neurology 38, 296–299 (2008).

57. Lopes-Cendes, I. et al. Somatic mosaicism in the central nervous system in spinocerebellar ataxia type 1 and machado-joseph disease. Ann Neurol. 40, 199–206 (1996).

58. Tanaka, F. et al. Differential pattern in tissue-specific somatic mosaicism of expanded CAG trinucleotide repeat in dentatorubral-pallidoluysian atrophy, Machado-Joseph disease, and X-linked recessive spinal and bulbar muscular atrophy. Journal of the Neurological Sciences 135, 43–50 (1996).

59. Hashida, H., Goto, J., Kurisaki, H., Mizusawa, H. & Kanazawa, I. Brain regional differences in the expansion of a CAG repeat in the spinocerebellar ataxias: Dentatorubral-pallidoluysian atrophy, machado-joseph disease, and spinocerebellar ataxia type 1. Ann Neurol. 41, 505–511 (1997).

60. Cancel, G. et al. Somatic mosaicism of the CAG repeat expansion in spinocerebellar ataxia type 3/Machado-Joseph disease. 5.

61. Paulson, H. L. et al. Machado-Joseph disease gene product is a cytoplasmic protein widely expressed in brain. Ann Neurol. 41, 453–462 (1997).

62. Burnett, B. The polyglutamine neurodegenerative protein ataxin-3 binds polyubiquitylated proteins and has ubiquitin protease activity. Human Molecular Genetics 12, 3195–3205 (2003).

63. Doss-Pepe, E. W., Stenroos, E. S., Johnson, W. G. & Madura, K. Ataxin-3 Interactions with Rad23 and Valosin-Containing Protein and Its Associations with Ubiquitin Chains and the Proteasome Are Consistent with a Role in Ubiquitin-Mediated Proteolysis. MCB 23, 6469–6483 (2003).

64. Chai, Y., Berke, S. S., Cohen, R. E. & Paulson, H. L. Poly-ubiquitin Binding by the Polyglutamine Disease Protein Ataxin-3 Links Its Normal Function to Protein Surveillance Pathways. Journal of Biological Chemistry 279, 3605–3611 (2004).

65. Berke, S. J. S., Chai, Y., Marrs, G. L., Wen, H. & Paulson, H. L. Defining the Role of Ubiquitin-interacting Motifs in the Polyglutamine Disease Protein, Ataxin-3. Journal of Biological Chemistry 280, 32026–32034 (2005).

66. Hershko, A. THE UBIQUITIN SYSTEM. 57 (1998).

67. Weissman, A. M. Themes and variations on ubiquitylation. Nat Rev Mol Cell Biol 2, 169–178 (2001).

68. Yi, J. J. & Ehlers, M. D. Emerging Roles for Ubiquitin and Protein Degradation in Neuronal Function. Pharmacol Rev 59, 14–39 (2007).

69. Nijman, S. M. B. et al. A Genomic and Functional Inventory of Deubiquitinating Enzymes. Cell 123, 773–786 (2005).

70. Clague, M. J., Coulson, J. M. & Urbe, S. Cellular functions of the DUBs. Journal of Cell Science 125, 277–286 (2012).

71. Wang, G. -h. Ataxin-3, the MJD1 gene product, interacts with the two human homologs of yeast DNA repair protein RAD23, HHR23A and HHR23B. Human Molecular Genetics 9, 1795–1803 (2000).

72. Dantuma, N. P., Heinen, C. & Hoogstraten, D. The ubiquitin receptor Rad23: At the crossroads of nucleotide excision repair and proteasomal degradation. DNA Repair 8, 449–460 (2009).

73. Ye, Y. Diverse functions with a common regulator: Ubiquitin takes command of an AAA ATPase. Journal of Structural Biology 156, 29–40 (2006).

74. Meyer, H. & Weihl, C. C. The VCP/p97 system at a glance: connecting cellular function to disease pathogenesis. Journal of Cell Science 127, 3877–3883 (2014).

75. Boeddrich, A. et al. An arginine/lysine-rich motif is crucial for VCP/p97-mediated modulation of ataxin-3 fibrillogenesis. EMBO J 25, 1547–1558 (2006).

76. Wang, Q., Li, L. & Ye, Y. Regulation of retrotranslocation by p97-associated deubiquitinating enzyme ataxin-3. Journal of Cell Biology 174, 963–971 (2006).

77. Scaglione, K. M. et al. Ube2w and Ataxin-3 Coordinately Regulate the Ubiquitin Ligase CHIP. Molecular Cell 43, 599–612 (2011).

78. Bai, J. J., Safadi, S. S., Mercier, P., Barber, K. R. & Shaw, G. S. Ataxin-3 Is a Multivalent Ligand for the Parkin Ubl Domain. Biochemistry 52, 7369–7376 (2013).

79. Liu, H. et al. The Machado–Joseph Disease Deubiquitinase Ataxin-3 Regulates the Stability and Apoptotic Function of p53. PLoS Biol 14, e2000733 (2016).

80. Zhou, L. et al. Ataxin-3 protects cells against H2O2-induced oxidative stress by enhancing the interaction between Bcl-XL and Bax. Neuroscience 243, 14–21 (2013).

81. Tu, Y. et al. Ataxin-3 promotes genome integrity by stabilizing Chk1. Nucleic Acids Research 45, 4532–4549 (2017).

82. Gao, R. et al. Inactivation of PNKP by Mutant ATXN3 Triggers Apoptosis by Activating the DNA Damage-Response Pathway in SCA3. PLoS Genet 11, e1004834 (2015).

83. Herzog, L. K. et al. The Machado–Joseph disease deubiquitylase ataxin-3 interacts with LC3C/GABARAP and promotes autophagy. Aging Cell 19, (2020).

84. Zhong, X. & Pittman, R. N. Ataxin-3 binds VCP/p97 and regulates retrotranslocation of ERAD substrates. Human Molecular Genetics 15, 2409–2420 (2006).

85. Evers, M. M., Toonen, L. J. A. & van Roon-Mom, W. M. C. Ataxin-3 Protein and RNA Toxicity in Spinocerebellar Ataxia Type 3: Current Insights and Emerging Therapeutic Strategies. Mol Neurobiol (2013) doi:10.1007/s12035-013-8596-2.

86. McCampbell, A. CREB-binding protein sequestration by expanded polyglutamine. Human Molecular Genetics 9, 2197–2202 (2000).

87. Chai, Y., Wu, L., Griffin, J. D. & Paulson, H. L. The Role of Protein Composition in Specifying Nuclear Inclusion Formation in Polyglutamine Disease. J. Biol. Chem. 276, 44889–44897 (2001).

88. Chai, Y., Shao, J., Miller, V. M., Williams, A. & Paulson, H. L. Live-cell imaging reveals divergent intracellular dynamics of polyglutamine disease proteins and supports a sequestration model of pathogenesis. Proceedings of the National Academy of Sciences 99, 9310–9315 (2002).

89. Chou, A.-H. et al. Polyglutamine-expanded ataxin-3 causes cerebellar dysfunction of SCA3 transgenic mice by inducing transcriptional dysregulation. Neurobiology of Disease 31, 89–101 (2008).

90. Chou, A.-H. et al. p53 activation mediates polyglutamine-expanded ataxin-3 upregulation of Bax expression in cerebellar and pontine nuclei neurons. Neurochemistry International 58, 145–152 (2011).

91. Shimohata, T. et al. Expanded polyglutamine stretches interact with TAFII130, interfering with CREB-dependent transcription. Nat Genet 26, 29–36 (2000).

92. Li, F., Macfarlan, T., Pittman, R. N. & Chakravarti, D. Ataxin-3 Is a Histone-binding Protein with Two Independent Transcriptional Corepressor Activities. J. Biol. Chem. 277, 45004–45012 (2002).

93. Carrozza, M. J., Utley, R. T., Workman, J. L. & Côté, J. The diverse functions of histone acetyltransferase complexes. Trends in Genetics 19, 321–329 (2003).

94. Evert, B. O. et al. Ataxin-3 Represses Transcription via Chromatin Binding, Interaction with Histone Deacetylase 3, and Histone Deacetylation. Journal of Neuroscience 26, 11474–11486 (2006).

95. Chou, A.-H., Chen, Y.-L., Hu, S.-H., Chang, Y.-M. & Wang, H.-L. Polyglutamine-expanded ataxin-3 impairs long-term depression in Purkinje neurons of SCA3 transgenic mouse by inhibiting HAT and impairing histone acetylation. Brain Research 1583, 220–229 (2014).

96. Evert, B. O. et al. Inflammatory Genes Are Upregulated in Expanded Ataxin-3-Expressing Cell Lines and Spinocerebellar Ataxia Type 3 Brains. J. Neurosci. 21, 5389–5396 (2001).

97. Evert, B. O. et al. Gene Expression Profiling in Ataxin-3 Expressing Cell Lines Reveals Distinct Effects of Normal and Mutant Ataxin-3. J Neuropathol Exp Neurol 62, 1006–1018 (2003).

98. Araujo, J. et al. FOXO4-dependent upregulation of superoxide dismutase-2 in response to oxidative stress is impaired in spinocerebellar ataxia type 3. Human Molecular Genetics 20, 2928–2941 (2011).

99. Ratovitski, T. et al. Post-Translational Modifications (PTMs), Identified on Endogenous Huntingtin, Cluster within Proteolytic Domains between HEAT Repeats. J. Proteome Res. 16, 2692–2708 (2017).

100. Pennuto, M., Palazzolo, I. & Poletti, A. Post-translational modifications of expanded polyglutamine proteins: impact on neurotoxicity. Human Molecular Genetics 18, R40–R47 (2009).

101. Fei, E. et al. Phosphorylation of ataxin-3 by glycogen synthase kinase 3β at serine 256 regulates the aggregation of ataxin-3. Biochemical and Biophysical Research Communications 357, 487–492 (2007).

102. Tao, R.-S., Fei, E.-K., Ying, Z., Wang, H.-F. & Wang, G.-H. Casein kinase 2 interacts with and phosphorylates ataxin-3. Neurosci. Bull. 24, 271–277 (2008).

103. Mueller, T. et al. CK2-dependent phosphorylation determines cellular localization and stability of ataxin-3. Human Molecular Genetics 18, 3334–3343 (2009).

104. Matos, C. A. et al. Ataxin-3 phosphorylation decreases neuronal defects in spinocerebellar ataxia type 3 models. Journal of Cell Biology 212, 465–480 (2016).

105. Kristensen, L. V., Oppermann, F. S., Rauen, M. J., Hartmann-Petersen, R. & Thirstrup, K. Polyglutamine expansion of ataxin-3 alters its degree of ubiquitination and phosphorylation at specific sites. Neurochemistry International 105, 42–50 (2017).

106. Todi, S. V. et al. Ubiquitination directly enhances activity of the deubiquitinating enzyme ataxin-3. EMBO J 28, 372–382 (2009).

107. Todi, S. V. et al. Activity and Cellular Functions of the Deubiquitinating Enzyme and Polyglutamine Disease Protein Ataxin-3 Are Regulated by Ubiquitination at Lysine 117*. Journal of Biological Chemistry 285, 39303–39313 (2010).

108. Tsou, W.-L. et al. Ubiquitination Regulates the Neuroprotective Function of the Deubiquitinase Ataxin-3 in Vivo. Journal of Biological Chemistry 288, 34460–34469 (2013).

109. Jana, N. R. et al. Co-chaperone CHIP Associates with Expanded Polyglutamine Protein and Promotes Their Degradation by Proteasomes. 7.

110. Yang, Y. et al. Protein SUMOylation modification and its associations with disease. 10.

111. Shen, L. et al. Research on screening and identification of proteins interacting with ataxin-3. Zhonghua Yi Xue Yi Chuan Xue Za Zhi 22, 242–247 (2005).

112. Zhou, Y.-F. et al. SUMO-1 Modification on K166 of PolyQ-Expanded aTaxin-3 Strengthens Its Stability and Increases Its Cytotoxicity. PLOS ONE 8, 9 (2013).

113. Tsai, H.-F., Tsai, H.-J. & Hsieh, M. Full-length expanded ataxin-3 enhances mitochondrial-mediated cell death and decreases Bcl-2 expression in human neuroblastoma cells. Biochemical and Biophysical Research Communications 324, 1274–1282 (2004).

114. Chou, A.-H. et al. Polyglutamine-expanded ataxin-3 activates mitochondrial apoptotic pathway by up-regulating Bax and downregulating Bcl-xL. Neurobiology of Disease 21, 333–345 (2006).

115. Yu, Y.-C., Kuo, C.-L., Cheng, W.-L., Liu, C.-S. & Hsieh, M. Decreased antioxidant enzyme activity and increased mitochondrial DNA damage in cellular models of Machado-Joseph disease. J. Neurosci. Res. 87, 1884–1891 (2009).

116. Kazachkova, N. et al. Patterns of Mitochondrial DNA Damage in Blood and Brain Tissues of a Transgenic Mouse Model of Machado-Joseph Disease. Neurodegener Dis 11, 206–214 (2013).

117. Liu, C.-S. et al. Depletion of mitochondrial DNA in leukocytes of patients with poly-Q diseases. Journal of the Neurological Sciences 264, 18–21 (2008).

118. Reina, C. P., Zhong, X. & Pittman, R. N. Proteotoxic stress increases nuclear localization of ataxin-3. Human Molecular Genetics 19, 235–249 (2010).

119. Hsu, J.-Y. et al. The Truncated C-terminal Fragment of Mutant ATXN3 Disrupts Mitochondria Dynamics in Spinocerebellar Ataxia Type 3 Models. Front. Mol. Neurosci. 10, 196 (2017).

120. Kwon, Y. T. & Ciechanover, A. The Ubiquitin Code in the Ubiquitin-Proteasome System and Autophagy. Trends in Biochemical Sciences 42, 873–886 (2017).

121. Mizushima, N. A brief history of autophagy from cell biology to physiology and disease. Nat Cell Biol 20, 521–527 (2018).

122. Kocaturk, N. M. & Gozuacik, D. Crosstalk Between Mammalian Autophagy and the Ubiquitin-Proteasome System. Front. Cell Dev. Biol. 6, 128 (2018).

123. Cortes, C. J. & La Spada, A. R. Autophagy in polyglutamine disease: Imposing order on disorder or contributing to the chaos? Molecular and Cellular Neuroscience 66, 53–61 (2015).

124. Chai, Y., Koppenhafer, S. L., Shoesmith, S. J., Perez, M. K. & Paulson, H. L. Evidence for Proteasome Involvement in Polyglutamine Disease: Localization to Nuclear Inclusions in SCA3/MJD and Suppression of Polyglutamine Aggregation in vitro. Human Molecular Genetics 8, 673–682 (1999).

125. de Pril, R. Accumulation of aberrant ubiquitin induces aggregate formation and cell death in polyglutamine diseases. Human Molecular Genetics 13, 1803–1813 (2004).

126. Neves-Carvalho, A. et al. Dominant negative effect of polyglutamine expansion perturbs normal function of ataxin-3 in neuronal cells. Human Molecular Genetics 24, 100–117 (2015).

127. Maria Cuervo, A. Autophagy: in sickness and in health. Trends in Cell Biology 14, 70–77 (2004).

128. Durcan, T. M. et al. The Machado–Joseph disease-associated mutant form of ataxin-3 regulates parkin ubiquitination and stability. Human Molecular Genetics 20, 141–154 (2011).

129. Nascimento-Ferreira, I. et al. Overexpression of the autophagic beclin-1 protein clears mutant ataxin-3 and alleviates Machado–Joseph disease. Brain 134, 1400–1415 (2011).

130. Ashkenazi, A. et al. Polyglutamine tracts regulate beclin 1-dependent autophagy. Nature 545, 108–111 (2017).

131. Sittler, A. et al. Deregulation of autophagy in postmortem brains of Machado-Joseph disease patients: Autophagy in Machado-Joseph disease. Neuropathology 38, 113–124 (2018).

132. Brini, M., Calì, T., Ottolini, D. & Carafoli, E. Neuronal calcium signaling: function and dysfunction. Cell. Mol. Life Sci. 71, 2787–2814 (2014).

133. Oliveira, A. M. M., Bading, H. & Mauceri, D. Dysfunction of neuronal calcium signaling in aging and disease. Cell Tissue Res 357, 381–383 (2014).

134. Chen, X. et al. Deranged Calcium Signaling and Neurodegeneration in Spinocerebellar Ataxia Type 3. Journal of Neuroscience 28, 12713–12724 (2008).

135. Seidel, K. et al. Axonal inclusions in spinocerebellar ataxia type 3. Acta Neuropathol 120, 449–460 (2010).

136. D'Abreu, A., França Jr, M., Appenzeller, S., Lopes-Cendes, I. & Cendes, F. Axonal Dysfunction in the Deep White Matter in Machado-Joseph Disease. Journal of Neuroimaging 19, 9–12 (2009).

137. Rosenthal, N. & Brown, S. The mouse ascending: perspectives for human-disease models. Nat Cell Biol 9, 993–999 (2007).

138. Chadman, K. K., Yang, M. & Crawley, J. N. Criteria for validating mouse models of psychiatric diseases. Am. J. Med. Genet. 150B, 1–11 (2009).

139. Colomer Gould, V. F. Mouse Models of Spinocerebellar Ataxia Type 3 (Machado-Joseph Disease). Neurotherapeutics 9, 285–296 (2012).

140. Silva-Fernandes, A. et al. Chronic Treatment with 17-DMAG Improves Balance and Coordination in A New Mouse Model of Machado-Joseph Disease. Neurotherapeutics 11, 433–449 (2014).

141. Rodríguez-Cueto, C. et al. Dysregulation of the endocannabinoid signaling system in the cerebellum and brainstem in a transgenic mouse model of spinocerebellar ataxia type-3. Neuroscience 339, 191–209 (2016).

142. Costa, M. do C. et al. In Vivo Molecular Signatures of Cerebellar Pathology in Spinocerebellar Ataxia Type 3. Mov Disord 35, 1774–1786 (2020).

143. Duarte-Silva, S. et al. Lithium Chloride Therapy Fails to Improve Motor Function in a Transgenic Mouse Model of Machado-Joseph Disease. Cerebellum 13, 713–727 (2014).

144. Duarte-Silva, S. et al. Neuroprotective Effects of Creatine in the CMVMJD135 Mouse Model of Spinocerebellar Ataxia Type 3: Creatine Therapeutic Effect in SCA3. Mov Disord. 33, 815–826 (2018).

145. Teixeira-Castro, A. et al. Serotonergic signalling suppresses ataxin 3 aggregation and neurotoxicity in animal models of Machado-Joseph disease. Brain 138, 3221–3237 (2015).

146. Esteves, S. et al. Preclinical Evidence Supporting Early Initiation of Citalopram Treatment in Machado-Joseph Disease. Mol Neurobiol 56, 3626–3637 (2019).

147. Esteves, S. et al. Limited Effect of Chronic Valproic Acid Treatment in a Mouse Model of Machado-Joseph Disease. PLoS ONE 10, e0141610 (2015).

148. Duarte-Silva, S. et al. Combined therapy with m-TOR-dependent and -independent autophagy inducers causes neurotoxicity in a mouse model of Machado–Joseph disease. Neuroscience 313, 162–173 (2016).

149. Ashraf, N. S. et al. Citalopram Reduces Aggregation of ATXN3 in a YAC Transgenic Mouse Model of Machado-Joseph Disease. Mol Neurobiol 56, 3690–3701 (2019).

150. Menzies, F. M. et al. Autophagy induction reduces mutant ataxin-3 levels and toxicity in a mouse model of spinocerebellar ataxia type 3. Brain 133, 93–104 (2010).

151. Marcelo, A. et al. Cordycepin activates autophagy through AMPK phosphorylation to reduce abnormalities in Machado–Joseph disease models. Human Molecular Genetics 28, 51–63 (2019).

152. Wang, H.-L. et al. H1152 promotes the degradation of polyglutamine-expanded ataxin-3 or ataxin-7 independently of its ROCK-inhibiting effect and ameliorates mutant ataxin-3-induced neurodegeneration in the SCA3 transgenic mouse. Neuropharmacology 70, 1–11 (2013).

153. Krause, T., Gerbershagen, M. U., Fiege, M., Weißhorn, R. & Wappler, F. Dantrolene – A review of its pharmacology, therapeutic use and new developments. 10 (2004).

154. Chou, A.-H., Chen, S.-Y., Yeh, T.-H., Weng, Y.-H. & Wang, H.-L. HDAC inhibitor sodium butyrate reverses transcriptional downregulation and ameliorates ataxic symptoms in a transgenic mouse model of SCA3. Neurobiology of Disease 41, 481–488 (2011).

155. Cunha-Santos, J. et al. Caloric restriction blocks neuropathology and motor deficits in Machado–Joseph disease mouse models through SIRT1 pathway. NATURE COMMUNICATIONS 14.

156. Galiniak, S., Aebisher, D. & Bartusik-Aebisher, D. Health benefits of resveratrol administration. Acta Biochim Pol (2019) doi:10.18388/abp.2018_2749.

157. Gonçalves, N. et al. Caffeine alleviates progressive motor deficits in a transgenic mouse model of spinocerebellar ataxia. Annals of Neurology 32.

158. Boy, J. et al. Reversibility of symptoms in a conditional mouse model of spinocerebellar ataxia type 3. Human Molecular Genetics 18, 4282–4295 (2009).

159. Schmidt, J. et al. In vivo assessment of riluzole as a potential therapeutic drug for spinocerebellar ataxia type 3. J. Neurochem. 138, 150–162 (2016).

160. Wang, R.-Y., Huang, F.-Y., Soong, B.-W., Huang, S.-F. & Yang, Y.-R. A randomized controlled pilot trial of game-based training in individuals with spinocerebellar ataxia type 3. Sci Rep 8, 7816 (2018).

161. D'Abreu, A., França, M. C., Paulson, H. L. & Lopes-Cendes, I. Caring for Machado–Joseph disease: Current understanding and how to help patients. Parkinsonism & Related Disorders 16, 2–7 (2010).

162. Silva, R. C. R. et al. Occupational therapy in spinocerebellar ataxia type 3: an open-label trial. Braz J Med Biol Res 43, 537–542 (2010).

163. de Rezende, T. J. R. et al. Cerebral cortex involvement in Machado–Joseph disease. Eur J Neurol 22, 277-e24 (2015).

164. Fahl, C. N. et al. Spinal Cord Damage in Machado-Joseph Disease. Cerebellum 14, 128–132 (2015).

165. Guimarães, R. P. et al. A multimodal evaluation of microstructural white matter damage in spinocerebellar ataxia type 3: Microstructural Damage In SCA3. Mov Disord. 28, 1125–1132 (2013).

166. Lei, L. et al. Magnetic resonance spectroscopy of the cerebellum in patients with spinocerebellar ataxia type 3/Machado-Joseph disease. Zhong Nan Da Xue Xue Bao Yi Xue Ban 36, 511–519 (2011).

167. Lirng, J.-F. et al. Differences between Spinocerebellar Ataxias and Multiple System Atrophy-Cerebellar Type on Proton Magnetic Resonance Spectroscopy. PLoS ONE 7, e47925 (2012).

168. Wüllner, U. et al. Dopamine Transporter Positron Emission Tomography in Spinocerebellar Ataxias Type 1, 2, 3, and 6. Arch Neurol 62, 1280 (2005).

169. C. França, M., D'abreu, A., Nucci, A., Cendes, F. & Lopes-Cendes, I. Prospective study of peripheral neuropathy in Machado-Joseph disease: Progression of PN in MJD. Muscle Nerve 40, 1012–1018 (2009).

170. Tort, A. B. L. et al. S100B and NSE serum concentrations in Machado Joseph disease. Clinica Chimica Acta 351, 143–148 (2005).

171. Zhou, J. et al. Serum concentrations of NSE and S100B in spinocerebellar ataxia type 3/Machado-Joseph disease. Zhong Nan Da Xue Xue Bao Yi Xue Ban 36, 504–510 (2011).

172. Saute, J. A. M. et al. Serum insulin-like system alterations in patients with spinocerebellar ataxia type 3: Insulin-Like System in SCA3. Mov. Disord. 26, 731–735 (2011).

173. Shi, Y. et al. MicroRNA profiling in the serums of SCA3/MJD patients. International Journal of Neuroscience 124, 97–101 (2014).

174. Zijlstra, M. P. et al. Levels of DNAJB family members (HSP40) correlate with disease onset in patients with spinocerebellar ataxia type 3: DNAJB levels and age of onset in SCA3. European Journal of Neuroscience 32, 760–770 (2010).

175. Li, Q.-F. et al. Neurofilament light chain is a promising serum biomarker in spinocerebellar ataxia type 3. Mol Neurodegeneration 14, 39 (2019).

176. Correia, M. et al. Evaluation of the effect of sulphametoxazole and trimethoprim in patients with Machado-Joseph disease. Rev Neurol 23, 632–634 (1995).

177. Mello, K. A. & Abbott, B. P. Effect of Sulfamethoxazole and Trimethoprim on Neurologic Dysfunction in a Patient With Joseph's Disease. Archives of Neurology 45, 210–213 (1988).

178. Monte, T. L. et al. Use of fluoxetine for treatment of Machado-Joseph disease: an open-label study: Fluoxetine in Machado-Joseph disease. Acta Neurologica Scandinavica 107, 207–210 (2003).

179. Kanai, K. Muscle cramp in Machado-Joseph disease: Altered motor axonal excitability properties and mexiletine treatment. Brain 126, 965–973 (2003).

180. Tuite, P. J., Rogaeva, E. A., St George-Hyslop, P. H. & Lang, A. E. Dopa-responsive parkinsonism phenotype of Machado-Joseph disease: Confirmation of 14q CAG expansion. Ann Neurol. 38, 684–687 (1995).

181. Wilder-Smith, E. et al. Spinocerebellar ataxia type 3 presenting as an l-DOPA responsive dystonia phenotype in a Chinese family. Journal of the Neurological Sciences 213, 25–28 (2003).

182. Takei, A. et al. Effects of Tandospirone on "5-HT1A Receptor-Associated Symptoms" in Patients with Machado-Josephe Disease: An Open-Label Study. Clinical Neuropharmacology 27, 9–13 (2004).

183. Liu, C.-S., Hsu, H.-M., Cheng, W.-L. & Hsieh, M. Clinical and molecular events in patients with Machado-Joseph disease under lamotrigine therapy. Acta Neurol Scand 111, 385–390 (2005).

184. Arpa, J. et al. Subcutaneous insulin-like growth factor-1 treatment in spinocerebellar ataxias: An open label clinical trial. Mov. Disord. 26, 358–359 (2011).

185. Yang, W.-Z. et al. Human umbilical cord blood-derived mononuclear cell transplantation: case series of 30 subjects with Hereditary Ataxia. J Transl Med 9, 65 (2011).

186. Jin, J.-L. et al. Safety and Efficacy of Umbilical Cord Mesenchymal Stem Cell Therapy in Hereditary Spinocerebellar Ataxia. 10.

187. Zesiewicz, T. A. et al. A randomized trial of varenicline (Chantix) for the treatment of spinocerebellar ataxia type 3. Neurology 78, 545–550 (2012).

188. Saute, J. A. M. et al. A randomized, phase 2 clinical trial of lithium carbonate in Machado-Joseph disease: Lithium Trial in Machado-Joseph Disease. Mov Disord. 29, 568–573 (2014).

189. Lei, L.-F. et al. Safety and efficacy of valproic acid treatment in SCA3/MJD patients. Parkinsonism & Related Disorders 26, 55–61 (2016).

190. Schulte, T. et al. Double-blind Crossover Trial of Trimethoprim-Sulfamethoxazole in Spinocerebellar Ataxia Type 3/Machado-Joseph Disease. Arch Neurol 58, 1451 (2001).

191. Schapel, G. J., Black, A. B., Lam, E. L., Robinson, M. & Dollman, W. B. Combination vigabatrin and lamotrigine therapy for intractable epilepsy. Seizure 5, 51–56 (1996).

192. Rollema, H. et al. Pharmacological profile of the α4β2 nicotinic acetylcholine receptor partial agonist varenicline, an effective smoking cessation aid. Neuropharmacology 52, 985–994 (2007).

193. Afonso-Reis, R., Afonso, I. T. & Nóbrega, C. Current Status of Gene Therapy Research in Polyglutamine Spinocerebellar Ataxias. IJMS 22, 4249 (2021).

194. Kaufmann, K. B., Büning, H., Galy, A., Schambach, A. & Grez, M. Gene therapy on the move. EMBO Mol Med 5, 1642–1661 (2013).

195. Choudhury, S. R. et al. Viral vectors for therapy of neurologic diseases. Neuropharmacology 120, 63–80 (2017).

196. Simoes, A. T. et al. Calpastatin-mediated inhibition of calpains in the mouse brain prevents mutant ataxin 3 proteolysis, nuclear localization and aggregation, relieving Machado-Joseph disease. Brain 135, 2428–2439 (2012).

197. do Carmo Costa, M. et al. Toward RNAi Therapy for the Polyglutamine Disease Machado–Joseph Disease. Molecular Therapy 21, 1898–1908 (2013).

198. Rodríguez-Lebrón, E. et al. Silencing Mutant ATXN3 Expression Resolves Molecular Phenotypes in SCA3 Transgenic Mice. Molecular Therapy 21, 1909–1918 (2013).

199. Konno, A. et al. Mutant Ataxin-3 with an Abnormally Expanded Polyglutamine Chain Disrupts Dendritic Development and Metabotropic Glutamate Receptor Signaling in Mouse Cerebellar Purkinje Cells. Cerebellum 13, 29–41 (2014).

200. Duarte-Neves, J. et al. Neuropeptide Y mitigates neuropathology and motor deficits in mouse models of Machado–Joseph disease. Hum. Mol. Genet. 24, 5451–5463 (2015).

201. Nóbrega, C. et al. Restoring brain cholesterol turnover improves autophagy and has therapeutic potential in mouse models of spinocerebellar ataxia. Acta Neuropathol 138, 837–858 (2019).

202. Mykowska, A., Sobczak, K., Wojciechowska, M., Kozlowski, P. & Krzyzosiak, W. J. CAG repeats mimic CUG repeats in the misregulation of alternative splicing. Nucleic Acids Research 39, 8938–8951 (2011).

203. Mills, J. D. & Janitz, M. Alternative splicing of mRNA in the molecular pathology of neurodegenerative diseases. Neurobiology of Aging 33, 1012.e11-1012.e24 (2012).

204. Furlanis, E. & Scheiffele, P. Regulation of Neuronal Differentiation, Function, and Plasticity by Alternative Splicing. Annu. Rev. Cell Dev. Biol. 34, 451–469 (2018).

205. Nik, S. & Bowman, T. V. Splicing and neurodegeneration: Insights and mechanisms. WIREs RNA e1532 (2019) doi:10.1002/wrna.1532.

206. Neves-Carvalho, A. et al. Regulation of neuronal mRNA splicing and Tau isoform ratio by ATXN3 through deubiquitylation of splicing factors. http://biorxiv.org/lookup/doi/10.1101/711424 (2019) doi:10.1101/711424.

207. Burkholder, T., Foltz, C., Karlsson, E., Linton, C. G. & Smith, J. M. Health Evaluation of Experimental Laboratory Mice. Current Protocols in Mouse Biology 2, 145–165 (2012).

208. Silva-Fernandes, A. et al. Motor uncoordination and neuropathology in a transgenic mouse model of Machado–Joseph disease lacking intranuclear inclusions and ataxin-3 cleavage products. Neurobiology of Disease 40, 163–176 (2010).

209. Carter, R. J. et al. Characterization of Progressive Motor Deficits in Mice Transgenic for the Human Huntington's Disease Mutation. J. Neurosci. 19, 3248–3257 (1999).

210. Kamens, H. M. & Crabbe, J. C. The parallel rod floor test: a measure of ataxia in mice. Nat Protoc 2, 277–281 (2007).

211. Livak, K. J. & Schmittgen, T. D. Analysis of Relative Gene Expression Data Using Real-Time Quantitative PCR and the 2−ΔΔCT Method. Methods 25, 402–408 (2001).

212. Palarz, K., Neves-Carvalho, A., Duarte-Silva, S., Maciel, P. & Khodakhah, K. Cerebellar neuronal dysfunction accompanies early motor symptoms in Spinocerebellar Ataxia Type 3 and is partially alleviated upon chronic citalopram treatment. http://biorxiv.org/lookup/doi/10.1101/2021.04.29.441865 (2021) doi:10.1101/2021.04.29.441865.

213. Goedert, M. & Jakes, R. Expression of separate isoforms of human tau protein: correlation with the tau pattern in brain and effects on tubulin polymerization. 6.

214. Fern, M. Huntington's disease is a four-repeat tauopathy with tau nuclear rods. nature medicine 20, 7 (2014).

215. Vuono, R. et al. The role of tau in the pathological process and clinical expression of Huntington's disease. Brain 138, 1907–1918 (2015).

216. Lucas, J. J. Altered Levels and Isoforms of Tau and Nuclear Membrane Invaginations in Huntington's Disease. Frontiers in Cellular Neuroscience 13, 12 (2020).

217. Yin, X. et al. Dyrk1A overexpression leads to increase of 3R-tau expression and cognitive deficits in Ts65Dn Down syndrome mice. Sci Rep 7, 619 (2017).

218. Hocquemiller, M., Giersch, L., Audrain, M., Parker, S. & Cartier, N. Adeno-Associated Virus-Based Gene Therapy for CNS Diseases. Human Gene Therapy 27, 478–496 (2016).

219. Hashad, D., Koichi Miyake, Noriko Miyake, & Takashi Shimada. Gene Delivery into the Central Nervous System (CNS) Using AAV Vectors, Gene Therapy - Principles and Challenges. (2015).

220. Gholizadeh, S., Tharmalingam, S., MacAldaz, M. E. & Hampson, D. R. Transduction of the Central Nervous System After Intracerebroventricular Injection of Adeno-Associated Viral Vectors in Neonatal and Juvenile Mice. Human Gene Therapy Methods 24, 205–213 (2013).

221. Yamazaki, Y., Hirai, Y., Miyake, K. & Shimada, T. Targeted gene transfer into ependymal cells through intraventricular injection of AAV1 vector and long-term enzyme replacement via the CSF. Sci Rep 4, 5506 (2014).

222. Toonen, L. J. A., Rigo, F., van Attikum, H. & van Roon-Mom, W. M. C. Antisense Oligonucleotide-Mediated Removal of the Polyglutamine Repeat in Spinocerebellar Ataxia Type 3 Mice. Mol Ther Nucleic Acids 8, 232–242 (2017).

223. McLoughlin, H. S. et al. Oligonucleotide therapy mitigates disease in spinocerebellar ataxia type 3 mice: ASO Therapy for SCA3. Ann Neurol. 84, 64–77 (2018).

224. Nobre, R. J. et al. MiRNA-Mediated Knockdown of ATXN3 Alleviates Molecular Disease Hallmarks in a Mouse Model for Spinocerebellar Ataxia Type 3. Nucleic Acid Therapeutics nat.2021.0020 (2021) doi:10.1089/nat.2021.0020.

225. Samaranch, L. et al. Adeno-Associated Virus Serotype 9 Transduction in the Central Nervous System of Nonhuman Primates. Human Gene Therapy 23, 382–389 (2012).

226. Samaranch, L. et al. Strong Cortical and Spinal Cord Transduction After AAV7 and AAV9 Delivery into the Cerebrospinal Fluid of Nonhuman Primates. Human Gene Therapy 24, 526–532 (2013).

227. Shababi, M. et al. Rescue of a Mouse Model of Spinal Muscular Atrophy With Respiratory Distress Type 1 by AAV9-IGHMBP2 Is Dose Dependent. Molecular Therapy 24, 855–866 (2016).

228. Roca, C., Motas, S., Marco, S. & Ribera, A. Disease correction by AAV-mediated gene therapy in a new mouse model of mucopolysaccharidosis type IIID. 17.

229. Baek, R. C. et al. AAV-mediated gene delivery in adult GM1-gangliosidosis mice corrects lysosomal storage in CNS and improves survival. PLoS One 5, e13468 (2010).

230. Bosch, M. K., Nerbonne, J. M. & Ornitz, D. M. Dual Transgene Expression in Murine Cerebellar Purkinje Neurons by Viral Transduction In Vivo. PLoS ONE 9, e104062 (2014).

231. Arendt, T., Stieler, J. T. & Holzer, M. Tau and tauopathies. Brain Research Bulletin 126, 238–292 (2016).

232. Franklin, K. B. J. & Paxinos, G. The mouse brain in stereotaxic coordinates. (Elsevier Academic Press, 2008).

233. Penrod, R. D., Wells, A. M., Carlezon, W. A. & Cowan, C. W. Use of Adeno-Associated and Herpes Simplex Viral Vectors for In Vivo Neuronal Expression in Mice. Current Protocols in Neuroscience 73, (2015).

234. Rüb, U. et al. Degeneration of the external cuneate nucleus in spinocerebellar ataxia type 3 (Machado–Joseph disease). Brain Research 953, 126–134 (2002).

235. Hernández, F., Merchán-Rubira, J., Vallés-Saiz, L., Rodríguez-Matellán, A. & Avila, J. Differences Between Human and Murine Tau at the N-terminal End. Front. Aging Neurosci. 12, 11 (2020).

236. Hölter, S. M. et al. Assessing Cognition in Mice. Curr Protoc Mouse Biol 5, 331–358 (2015).

237. Rösler, T. W. et al. Four-repeat tauopathies. Progress in Neurobiology 180, 101644 (2019).

238. Espíndola, S. L. et al. Modulation of Tau Isoforms Imbalance Precludes Tau Pathology and Cognitive Decline in a Mouse Model of Tauopathy. Cell Reports 23, 709–715 (2018).

239. Wobst, H. J. et al. Increased 4R tau expression and behavioural changes in a novel MAPT-N296H genomic mouse model of tauopathy. Sci Rep 7, 43198 (2017).

240. Vandenberg, L. N. & Blumberg, B. Alternative Approaches to Dose–Response Modeling of Toxicological Endpoints for Risk Assessment: Nonmonotonic Dose Responses for Endocrine Disruptors. in Comprehensive Toxicology 39–58 (Elsevier, 2018). doi:10.1016/B978-0-12-801238-3.64298-8.

241. Nakamura, S. et al. Gene therapy for a mouse model of glucose transporter-1 deficiency syndrome. Molecular Genetics and Metabolism Reports 10, 67–74 (2017).

242. Vogels, T., Vargová, G., Brezováková, V., Quint, W. H. & Hromádka, T. Viral Delivery of Non-Mutated Human Truncated Tau to Neurons Recapitulates Key Features of Human Tauopathy in Wild-Type Mice. JAD 77, 551–568 (2020).

243. Dassie, E. et al. Focal expression of adeno-associated viral-mutant tau induces widespread impairment in an APP mouse model. Neurobiology of Aging 34, 1355–1368 (2013).

244. Samaranch, L. et al. Adeno-associated viral vector serotype 9–based gene therapy for Niemann-Pick disease type A. Sci. Transl. Med. 11, eaat3738 (2019).

245. Cetin, A., Komai, S., Eliava, M., Seeburg, P. H. & Osten, P. Stereotaxic gene delivery in the rodent brain. Nat Protoc 1, 3166–3173 (2006).

246. Hammelrath, L. et al. Morphological maturation of the mouse brain: An in vivo MRI and histology investigation. NeuroImage 125, 144–152 (2016).

247. Rafii, M. S. A phase1 study of stereotactic gene delivery of AAV2-NGF for Alzheimer's disease. 11 (2014).

248. LeWitt, P. A. AAV2-GAD gene therapy for advanced Parkinson's disease: a double-blind, sham-surgery controlled, randomised trial. 10, 11 (2011).

249. Mendell, J. R. et al. Single-Dose Gene-Replacement Therapy for Spinal Muscular Atrophy. n engl j med 10 (2017).

SUPPLEMENTARY DATA

Table S1. Statistical report for all behavioral analyses performed in the SCA3 mice.

Figure	Statistical report		Sample size
CAG repeat	t(31) = ,302 , p = 0.765, Cohen's d = 0.105		16 to 17 mice/group
Body weight	Females	Group: $F_{(3,20)}$ = 5.128, p = 0.009 , η^2_p = 0.435 Genotype: $F_{(1,20)}$ = 12.430, p = 0.002 , η^2_p = 0.393 Treatment: $F_{(1,20)}$ < 0.001, p = 0.988 , η^2_p < 0.001 Genotype x Treatment: $F_{(1,20)}$ = 1.990, p = 0.174 , η^2_p = 0.091	5 to 7 mice/group
	Males	Group: $F_{(3,23)}$ = 9.458, p < 0.001 , η^2_p = 0.552 Genotype: $F_{(1,23)}$ = 25.171, p < 0.001 , η^2_p = 0.523 Treatment: $F_{(1,23)}$ = 0.112, p = 0.714 , η^2_p = 0.005 Genotype x Treatment: $F_{(1,23)}$ = 0.849 , p = 0.366, η^2_p = 0.036	4 to 8 mice/group
Hanging Wire Grid Test	6 weeks of age: H(3) = 35.013, p < 0.001 8 weeks of age: H(3) = 34.117, p < 0.001 10 weeks of age: H(3) = 38.889, p < 0.001 12 weeks of age: H(3) = 45.096, p < 0.001 14 weeks of age: H(3) = 43.637, p < 0.001 16 weeks of age: H(3) = 33.752, p < 0.001 18 weeks of age: H(3) = 37.074, p < 0.001 20 weeks of age: H(3) = 36.647, p < 0.001		11 to 14 mice/group
Horizontal spontaneous activity	6 weeks of age: H(3) = 0.140, p = 0.987 8 weeks of age: H(3) =4.270, p = 0.234 10 weeks of age: H(3) = 17.739, p < 0.001 12 weeks of age: H(3) = 11.148, p = 0.011 14 weeks of age: H(3) = 15.152, p = 0.002 16 weeks of age: H(3) = 14.156, p = 0.003 18 weeks of age: H(3) = 3.726, p = 0.293 20 weeks of age: H(3) = 12.852, p = 0.005		11 to 15 mice/group
Motor swimming test	Group: $F_{(3, 47)}$ = 4.733, p = 0.006, η^2_p = 0.232 Genotype: $F_{(1, 47)}$ = 12.949, p < 0.001, η^2_p = 0.216 Treatment: $F_{(1, 47)}$ = 0.156, p = 0.695, η^2_p = 0.003		10 to 14 mice/group
Parallel Rod Floor	Group: $F_{(3,48)}$ = 0.611, p = 0.611, η^2_p = 0.037 Genotype: $F_{(1, 48)}$ = 1.473, p < 0.231, η^2_p = 0.030 Treatment: $F_{(1, 48)}$ = 0.117, p = 0.734, η^2_p = 0.002		11 to 15 mice/group
Square Beam 12mm	Group: $F_{(3, 43)}$ = 8.910, p < 0.001, η^2_p = 0.383 Genotype: $F_{(1, 43)}$ =13.717, p < 0.001, η^2_p = 0.242 Treatment: $F_{(1, 43)}$ =13.695, p < 0.001, η^2_p = 0.242		8 to 14 mice/group
Circle Beam 17mm	Group: $F_{(3, 37)}$ = 10.399, p < 0.001, η^2_p = 0.457 Genotype: $F_{(1, 37)}$ = 26.041, p < 0.001, η^2_p = 0.413 Treatment: $F_{(1, 37)}$ = 8.409, p = 0.006, η^2_p = 0.185		8 to 12 mice/group
Circle Beam 11mm	Group: $F_{(3, 39)}$ = 4.455, p = 0.009, η^2_p = 0.255 Genotype: $F_{(1, 39)}$ = 4.390, p = 0.043, η^2_p = 0.101 Treatment: $F_{(1, 39)}$ =5.841, p = 0.020, η^2_p = 0.130		9 to 12 mice/group

Table S2. Statistical report of mRNA relative expression of 3R-Tau and 4R-Tau isoforms in the cerebellum and in the brainstem of SCA3 mice.

Brain region	Gene	Statistical report: Independent T-test	Sample size
Cerebellum	3R-Tau	t(5) = 0.628, p = 0.558 Cohen's d = 0.480	3 to 4 samples/group N=2 technical replicates
	4R-Tau	t(5) = 1.176, p = 0.293 Cohen's d = 0.898	
Brainstem	3R-Tau	t(5) = 1.507, p = 0.192 Cohen's d = 1.151	3 to 4 samples/group N=2 technical replicates
	4R-Tau	t(5) = 2.105, p = 0.089 Cohen's d = 1.608	

Table S3. Conditions tested in the first pilot study.

AAV vector	Volume (µL)	Titer	Total volume (V_{TOTAL}) and Infusion rate (IR)	Number of animals per condition
AAV-CAG-4R-Tau	0.5 1 2	$1.3x10^{13}$ GC/ml	V_{TOTAL}= 2 µL IR= 200 nL/min	1 animal / condition
AAV-CAG-GFP		$1.0x10^{13}$ GC/ml		

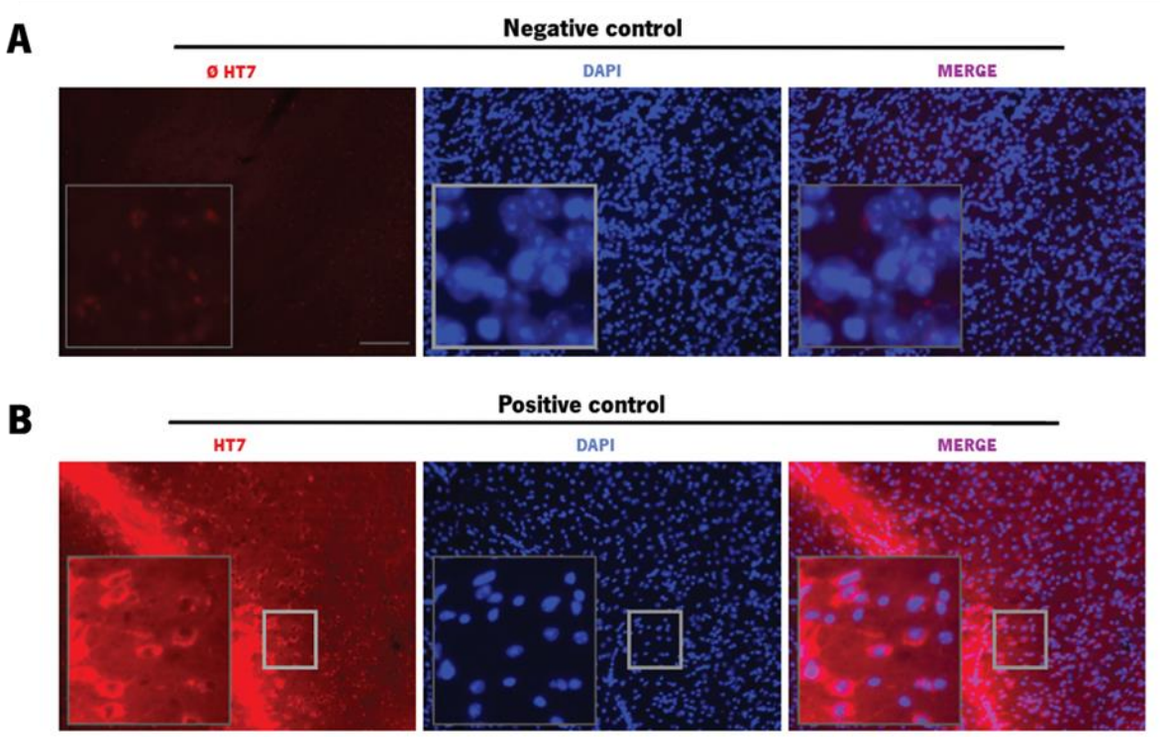

Figure S1. Controls used for the immunofluorescence technique in mouse brain sections (20 µm-thickness) at 3- and 4-weeks post-injection. (A) A negative control, without the presence of primary antibody (øHT7), was used to confirm the specificity of the secondary antibody (fluorophore-conjugated anti-mouse 594). **(B)** P301L mouse hippocampus slice labelled with the HT7 antibody was used as positive control. This transgenic mouse line expresses mutant human Tau under a CAMKII promoter. 20x magnification. The HT7 antibody detects the presence of human Tau (red). Cell nuclei were counterstained with DAPI (blue). Scale bars represent 100 µm.

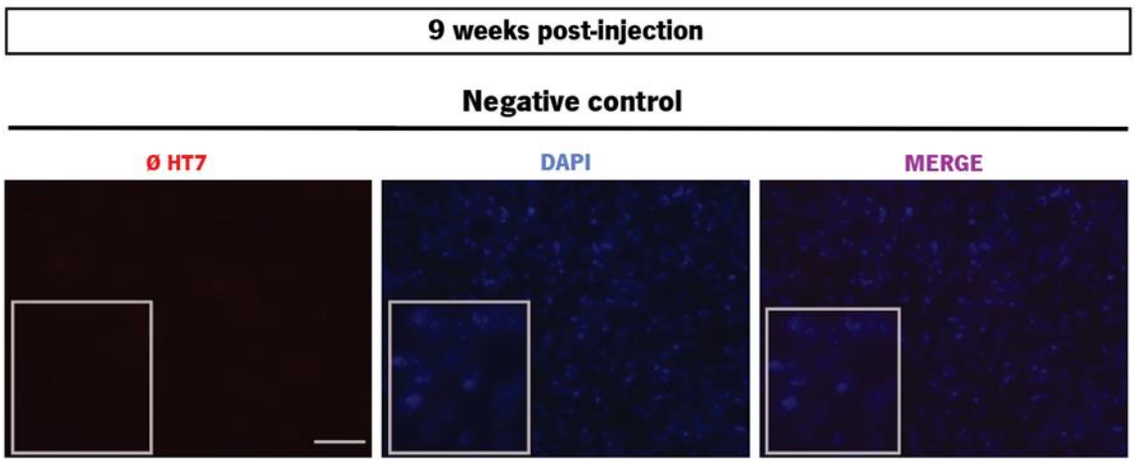

Figure S2. Controls used for the immunofluorescence technique in mouse brain sections (20 µm-thickness) at 9-weeks post-injection. A negative control, without the presence of primary antibody (øHT7), was used to confirm the specificity of the secondary antibody. The HT7 antibody detects the presence of human Tau (red). Cell nuclei were counterstained with DAPI (blue). 20x magnification. Scale bars represent 100 µm.

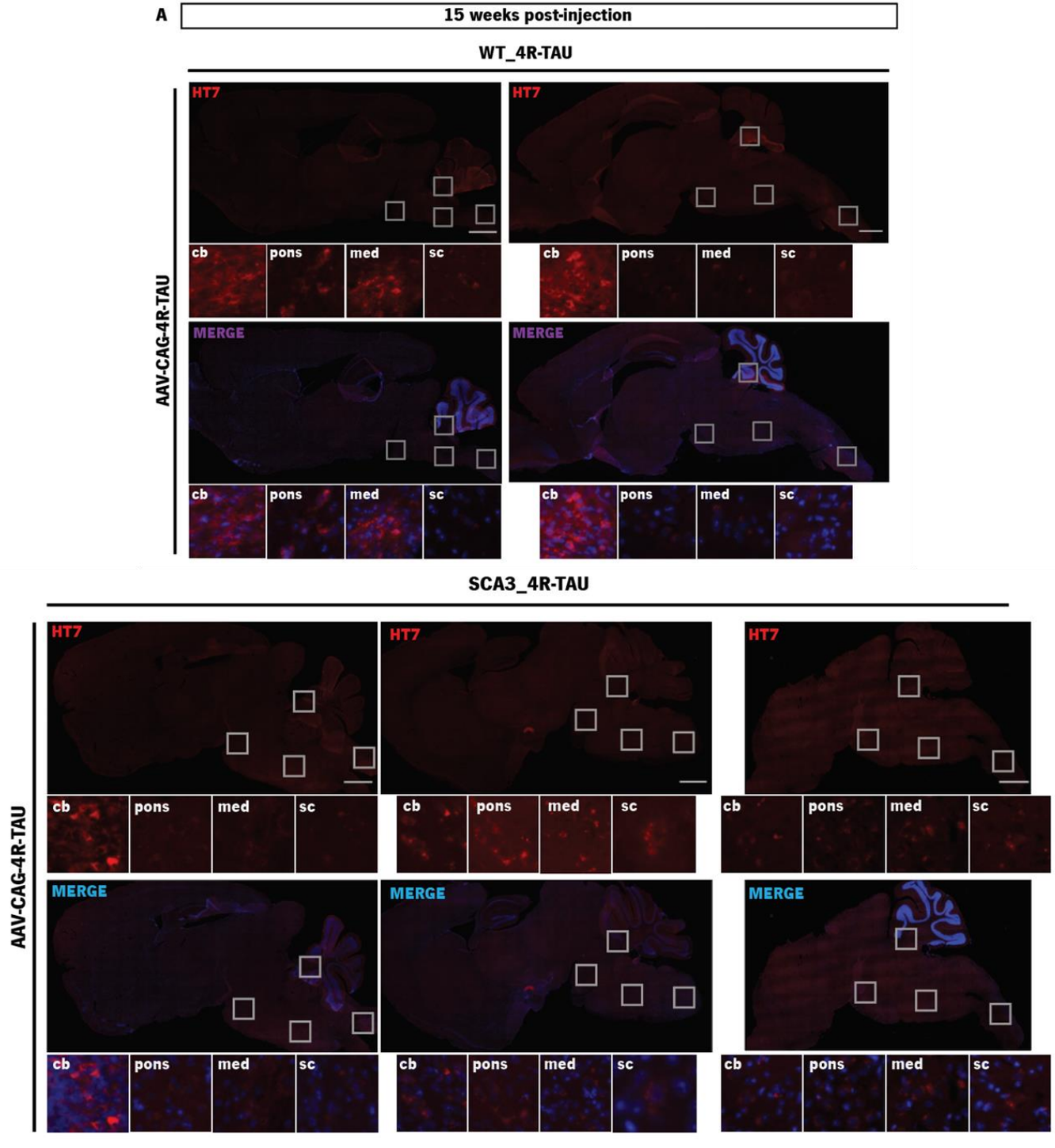
A
15 weeks post-injection
WT_4R-TAU
SCA3_4R-TAU
AAV-CAG-4R-TAU
HT7
MERGE
cb
pons
med
sc

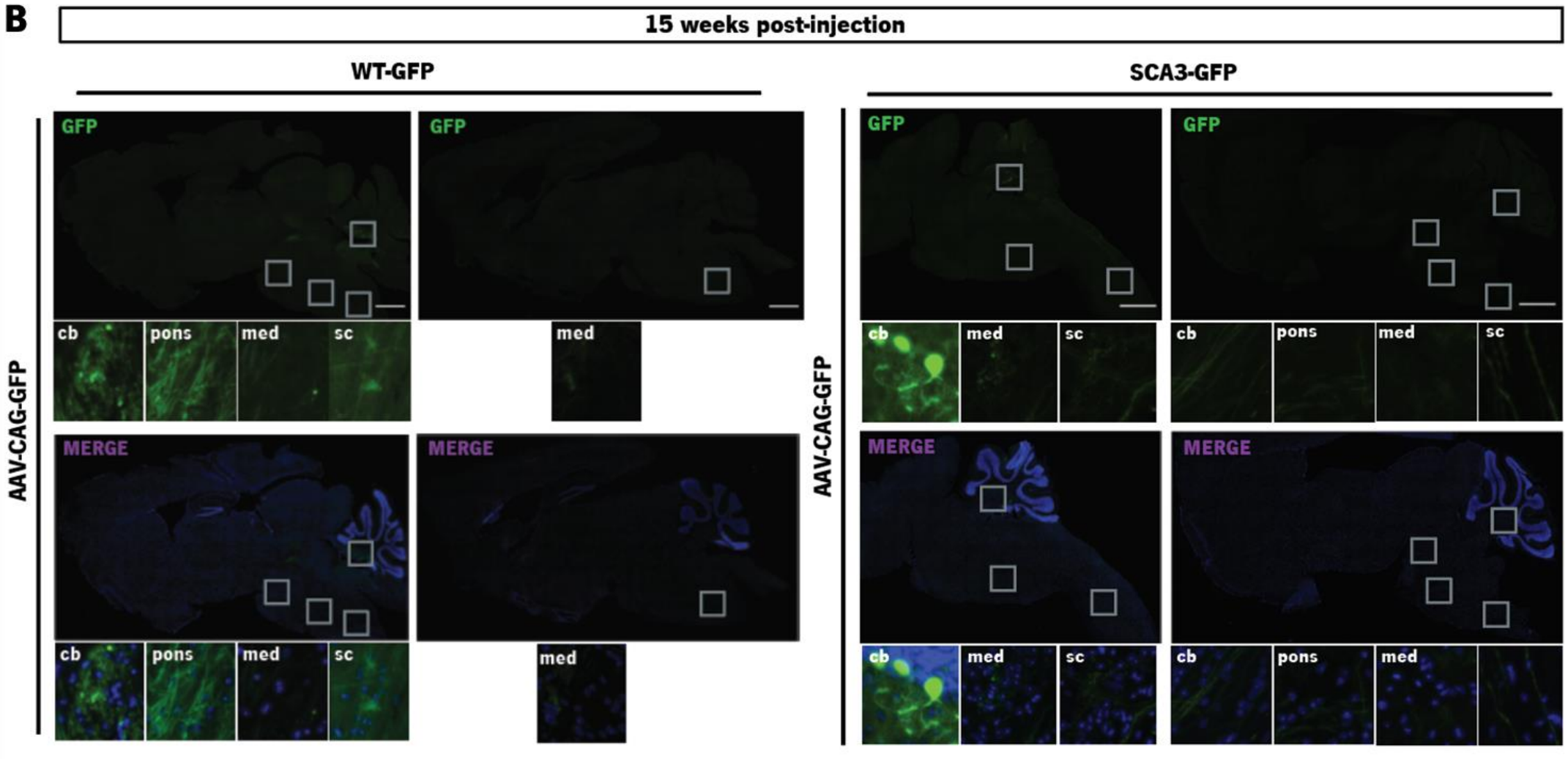
B
15 weeks post-injection
WT-GFP
SCA3-GFP
AAV-CAG-GFP
AAV-CAG-GFP
GFP
GFP
GFP
GFP
cb
pons
med
sc
med
cb
med
sc
cb
pons
med
sc
MERGE
MERGE
MERGE
MERGE
cb
pons
med
sc
med
cb
med
sc
cb
pons
med

Figure S3. AAV-CAG-4R-Tau and AAV-CAG-GFP administration into mouse brains led to high viral transduction and expression at 15-weeks post-injection. Representative mouse brain sagittal sections (20 µm-thickness) of both WT and SCA3 mice, injected with a total volume of 3 µL of **(A)** human 4R-Tau protein driven by AAV-CAG-4R-Tau (n= 4 to 5 mice/group) or **(B)** GFP driven by AAV-CAG-GFP (n=4 mice/group) showing expression in several brain areas, including the cerebellum (cb), pons, medulla oblongata (med) and spinal cord (sc) at 15-weeks post-injection. The HT7 antibody detects the presence of human Tau (red). Cell nuclei were counterstained with DAPI (blue). 20x magnification. Scale bars of whole mouse brain sections represent 1000 µm. Scale bars of insets of each mosaic picture represent 100 µm.

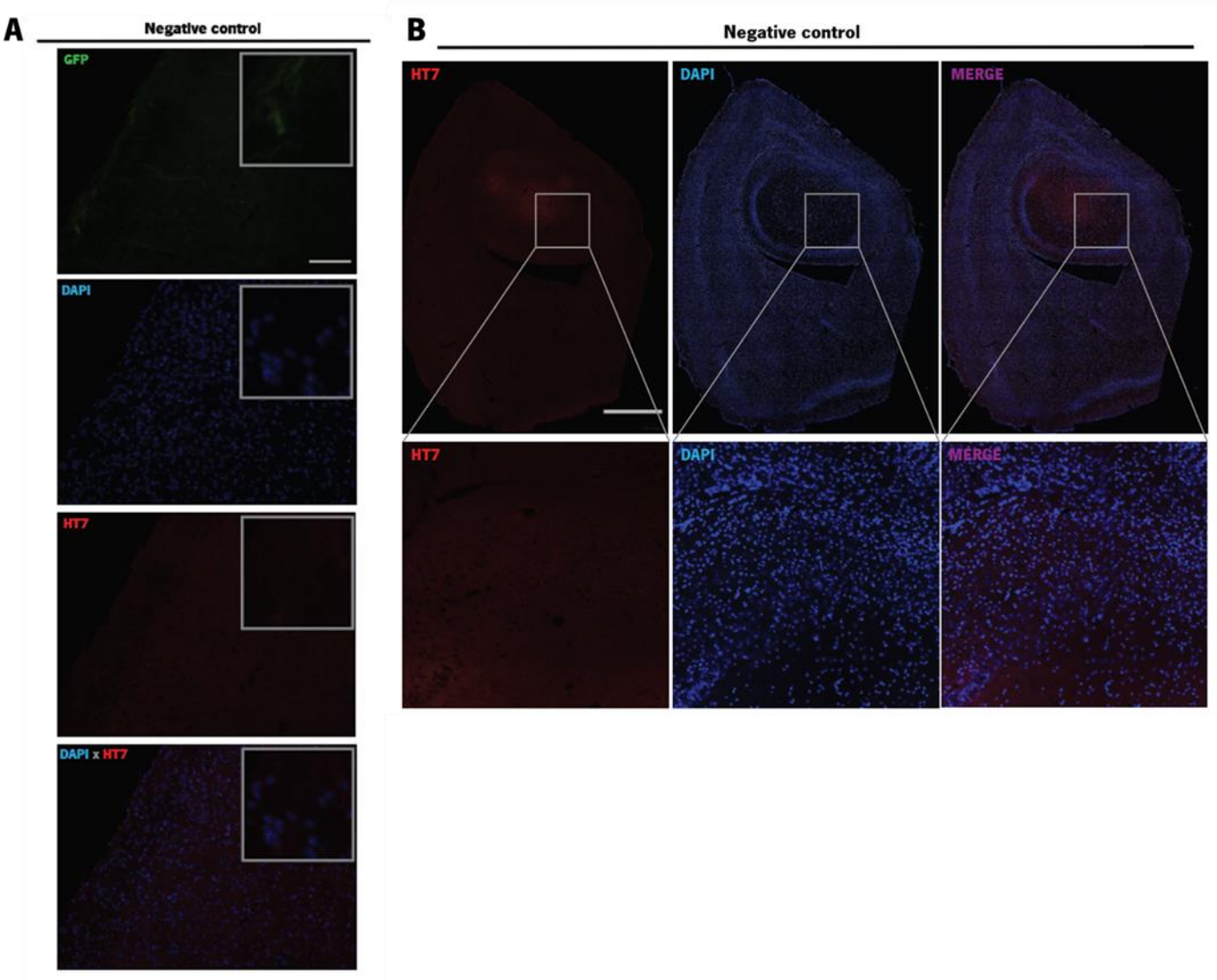

Figure S4. Controls used for the immunofluorescence technique in mouse brain sections (20 µm-thickness) at 15-weeks post-injection. (A) Mouse brain sections expressing GFP were stained with HT7 antibody to confirm if it would be specific to detect exclusively human Tau **(B)** A negative control, without the presence of primary antibody (HT7), was used to confirm the specificity of the secondary antibody. The HT7 antibody detects the presence of human Tau (red). Cell nuclei were counterstained with DAPI (blue). 20x magnification. Scale bars represent 100 µm.